DEVELOPING A NEW SPATIO-TEMPORAL FRAMEWORK FOR ASSESSMENT OF THE NOVA SCOTIA INSHORE SEA SCALLOP (*PLACOPECTEN MAGELLANICUS*) FISHERY

by

Raphaël McDonald

Submitted in partial fulfillment of the requirements
for the degree of Master of Science

at

Dalhousie University
Halifax, Nova Scotia
July 2020

A mes parents, qui m'ont toujours soutenu et encouragé pendant toutes ces années d'études

To my partner, who supported me every step of the way

Table of Contents

List of Tables

List of Figures

Abstract

The Nova Scotia Inshore Sea Scallop (*Placopecten Magellanicus*) Fishery is the fourth most valuable fishery in the province and has been in existence since the 1960s. Covering the Bay of Fundy and areas close to the shore of Nova Scotia, it is split up into multiple Scallop Production Areas (SPA) and Scallop Fishing Areas (SFA). Most areas are assessed separately with a different yearly Total Allowable Catch (TAC) set to limit maximum landings. SPA 3, encompassing St-Mary's Bay and a good portion of the western shore of Nova Scotia, has been difficult to assess due to its strong spatial patterns in both biological characteristics and fishing effort.

The current model typically used to assess areas of this fishery is a delay-difference model, a type of biomass dynamics model which only requires an index of abundance and commercial landings. However, even after recasting it into a frequentist framework, this model has been found to be unable to reliably model SPA 3. The focus of this work is to incorporate spatial information into this assessment model in two steps. The first step involves reconsidering abundance indices to reduce the amount of necessary pre-processing and directly model all intra-annual variability, while simultaneously accounting for the large number of zeroes. The second step involves explicitly modeling the location of survey tows and commercial fishing by modifying the error structure of the model by using Gaussian Markov Random Fields such that a spatio-temporal model results.

The new framework for abundance indices is shown to better capture population changes and can be viewed as a hybrid between a traditional temporal model and a spatio-temporal version. The full spatio-temporal stock assessment framework is further able to capture both local population changes reliably and population trends for the entire area of interest. This novel framework shows promise to improve the reliability of scientific advice given to fisheries managers while opening up new possibilities for spatial management.

Acknowledgements

This research was undertaken thanks in part to funding from the Canada First Research Excellence Fund, through the Ocean Frontier Institute.

Chapter 1

Introduction

Nova Scotia's relationship with fishing the Atlantic Ocean and the Bay of Fundy is a long and enduring one. Both pre-European inhabitants and European colonists have been attracted to and depended on the rich fishing done in and around the Canadian east coast (Lelièvre, 2017). Over time, technological developments have allowed access to new fisheries and new species of fish previously inaccessible, such as yellowtail (*Pleuronectes ferroginea*) (Merrill and Posgay, 1964), while increasing fisher's capacity to capture large amounts of fish. This led to a steady global increase in amount of fish caught up until recent times, where this amount has stabilized (FAO, 2018). This increase in exploitation of wild fish and shellfish has led to intense debate over the global status of fish stocks throughout the last few decades. The well-documented collapse of the Northwest Atlantic population of Atlantic cod (*Gadus morhua*) (Hutchings and Myers, 1994; Myers et al., 1996) underlined the necessity for a global discussion on the causes of worldwide population declines (Myers and Worm, 2003) to prevent global population collapses. Unsustainable practices such as overfishing and mismanagement have been identified as causal factors, albeit with varying degrees of emphasis and mitigative solutions (Worm et al., 2006; Hilborn, 2007).

Ecological theory, while often developed on terrestrial species, has long been applied with varying levels of success to understand how marine species vary. Evidence of density dependence in fish populations, wherein population growth depends on the size of the population (Smith, 1961), has been empirically detected for a long time (Raitt, 1939). The climate can also have a profound effect on fish populations (Sissenwine, 1984), just as preferred habitat (Jones and Martin, 1981), fish behaviour, and movement/migration (Callihan et al., 2014) can impact population variability.

More specifically, fisheries ecology has focused on attempting to explain variability in population abundance of commercially important fish stocks (Sissenwine, 1984).

Many of these stocks have historically been very difficult to monitor in an attempt to manage these fisheries in a sustainable manner. Dozens of theories have been developed to try to explain commonly observed large or ephemeral spikes in populations. These theories have ranged from extensive migrations to patterns of larval dispersal (Houde, 2008). One key component of most approaches has been to focus on recruitment (wherein young fish grow old or large enough to be of commercial interest) since it is ultimately responsible for the maintenance and health of a stock (Sissenwine, 1984). Due to the practical impossibility of directly observing most of these traits and variables, changes in fish populations must be estimated or predicted, using different types of deterministic and statistical models.

1.1 Stock Assessment Approaches

Far from a strictly modern phenomena, models in ecology have a very long history stretching all the way back to Malthus' original exponential population growth model (Malthus, 1798, as seen in Angelini and Moloney, 2007). Early statistical approaches can even be seen pre-20^{th} century with the use of the least squares method to compare different herring (*Clupea harengus*) populations (Angelini and Moloney, 2007). Unfortunately, lack of appropriate statistical and computational tools long hindered the progress of modeling fish stocks (Goethel et al., 2011), and led to the development of many different methods dependent on the types of data available.

When environmental variables or other types of predictors are available along with measures of abundance, linear models have formed the basis of many statistical approaches via the following general form (Venables and Dichmont, 2004)

$$y = \mathbf{X}\boldsymbol{\beta} + \epsilon \tag{1.1}$$

where y is the response variable of interest (e.g. fish length at age), $\mathbf{X}\boldsymbol{\beta}$ is the linear predictor that represents the dynamic process impacting the response variable (for example, β could be the coefficient for temperature x and ϵ is some error term, often assumed to be distributed normally). However, fisheries data rarely follow the assumptions of ordinary linear regression and tend to be inherently noisy (Aeberhard et al., 2018). For example, standard deviations often increase with the mean (e.g.

Punt et al., 2000), there can be non-linear relationships between response and explanatory variables (Froese, 2006 for fish weight-length relationships), and data are often distributed non-normally (e.g. Martin et al., 2005; Yin et al., 2019). Multiple approaches have been developed to extend and generalize ordinary linear models to account for these complexities. These include generalized linear models (GLM), generalized additive models (GAM) and generalized linear mixed models (GLMM) (Venables and Dichmont, 2004; Bolker et al., 2009).

When few or no environmental variables are available, three main approaches have historically been taken for fisheries stock assessments: catch-at-age methods if the age distribution is available, biomass dynamics (also called surplus production) if an index of abundance is available, and length frequency analysis if only length data is available (Hilborn, 1992). Of interest here are biomass dynamics models, which are based on logistic growth models. Their main attraction is that they only require total catch and an index of fish abundance to work (Hilborn, 1992). A good example of a biomass dynamics model would be the delay-difference model, created as a compromise between overly simplistic traditional models and overly complex but more realistic models (Deriso, 1980). The main equation of interest for this type of model resembles the following:

$$B_{t+1} = (1+\rho)lS_t - \rho l^2 \frac{S_t}{B_t} S_{t-1} + F(S_{t+1-k}) \tag{1.2}$$

where B_t is the biomass of the catchable population before fishing in year t, ρ is Brody's growth coefficient with $0 \leq \rho \leq 1$, $S_t = B_t - C_t$ where S_t is the escapement of adults and C_t is the total catch in year t, l is the annual natural survival fraction for catchable adults, and $F(S_{t+1-k})$ is a spawner-recruit relationship with k being the age at recruitment (Deriso, 1980). This type of equation is conceptually simple: to obtain the next year's total fishable biomass, one must simply take those from the previous year, remove those that died either through natural mortality (l) or through fishing mortality (C_t), grow the survivors (ρ) and add the recruits ($F(S_{t+1-k})$).

Even when these types of equations had strong conceptual roots, they are difficult to apply when dealing with real data (Schnute, 1985). Real data are often thought to have two main sources of error: observation errors, which come from the observation process and often called measurement errors, and process errors, which

come from the imperfect knowledge of the true underlying dynamical process (Cressie et al., 2009; Aeberhard et al., 2018). A classical method was to take a "curve-fitting" approach when applying these models to real data (Quinn and Deriso, 1999). This type of approach consisted of fitting different theoretical curves, such as nonlinear Ricker or Gompertz curves, and picking out the one that best fits the data (Cressie et al., 2009). Early implementations of these models often struggled to account for variability coming from observation errors or imperfect knowledge of the underlying process. Attempts to deal with these issues included the incorporation of assumptions like assuming that one type of error was absent (e.g. Kinas, 1996) or that the ratio between the two forms of errors was known (e.g. Schnute and Richards, 1995). A common way of incorporating both types of errors came in the form of hierarchical models, such as state-space models (SSMs) (Cressie et al., 2009), although these models can sometimes exhibit problematic behaviors when measurements errors are larger than process errors (Auger-Méthé et al., 2016). These models are also able to predict future states, making them useful for the purpose of fisheries management.

A basic SSM is defined by two stochastic processes: $\mathbf{X}_t$ representing the unobserved state of a dynamic process of interest (e.g. stock biomass) and $\mathbf{Y}_t$ representing a directly observed response variable with the index t indicating time-steps (Aeberhard et al., 2018). These models often include an associated covariate vector $\mathbf{z}_t$ and underlying fixed parameters $\boldsymbol{\theta}$ (Schnute, 1994; Aeberhard et al., 2018). SSMs fit in a frequentist framework can be represented by a 2-tiered hierarchical set of equations (Aeberhard et al., 2018). The first set of equations, which models directly observed variables, is conditioned on the underlying variables, modeled by the second set of equations (e.g. $E[\mathbf{Y}_t|\mathbf{X}_t]$) (Aeberhard et al., 2018). The states of the underlying process at time t are conditioned on their state at the previous time-step. A general SSM can therefore be modeled the following way (Aeberhard et al., 2018):

$$E[\mathbf{Y}_t|\mathbf{X}_t] = g(\mathbf{X}_t, \boldsymbol{\theta}_Y) \tag{1.3}$$

$$E[\mathbf{X}_t|\mathbf{X}_{t-1}] = h(\mathbf{X}_{t-1}, \boldsymbol{\theta}_X) \tag{1.4}$$

where g and h are functions following regular time-steps (e.g. $t = 1, 2, ..., T$). If a Bayesian framework is selected, a third level of equations would be added to include

prior distributions for parameters $\boldsymbol{\theta}$.

1.2 Classical Geostatistics

While SSMs have been used effectively to describe temporal trends (e.g. Linton and Bence, 2008; Yin et al., 2019), the direct inclusion of spatial information is far less common. Recent work in fisheries science has started to emphasize the importance of including spatial information to accurately predict species distribution and abundance (e.g. Ciannelli et al., 2008; Thorson et al., 2015a; Berger et al., 2017). The effect of spatial variation on fish populations has long been acknowledged (e.g. Baranov, 1918; Beverton and Holt, 1957; Legendre, 1993) but rarely directly included in statistical models due to lack of technological and conceptual tools (Goethel et al., 2011). It has only recently been more widely achieved in general population ecology (e.g. Hooten et al., 2003; Gelfand et al., 2005) and even more recently in SSMs (e.g. Thorson et al., 2015c; Cadigan et al., 2017).

Spatial approaches in fisheries science have either borrowed from geostatistics with a focus on the error structure or modified common regression techniques with a focus on the mean effect (Ciannelli et al., 2008). Geostatistical methods are of particular interest since they can be applied to models that do not require plentiful information on environmental covariates such as biomass dynamics models. In other words, given that $y = \mu + \epsilon$ where y is a spatial response with mean μ and error term ϵ, regression approaches will focus on spatially modeling μ while geostatistical methods focuses on spatially modeling ϵ (Ciannelli et al., 2008), which lets the mean be modeled through other approaches such as traditional stock assessment models.

Classical geostatistical approaches, originally from the field of geology (Matheron and Krumbein, 1970), focused on cases where the variable of interest is continuous throughout space with the goal of predicting at unsampled locations through both large-scale and small-scale variations (Zimmerman and Stein, 2010). This is done by assuming that the observations are a sample of a single realization of a continuous stochastic spatial process $Y(\cdot)$, called a random field, where $Y(\cdot) \equiv Y(\mathbf{s}) : \mathbf{s} \in D$ (Zimmerman and Stein, 2010). This leads to the unintuitive fact that, because the observations are only a partial representation of a single realization of this spatial

process $Y(\cdot)$, the sample size for this process is 1. This therefore requires the statistician to include constraints to model this type of process. For example, structure is often imposed so that $Y(\mathbf{s}) = \mu(\mathbf{s}) + e(\mathbf{s})$ where $\mu(\mathbf{s})$ is some mean function and $e(\mathbf{s})$ is a zero-mean random error process (Zimmerman and Stein, 2010).

These approaches, however, require a few assumptions in order to be valid. The first is stationarity, which can be second-order stationarity or intrinsic stationarity (Zimmerman and Stein, 2010). Intrinsic stationarity, more commonly used than second-order stationarity, specifies that:

$$\frac{1}{2}var[e(\mathbf{s}) - e(\mathbf{t})] = \gamma(\mathbf{s} - \mathbf{t}), \ \ for\ all\ \mathbf{s}, \mathbf{t} \in D. \tag{1.5}$$

where $\gamma(\mathbf{s} - \mathbf{t})$ is the semivariogram tracking the covariance between two locations $\mathbf{s}$ and $\mathbf{t}$ (Zimmerman and Stein, 2010). Second-order stationarity is a more stringent assumption, where the semivariogram $\gamma(\cdot)$ is replaced by an unspecified covariance function $C(\cdot)$ (Zimmerman and Stein, 2010). In practice, this approach is usually done by estimating an empirical semivariogram $\gamma(h)$ through the semivariance at all points N separated by distance h:

$$\gamma(h) = \frac{1}{2N(h)} \sum_{i=1}^{N(h)} (x_i - x_{i+h})^2 \tag{1.6}$$

where x_i is some observation i of interest such as fish abundance (Ciannelli et al., 2008). This empirical variogram is then fit to the most appropriate theoretical variogram (e.g. Gaussian, exponential, Matérn) (Ciannelli et al., 2008), after which the estimation of large-scale and small-scale trends can be made (Zimmerman and Stein, 2010).

Another important assumption often made in these models is that of isotropy, either second-order or intrinsic. Intrinsic isotropy implies that the semivariogram $\gamma(h)$ is a function of the locations through the Euclidean distance between them, meaning that direction has no impact on this semivariogram (Zimmerman and Stein, 2010). Second-order isotropy assumes a similar constraint over an unspecified covariance functions. Real life examples, especially in near-shore fisheries (Thorson et al., 2015c), often does not respect this important assumption. A simple modification can be used to account for geometric anisotropy in these cases, wherein a simple positive definite

matrix (analogous to a rotation matrix) can be introduced in the implementation of the covariance structures (Zimmerman and Stein, 2010; Lindgren and Rue, 2011; Thorson et al., 2015c).

1.3 Gaussian Markov Random Fields

Geostatistical methods have since developed into multiple different avenues (e.g. predictive processes in Banerjee et al., 2008), including extensions into spatially discrete cases (Rue and Held, 2010). Of greatest interest here are Markov Random Fields (MRFs) and Gaussian Markov Random Fields (GMRFs). MRFs are a type of random field that are specified by conditioning each component on all the others, with GMRFs being a special case where these conditional distributions are Gaussian (Rue and Held, 2010). This conditional distribution approach further implies that each location is only directly dependent on its set of direct neighbours (Besag, 1974, 1975), which has very convenient computational properties when it comes to covariance structures (Rue and Held, 2010; Lindgren and Rue, 2011). MRFs can be visualized through a graph $\mathscr{G} = (\mathscr{V}, \mathscr{E})$ where $\mathscr{V} = \{1, ..., n\}$ is the set of vertices (e.g. locations of interest) and $\mathscr{E} = \{\{i, j\} : i, j \in \mathscr{E}\}$. Using the example in Figure 1.1, one can see how the value of vertex 1 is conditionally independent of the value of vertex 3 given the values of vertices 2 and 4 ($x_1 \perp x_3 | x_{\{2,4\}}$).

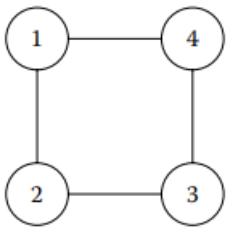

Figure 1.1: Conditional independence graph (taken from Rue and Held, 2010).

GMRFs and, more broadly, Gaussian Fields (GFs) are usually specified through a mean $\boldsymbol{\mu} = \mu(\mathbf{s})$ with mean function $\mu(\cdot)$ and covariance $\boldsymbol{\Sigma} = C(\mathbf{s}_i, \mathbf{s}_j)$ with covariance function $C(\cdot)$ (Lindgren and Rue, 2011). However, it can be very computationally expensive to work with the complete covariance matrix $\boldsymbol{\Sigma}$, and one of the advantages of using GMRFs is the use of the sparse precision matrix $\mathbf{Q} = \boldsymbol{\Sigma}^{-1}$ (Rue and

Held, 2010; Lindgren and Rue, 2011). The zero structure inside this precision matrix is directly analogous to the neighbouring structure of the vertices, meaning that $Q_{ij} \neq 0 \leftrightarrow i \in \delta j \cup j$ where δj is the set of neighbours to location j (Lindgren and Rue, 2011). Furthermore, they can be used to represent underlying GRFs through the Stochastic Partial Differential Equations (SPDE) approach (for more details see Lindgren and Rue, 2011), bridging the gap between continuously defined random fields and discretely defined variables or observations of interest. The modeling approach has therefore recently consisted of assuming an underlying GF, representing it through a GMRF whose precision matrix is very close to the real covariance matrix ($\mathbf{Q}^{-1}$ is close to $\mathbf{\Sigma}$) and modeling on the GRMF discrete locations (Lindgren and Rue, 2011; Carson et al., 2017)

While there are many types of covariance structures that can be specified, this specific approach using GMRFs has been demonstrated to be appropriate when using Matérn covariance structures, which are widely used structures (Lindgren and Rue, 2011). This structure specifies how the correlation between two locations decays over distance in the following way:

$$\mathbf{\Sigma}(s_1, s_2) = \sigma^2 \frac{1}{\Gamma(\nu)2^{\nu-1}} (\kappa d(s_1, s_2))^{\nu} K_{\nu}(\kappa d(s_1, s_2)) \tag{1.7}$$

where $\mathbf{\Sigma}(s_1, s_2)$ is the covariance between two locations, σ^2 is the spatial variance, ν determines smoothness and is often fixed in practical applications (e.g. Thorson et al., 2015c; Carson et al., 2017), κ is the parameter setting the distance at which two locations are effectively uncorrelated, $\Gamma(\cdot)$ is the gamma function, $K(\cdot)$ is the Besel function of the second kind and $d(s_1, s_2)$ is the Euclidean distance between two points ($d(s_1, s_2) = \sqrt{(x_1 - x_2)^2 + (y_1 - y_2)^2}$ with x_i and y_j being coordinates).

One of the advantages of the SPDE approach is that it avoids the need for a regular grid. Instead, the area of interest is subdivided in non-intersecting triangles with vertices where the triangles meet and edges connecting those vertices, with additional vertices usually added to obtain a more useful triangulation (Lindgren and Rue, 2011). An example triangulation can be seen in Figure 1.2.

This approach will represent some underlying GF $X(s)$ by using piece-wise linear

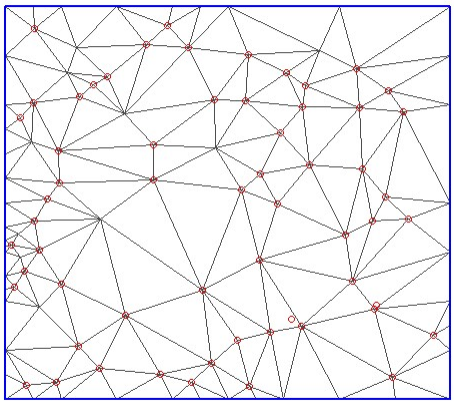

Figure 1.2: Example of a triangulation created for the SPDE approach on randomly simulated locations

interpolation from one vertex to the next in the following way:

$$X(s) = \sum_{i=1}^{n} \psi_i(s)\epsilon_i \tag{1.8}$$

where n is the number of vertices, $\psi_i(s)$ are basis functions that take the value 1 at vertex i and 0 at all other vertices, and ϵ_i are gaussian weights (Carson et al., 2017).

Spatial approaches and geostatistical methods are not particularly new in fisheries science, with known issues created by spatially-aggregated commercial catch (Paloheimo and Dickie, 1964) and by intrinsically spatial life-history characteristics of certain species, such as scallops (Caddy, 1975). Geostatistical approaches have been used sparingly in the past, often on a regular grid (e.g. Petitgas, 1993) or on non-traditional data such as accoustic surveys (e.g. Mello and Rose, 2005), but the widespread interest in spatial statistics applied to stock assessments is relatively recent (Ciannelli et al., 2008). The development of tools for easily and rapidly applying GMRFs within SSMs has recently expanded, from improvements to generalized linear frameworks (Thorson et al., 2015c; Thorson, 2019) to implementations in spatio-temporal state-space models (e.g. Cadigan et al., 2017).

1.4 Computational Approaches

While classical geostatistical approaches using semivariograms do not necessarily make any parametric distributional assumptions, stock assessment methods necessitate the estimation of multiple parameters and the prediction of random effects. SSMs often use Bayesian approaches (e.g. Kinas, 1996; Smith and Hubley, 2014; Best and Punt, 2020). However, issues with the use of prior distributions have recently been identified wherein these distributions can impact posterior distributions in non-intuitive ways, potentially rendering these output unreliable. For example, it can result in erroneous conclusions based on estimated carrying capacity in the absence or fishing (Thorson and Cope, 2017) or can mask identifiability and estimability issues (Yin et al., 2019). The frequentist framework, on the other hand, does not tend to inadvertently mask those issues (Yin et al., 2019). It uses methods where parameters are estimated by maximizing a likelihood function (often through the log-likelihood). In the case of SSMs and given some data $\mathbf{y}$, random effects to be predicted $\mathbf{x}$ and unknown parameters $\boldsymbol{\theta}$, the log-likelihood function $\mathscr{L}(\cdot)$ and the joint log-likelihood of interest (where random effects are integrated out), which are based on likelihood function $L(\cdot)$, resemble the following:

$$\mathscr{L}(\boldsymbol{\theta}|\mathbf{y}) = \sum_{i=1}^{n} log(f(y_i, \boldsymbol{\theta})) \tag{1.9}$$

$$\mathscr{L}(\boldsymbol{\theta}, \mathbf{y}) = log \int L(\boldsymbol{\theta}, \mathbf{y}, \mathbf{x}) d\mathbf{x} \tag{1.10}$$

In the case of complex state-space and spatial models, the integral in equation 1.10 becomes high-dimensional and must be approximated. The Template Model Builder (TMB) package (Kristensen et al., 2016), optimized in the R environment (R Core Team, 2020), is a cutting-edge approach for fitting these complicated SSMs. TMB uses the Laplace approximation to get the marginal likelihood of the parameters $\boldsymbol{\theta}$ in the following way:

$$L(\boldsymbol{\theta}|\mathbf{y}) = \sqrt{2\pi}^{n} det(H(\boldsymbol{\theta}))^{-\frac{1}{2}} exp(-f(\mathbf{y}, \hat{\mathbf{x}}, \boldsymbol{\theta})) \tag{1.11}$$

where $\hat{\mathbf{x}}$ is the optimized value of the random effects $\mathbf{x}$, $H(\cdot)$ is the Hessian matrix evaluated at $\hat{\mathbf{x}}$, and n is the number of random effects (Kristensen et al., 2016). This

approximation has been shown to be appropriate for a myriad of different models, from state-space to non-linear mixed effects, and for the use of GMRFs (Kristensen et al., 2016). TMB has also been shown to be more computationally efficient and faster than other generally available packages due to its use of automatic differentiation to keep track of higher order derivatives (Kristensen et al., 2016; Auger-Méthé et al., 2017). Furthermore, it has shown great success in applications for fisheries and stock assessments (e.g. (Albertsen et al., 2017; Cadigan et al., 2017; Thorson, 2019).

1.5 Case Study

While the importance of incorporating spatial information into SSMs is clear, a concrete setting is necessary to demonstrate the improvements it brings. The work contained in this thesis has been motivated by the sea scallop (*Placopecten magellanicus*) fishery of Nova Scotia, Canada. The second largest fishery in the province in terms of value, it represents a highly important economical driver that has to be managed very carefully to both maximize its economical impact while minimizing the risk of overexploitation. The inshore portion of this fishery has been using a delay-difference model, similar to the version proposed by Schnute (1985), since the early 2000s (Smith and Lundy, 2002), with the following main population dynamics equation:

$$B_t = (e^{-M_{t-1}}(\rho + \frac{\alpha}{\overline{w}_{t-1}})(B_{t-1} - C_{t-1}) + w_k R_t)\mu_t \tag{1.12}$$

where B_t is the biomass in year t, M_t is the natural mortality, $\rho + \frac{\alpha}{\overline{w}_{t-1}}$ is a growth factor that decreases as average size increases (to represent slower growing older populations) where α and ρ are unknown parameters estimated from separate growth data, C_t is the commercial catch, w_k is the weight at recruitment size k, R_t is the number of scallop recruits and μ_t is a log-normal error term (Smith and Lundy, 2002). While there are more modern versions of this model (Smith and Hubley, 2014; Yin et al., 2019), they all follow a similar form.

This fishery, which has been commercially exploited since the early 1960s (Caddy and Chandler, 1968), is an ideal case in which to incorporate spatial information into SSMs. Sea scallops have inherent biological properties that makes them very intuitive

for spatial modeling. Their aggregation behaviors, their recurring colonization of specific areas (called scallop beds) and their minimal dispersal and movement as adults (Smith and Rago, 2004) are all inherently spatial characteristics that can intuitively be modeled through the implementation of spatial statistics in SSMs. Strong spatial patterns have also been acknowledged in this specific fishery for a long time (Caddy, 1975; Smith and Rago, 2004). Furthermore, many subareas are also known to have highly aggregated commercial fishing (Nasmith et al., 2016; Smith et al., 2017), which has long been known to impact the quality of predictions and estimates from strictly temporal models (Baranov, 1918; Caddy, 1975). These spatial patterns have historically not been incorporated in models due to lack of available data (Smith and Rago, 2004). However, this has recently changed, with the implementation of a mandatory satellite Vessel Monitoring System (VMS) for all vessels since 2002 (Smith et al., 2012, 2017). Furthermore, a strong link between habitat suitability and fishing intensity has been identified, with serious implications for population productivity and long-term sustainability if not incorporated in the stock assessment (Smith et al., 2017).

The latest work undertaken on the SSM for the inshore Nova Scotia scallop fishery focused on identifying and solving identifiability issues related to the Bayesian framework currently in use (Yin et al., 2019). This work demonstrated that even non-informative priors can sometimes overwhelm the information in the data, especially when the sample size is very low, which can result in unreliable estimates and predictions. Focused on the Scallop Production Area (SPA) 4 in the Bay of Fundy, an alternative frequentist framework added new process equations and modeled the commercial catch directly to overcome these issues (Yin et al., 2019). Attempts to apply this alternative approach, part of this body of work, to a more difficult and variable area, SPA 3, were unfortunately unsuccessful due to problems in estimating variance parameters. This area and neighboring areas are known to have highly aggregated commercial fishing (Nasmith et al., 2016; Smith et al., 2017) and strong spatial patterns in biomass and mortality. This motivated the development of new approaches that could explicitly model the unused information already present in the data, both strictly temporally and spatio-temporally.

1.6 Thesis Outline

This thesis aims to integrate spatial information available about a fishery into pre-existing SSMs to improve the predictive ability and resolution of those predictions of this model with the broad goal of accurately estimating the current status of the SPA 3 sea scallop stock. Chapter 1 presented the relevant background information, theoretical approaches and computational methods necessary for the subsequent chapters. Chapter 2 and 3 are constructed as manuscripts for publication. Chapter 2 concerns the expansion of a temporal state-space model developed by Yin et al. (2019) to account for the intra-annual variability obtained by fishery-independent surveys, avoiding the need to use a single data point per year as has been done in many biomass dynamics models (Nasmith et al., 2016). Simulation experiments will be utilized to test model performance before being tested on a real setting as a case study, utilizing data from SPA 3 in the Inshore Scallop Fishery in Nova Scotia, Canada (Nasmith et al., 2016). While not incorporating any spatial information, these developments were necessary before the application of the spatial methods described in Chapter 1. Chapter 3 will further develop this state-space model to directly incorporate the spatial locations of both survey tows and commercial fleet catches into a stock assessment framework with the ultimate objective of predicting the spatial distribution and abundance of scallop biomass in SPA 3. Simulation experiments will also be used to test model performance before being applied to the SPA 3 data. Further simulation experiments will be run wherein data will be simulated from a spatial model before fitting the temporal model described in Chapter 2 to test the effect of the spatial aggregation of commercial catch. Chapter 4 will present the important conclusion from this body of work before expanding into future work and application of these approaches.

Chapter 2

Diagnosing and solving identifiability issues related to fisheries abundance indices in the Assessment of the Nova Scotia Inshore Sea Scallop *Placopecten magellanicus* Fishery

Abstract

Biomass dynamics stock assessment models have seen widespread use in fisheries science. Often implemented in a state-space framework, these models tend to rely solely on indices of abundance and commercial landings data. Much effort has gone into improving the reliability of abundance indices, either from fishery-dependent or independent sources. However, standard practice often still involves simply taking mean values over large temporal and spatial ranges. This reduces the ability of biomass dynamics models, including delay-difference models, to accurately track changes in populations. We explore these issues with the stock assessment model used for the Nova Scotia Inshore Scallop Fishery, which calculates its abundance indices based on annual fishery-independent surveys. Using a state-space stock assessment model based upon a delay-difference model, our proposed approach treats each individual survey tow as an independent realization of the true underlying biomass. Given the abundance of zeroes in these tows, a delta model is incorporated. Results from fitting this approach to a highly variable sea scallop production area in and around St-Mary's Bay, Nova Scotia shows significant improvement in the estimation of variance parameters over previous model implementations. This increases the reliability of the patterns predicted by the stock assessment, can easily be generalized to other stock assessment frameworks, and is the first step to developing a fully spatio-temporal model for this area.

2.1 Introduction

Fisheries stock assessment has long used deterministic and statistical models to quantify and predict variation in fish populations, often with the goal of providing reliable information for the purpose of fisheries management. Since many fisheries set quotas or use other forms of regulation to ensure their long-term viability, the scientific advice they receive must be as accurate and precise as possible to minimize the risk of overexploitation. The collapse of Atlantic cod (*Gadus morhua*) in Eastern Canada (Hutchings and Myers, 1994; Myers et al., 1996) had severe social and economic consequences on the Maritime provinces, which underlined the importance of developing accurate and reliable stock assessment models. A key part of modern stock assessment is the ability to account for multiple sources of uncertainty (e.g. Schnute and Richards, 1995; Aeberhard et al., 2018).

State-space models (SSMs) have become increasingly popular for incorporating multiple sources of uncertainty into a unified framework. SSMs are able to account for both measurement errors, which occur in the observation of data, and process errors, which come from the imperfect knowledge of the underlying dynamical processes of interest (De Valpine, 2002; Cressie et al., 2009; Aeberhard et al., 2018). These models can be built to account for noisy data (e.g. Punt et al., 2000), complex non-linear population dynamics (e.g. Froese, 2006; Linton and Bence, 2008) or non-Gaussian distributions (e.g. Martin et al., 2005; Cressie et al., 2009), all of which are common with fisheries data. Estimation frameworks for SSMs, traditionally difficult to fit in practice, have only recently become easily accessible through innovations facilitating the approximation of intractable integrals. Multiple approaches have been developed, such as Bayesian methods usually involving the use of Markov Chain Monte Carlo (MCMC) (Meyer and Millar, 1999; Linton and Bence, 2008; Smith and Hubley, 2014), and frequentist methods involving the use of automatic differentiation and the Laplace approximation (Skaug and Fournier, 2006; Kristensen et al., 2016). Both approaches have been used extensively when incorporating traditional stock assessment models, such as biomass dynamics models, into SSM frameworks.

Biomass dynamics models are historically one of the three most important types of models available to fisheries scientists (Hilborn, 1992). Requiring only an index of

population abundance and commercial landings, their implementation in SSM frameworks has led to their widespread applicability to modern stock assessment (e.g. Smith and Hubley, 2014; Xu et al., 2019; Best and Punt, 2020). A common example is the delay-difference model, derived as a compromise between intractable realistically complex models and overly simplistic models (Deriso, 1980; Schnute, 1985). Since biomass dynamics models only require two inputs, it is imperative that these inputs be reliable. This is especially the case for abundance indices, which often require extensive data processing before being considered suitable for modeling purposes.

An index of abundance can be calculated from two different sources: fishery-dependent (e.g. commercial landings, fishing logbooks, etc.) or fishery-independent (e.g. surveys). A significant amount of work has gone into developing better methods to obtain reliable indices from fishery-dependent sources (Harley et al., 2001; Maunder and Punt, 2004; Maunder et al., 2006), but even indices calculated from more reliable fishery-independent sources usually result in a single datum per year. Even if that may be enough for some SSMs, situations where time-series are relatively short can lead to overparameterization and identifiability issues (e.g. Yin et al., 2019). While Bayesian methods have been highly popular for fitting stock assessment SSMs (e.g. Best and Punt, 2020), they sometimes simply mask these issues (Thorson and Cope, 2017; Yin et al., 2019). Modeling these data directly requires dealing with the complications inherent to fisheries data, such as zero-inflation.

Zero-inflation occurs when a dataset includes a large proportion of zeroes which cannot be accurately represented by standard distributions (e.g. Gaussian, Poisson, etc.) (Martin et al., 2005). Ignoring these zeroes can lead to bias in parameter estimates and negatively impact the resulting inference (e.g. Mackenzie et al., 2002). These zeroes can either be "true" zeroes, which would be a real representation of the underlying process, or "false" zeroes, when they stem from the observation process itself (Martin et al., 2005). Using the example of fisheries survey data, "true" zeroes could come from fishing in an area without the species of interest, and "false" zeroes could be because the animals managed to escape the fishing gear but were indeed present. The delta approach has shown great success accounting for this zero-inflation. This approach models the probability of a zero separately as p, often through a binomial distribution, and the probability of a positive observation as $1 - p$ (Fletcher

et al., 2005). Used extensively for both standard regression frameworks (e.g. Fletcher et al., 2005) and spatial approaches (e.g. Thorson et al., 2015c), the delta approach is readily applicable to the SSM framework.

This work aims to demonstrate how to incorporate survey abundance data directly into SSMs to increase the reliability of parameter estimation with the broad goal of reliably estimating the current status of the stock of interest. The model presented in Yin et al. (2019) is modified here to incorporate each individual survey observation directly (instead of a single index of abundance per year) while explicitly accounting for both the variability and zero-inflation present in these data. We view this approach as a hybrid between a traditional biomass dynamics model and a fully spatio-temporal model. This framework is vetted using the Nova Scotia Inshore sea scallop (*Placopecten magellanicus*) fishery as a case study.

The Nova Scotia Inshore sea scallop fishery is the fourth most important fishery in the province, worth millions of dollars in revenue each year. Fisheries and Oceans Canada (DFO) has conducted surveys since the 1980s and currently sets annual quotas to manage the exploitation of this species (Nasmith et al., 2016). For this fishery, DFO uses a simplified version of the delay-difference model (Deriso, 1980; Schnute, 1985), originally presented in Smith and Lundy (2002) and more recently described in Nasmith et al. (2016). Identifiability issues masked by a Bayesian framework were recently diagnosed, and a modified alternative frequentist version was proposed to help solve many of these issues (Yin et al., 2019). However, while this SSM framework worked well for the Scallop Production Area 4 (SPA 4, labeled by DFO) in the Bay of Fundy, it struggled to reliably assess the population of sea scallops in the more highly variable Area 3 (SPA 3), located in and around St-Mary's Bay. In later sections we show that, while it successfully converged, this model could not reliably estimate certain variance and catchability parameters. It is likely that strong spatial patterns in population dynamics, habitat suitability and fishing effort (Caddy, 1975; Smith et al., 2017) in SPA 3 are the culprit. Due to the increased difficulty in assessing SPA 3, DFO restratified the area based on the locations of fishing vessels using a Vessel Monitoring System (VMS) (Nasmith et al., 2016). The three resulting strata are defined as St-Mary's Bay, the Inside VMS stratum and the Outside VMS stratum (seen in Nasmith et al., 2016), of which only St-Mary's Bay and the Inside VMS are

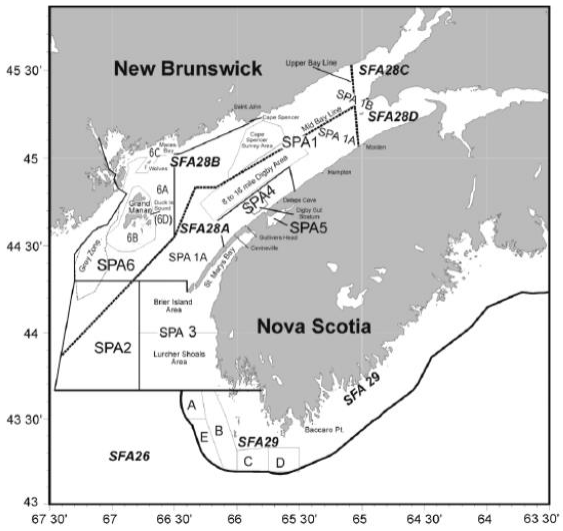

Figure 2.1: Map of Scallop Production Areas (SPA) and Scallop Fishing Areas (SFA) in Bay of Fundy and surroundings (taken from Nasmith et al., 2016). SPAs and SFAs are regulated differently, hence the difference in labeling.

modeled. This motivated the development of our new model formulation to better harness existing data and more reliably capture the trends in biomass in SPA 3, with the ultimate goal of later expanding it into a fully spatio-temporal stock assessment model.

Section 2.2 describes the specific characteristics of the sea scallop data from SPA 3. It also contains descriptions of the 3 models of interest here: the original Bayesian model presented in Nasmith et al. (2016), the alternative frequentist model presented in Yin et al. (2019), and our novel approach treating each survey tow as a separate observation. Section 2.3 presents the result of a simulation study to assess the reliability and identifiability properties of our new approach. All 3 models are fitted to SPA 3 in Section 2.4. Finally, Section 2.5 discusses our important findings.

2.2 Model and Data Descriptions

2.2.1 Data Description

SPA 3, shown in Figure 2.1, is surveyed annually using a stratified random sampling design with partial replacement (Nasmith et al., 2016). Two types of survey drag are used, either with a lined mesh of 38mm (with the goal of capturing recruit-sized scallops) or without. Every live scallop and clapper (dead scallop whose shell is still

attached by a hinge) is counted and binned by size (5mm bins), with commercial size scallops defined as having shell heights larger than 80mm, recruits defined as those between 65mm and 79mm, and everything smaller deemed pre-recruits. A subset of live scallops (3 per 5mm bins that are 50mm and larger) are set aside in order to record their individual shell height, their meat weight (weight of the adductor muscle) and their age so as to obtain a yearly shell height to meat weight relation. Although DFO typically incorporates the condition of the scallop into this relationship (Nasmith et al., 2016), a simplified approach was used here where:

$$w_i = Ah_i^3 d_i^\beta \epsilon_i, \quad \epsilon_i \overset{Ind}{\sim} u\ell N(\sigma_\epsilon^2) \tag{2.1}$$

where w_i is the meat weight of scallop i, A is the intercept parameter on the log-scale, h_i is the shell height of scallop i, d_i is the depth where it was caught with associated slope parameter β on the log-scale, and ϵ_i is a log-normally distributed error term. This model follows a simple cube law (Froese, 2006) and is fitted separately for each year. Once the parameters A and β are estimated, the equation is applied deterministically (i.e. without error) to the live scallops using the size bin midpoints to predict the meat weight for all scallops in each tow.

The commercial size biomass survey index is typically obtained by summing up the the predicted biomass of the shells 80mm or larger from the unlined gear (7 drags out of 9 in each tow). The same process is done for scallops between 65mm and 79.9mm from the lined gear (2 drags out of 9) to obtain a recruitment biomass survey index. The mean is then taken across all tows in a stratum and these are then scaled up to their respective strata by multiplying this mean value by the number of towable units (number of tows that would be necessary to cover the whole area) in this stratum. The approach taken for the DFO model and the one described by Yin et al. (2019) only models the St-Mary's Bay and the Inside VMS strata. The clapper and live scallop index is obtained by taking the scaled up mean number of clappers or live scallops per stratum.

For our novel approach, we instead consider each individual survey tow as a separate observation of the true underlying processes. Only the data from the St-Mary's Bay and Inside VMS strata are taken, but they are treated as if from a single stratum in this case. For the biomass and recruitment processes, the number of towable

units is first computed. Each observed commercial size and recruit biomass is then multiplied by this number of towable units. In this way, each individual tow can be thought of as a replicate of the traditional single index of abundance. We do not modify the number of clappers and live scallops caught in each tow.

The last data inputs required are commercial landings. There are two different commercial catch time series used here. The commercial catch used to fit the Bayesian model are simply the official landings in a given fishing year, since this is the approach currently taken by DFO. However, since the surveys tend to be done between June and August but the fishing period is from October to September (Nasmith et al., 2016), the commercial catch needs to be temporally aligned so that landings are appropriately attributed to each survey year (e.g. fishing done in September 2015 is taken out after 2015 survey). This was done for both frequentist models from fishing logbooks obtained from DFO. Due to a mismatch between the yearly sums of the logbook catches and the official landings, which are considered highly reliable, this difference is also proportionally added to the commercial catches in a given survey year. Visualizations of all these data inputs can be seen in Appendix A.

2.2.2 Model Descriptions

State-space models (SSMs) are hierarchical models defined by two stochastic processes: $\mathbf{X}_t$, $t = 1, ..., T$, representing the unobserved dynamic state process describing real population dynamics between discrete time-steps t, and $\mathbf{Y}_t$, which are the observations linked to the true underlying dynamical processes of interest (Aeberhard et al., 2018). All models of interest for this study follow the state-space hierarchical approach, with the model described in Nasmith et al. (2016) referred to as the Bayesian model (BM), the model described in Yin et al. (2019) referred to as Frequentist Model A (FMA) and the novel model described here referred to as Frequentist Model B (FMB). For all, the unobserved states are labeled in $\mathbf{X}_t$, and the observed states are labeled $\mathbf{Y}_t$, the model parameters are combined in a p-vector $\theta \in \Theta \subseteq \mathbb{R}^p$, while fixed covariates are indicated by $\mathbf{z}_t$.

BM

The implementation of a Bayesian approach allows the scientist to include prior knowledge (such as expert opinion, biological knowledge, historical experience, etc.) into any statistical analysis or modeling exercise (Meyer and Millar, 1999) through prior distributions $\pi(\boldsymbol{\theta})$. This is done by using observed data $\mathbf{Y}_{1:T}$, unobserved variables $\mathbf{X}_{1:T}$, and $\boldsymbol{\theta}$ to set up the joint density $p(\mathbf{Y}_{1:T}, \mathbf{X}_{1:T}, \boldsymbol{\theta})$. Since only the data are observed, the unobserved variables are conditioned on the observations to obtain the posterior distribution from which conclusions can be drawn (Meyer and Millar, 1999). In this case, the posterior distribution is the following (using notation borrowed from Yin et al., 2019):

$$p(\boldsymbol{\theta}, \mathbf{X}_{1:T}|\mathbf{Y}_{1:T}) = \frac{p(\boldsymbol{\theta}, \mathbf{Y}_{1:T}, \mathbf{X}_{1:T})}{\int\int p(\boldsymbol{\theta}, \mathbf{Y}_{1:T}, \mathbf{X}_{1:T}) d\mathbf{X}_{1:T} d\boldsymbol{\theta}} \tag{2.2}$$

A Markov Chain Monte Carlo (MCMC) algorithm, whose goal is to sample from the posterior distribution for the purpose of inference (Best and Punt, 2020), is used to fit the model in R using the WinBUGS package (Lunn et al., 2000). This approach used a Gibbs Sampling method wherein a sample can be simulated from the posterior distribution without knowing what it is, meaning that with enough simulations one can calculate any characteristic of this distribution or any of its components to a desired accuracy (Casella et al., 1992).

The first level of the hierarchical framework includes the following equations linking observed $\mathbf{Y}_t$ to unobserved states $\mathbf{X}_t$:

$$I_t = qB_t\epsilon_t, \quad \epsilon_t \overset{Ind}{\sim} u\ell N(\sigma^2_{\epsilon,t}) \tag{2.3}$$

$$I^R_t = qr_tR_t\upsilon_t, \quad \upsilon_t \overset{Ind}{\sim} u\ell N(\sigma^2_{\upsilon,t}) \tag{2.4}$$

$$L_t = m_tS(\frac{S}{2}N_{t-1} + (1 - \frac{S}{2}N_t))\kappa_t, \quad \kappa_t \overset{Ind}{\sim} u\ell N(\sigma^2_{\kappa}) \tag{2.5}$$

$u\ell N(\sigma^2)$ denotes a log-normal distribution with unit mean on the natural scale ($\mu_l = -0.5\sigma^2$ on the log scale) and variance σ^2 on the log scale. Equation 2.3 links the survey commercial size biomass index (mean biomass per tow scaled up to modeled area) I_t to the underlying biomass B_t, scaled by a catchability parameter q, and with

a multiplicative error term ϵ_t and its associated log-normal variance $\sigma^2_{\epsilon,t}$. Equation 2.4 links the recruit commercial size biomass index I^R_t to the underlying recruit biomass R_t, scaled by the same catchability parameter q modified by the ratio of lined to unlined gear r_t, and with a multiplicative error term υ_t and its associated log-normal variance $\sigma^2_{\upsilon,t}$. q and variances $\sigma^2_{\epsilon,t}$, $\sigma^2_{\upsilon,t}$ and σ^2_κ are parameters estimated from the data, although $\sigma^2_{\epsilon,t}$ and $\sigma^2_{\upsilon,t}$ are only allowed to vary through time due to the availability of survey coefficients of variations (CVs) used in the prior distributions (Yin et al., 2019).

Equation 2.5, called the "popcorn" model (Smith and Lundy, 2002), links the number of clappers (dead scallops with hinges still attached) L_t to the number of live scallops N_t and natural mortality m_t using parameter S, which represents the average hinge separation time in years for a clapper (known as dissolution rate). This assumes a fixed lifespan for clappers and that hinges for clappers of the same age dissolve in a short time-span.

The second hierarchical level models the population dynamics the following way:

$$\frac{B_t}{K} = [e^{-m_t} g_{t-1} \frac{B_{t-1} - C_{t-1}}{K} + e^{-m_t} g^R_{t-1} \frac{R_{t-1}}{K}]\tau_t \tag{2.6}$$

Here, $\tau_t \overset{Ind}{\sim} u\ell N(\sigma^2_\tau)\mathbf{1}_{[0,8]}$ for $t = 2, ..., T$. Equation 2.6 moves the biomass B_t from one year to the next after removing the commercial catch C_t, removing those that died from natural mortality m_t, and growing the surviving scallop biomass by growth scalar g_{t-1}. The natural mortality is afterwards applied to the recruitment biomass R_t, which is then grown by recruit growth scalar g^R_{t-1} and added to the biomass to obtain the final value, which is then associated with error term τ_t and its associated log-normal variance σ^2_τ. Both scaling constant K and $\mathbf{1}_{[a,b]}$, an indicator function indicating censoring within the interval $[a, b]$, are present for numerical stability and convergence reasons (Yin et al., 2019). The growth scalars g_t and g^R_t are assumed known and are estimated through separate work done by DFO and unreported here. Equation 2.6 is a simplified version of the delay-difference model shown in (Hilborn, 1992, p.335). The biomass in year 1 is specified as $B_1/K \sim u\ell N(\sigma^2_\tau)$. K and σ^2_τ are both estimated parameters.

There are no underlying process equations for recruitment R_t and natural mortality m_t. Instead, both the ratio R_t/K and m_t are assumed to independently and

identically distributed (i.i.d.) following log-normal distributions with mean -1.9 and variance 2 on the natural logarithm scale. A third hierarchical level is included to use the Bayesian framework wherein prior distributions $\pi(\boldsymbol{\theta})$ are specified.

In summary, BM contains the observed states $\mathbf{Y}_t = (I_t, I_t^R, L_t)^T$, the unobserved states $\mathbf{X}_t = (B_t, R_t, m_t)^T$, the fixed covariates $\mathbf{z}_t = (N_t, C_t, g_t, g_t^R, r_t, CV_{\epsilon,t}, CV_{\upsilon,t})^T$ and the parameters $\boldsymbol{\theta} = (K, q, S, \sigma^2_{\epsilon,t}, \sigma^2_{\upsilon,t}, \sigma^2_{\kappa}, \sigma^2_{\tau})^T$. Identifiability issues have been identified for BM, wherein priors intended to be non-informative had a strong impact on the model output, which motivated its reformulation using a frequentist perspective (Yin et al., 2019).

Frequentist Approaches

A frequentist perspective was proposed as an alternative (Yin et al., 2019) wherein $\boldsymbol{\theta}$ is considered a vector of fixed effects and $\mathbf{X}_{1:T}$ a vector of random effects predicted from estimates of $\boldsymbol{\theta}$. These variables can be combined into the following joint likelihood and marginal log-likelihood:

$$L(\boldsymbol{\theta}, \mathbf{Y}_{1:T}, \mathbf{X}_{1:T}) = p(\mathbf{Y}_1|\mathbf{X}_1, \boldsymbol{\theta}) \prod_{t=2}^{T} p(\mathbf{Y}_t|\mathbf{X}_t, \boldsymbol{\theta}) p(\mathbf{X}_t|\mathbf{X}_{t-1}, \boldsymbol{\theta}) \tag{2.7}$$

$$\mathscr{L}(\boldsymbol{\theta}, \mathbf{Y}_{1:T}) = log \int L(\boldsymbol{\theta}, \mathbf{Y}_{1:T}, \mathbf{X}_{1:T}) d\mathbf{X}_{1:T} \tag{2.8}$$

The approximation for these high-dimensional integral is done using the Laplace method using the TMB package in R (Kristensen et al., 2016). Aside from consistency, TMB's use of Automatic Differentiation, which keeps track of higher order derivatives for all modeled functions, has been shown to be computationally more efficient than most other packages without losing accuracy (Kristensen et al., 2016; Auger-Méthé et al., 2017).

FMA

The original goal for FMA was to be fully identifiable without the use of Bayesian priors or constraints between parameters while staying as close as possible to BM (Yin et al., 2019). FMA is reproduced here with the exception of the commercial catch equation for a few reasons. First, to preserve a higher degree of similarity with

BM. Furthermore, one of the commercial catch parameters had a proportionally large standard error associated with it (Yin et al., 2019) and preliminary analyses of SPA 3 using FMA showed no improvement in model fit when using the catch equation than without. Finally, the landings are considered highly reliable in this area (Nasmith et al., 2016), so the necessity of modeling the catch was not clear. Commercial catch is therefore not explicitly modeled here.

The first level of the hierarchical framework of FMA includes the following equations linking observed $\mathbf{Y}_t$ to unobserved states $\mathbf{X}_t$:

$$I_t = q_I B_t \epsilon_t, \quad \epsilon_t \overset{Ind}{\sim} u\ell N(\sigma_\epsilon^2) \tag{2.9}$$

$$I_t^R = q_R R_t \upsilon_t, \quad \upsilon_t \overset{Ind}{\sim} u\ell N(\sigma_\upsilon^2) \tag{2.10}$$

$$L_t = m_t S(\frac{S}{2} N_{t-1} + (1 - \frac{S}{2} N_t))\kappa_t, \quad \kappa_t \overset{Ind}{\sim} u\ell N(\sigma_\kappa^2) \tag{2.11}$$

Equations 2.9 and 2.10 are almost the same as Equations 2.3 and 2.4. The only differences are that commercial size biomass and recruit biomass have separate catchability parameters q_I and q_R and their variances are not allowed to vary across time. This last modification was introduced to reduce the number of parameters that needed to be estimated in a frequentist framework (Yin et al., 2019). Equation 2.11 is unmodified from Equation 2.5. For year 1, since there is no N_{t-1}, Equation 2.11 is simplified to $L_1 = m_1 S N_1 \kappa_1$.

The second level of the hierarchical structure includes the following equations that model the population dynamics:

$$B_t = [e^{-m_t} g_{t-1}(B_{t-1} - C_{t-1}) + e^{-m_t} g_{t-1}^R R_{t-1}]\tau_t \tag{2.12}$$

$$R_t = R_{t-1}\phi_t, \quad \phi_t \overset{Ind}{\sim} u\ell N(\sigma_\phi^2) \tag{2.13}$$

$$m_t = m_{t-1}\eta_t, \quad \eta_t \overset{Ind}{\sim} u\ell N(\sigma_\eta^2) \tag{2.14}$$

Aside from the removal of scaling constant K, Equation 2.12 is identical to Equation 2.6. The largest modifications is the addition of process equations for recruitment

and natural mortality. Equation 2.13 and 2.14 move the recruitment biomass and the natural mortality through time with a simple random walk through the error terms ϕ_t and η_t and their associated constant log-normal variances σ^2_ϕ and σ^2_η. Although not designed to capture realistic dynamics of these processes, they include some temporal dependency while minimizing the number of new parameters to estimate and were considered adequate for this purpose (Yin et al., 2019). While log-normal random walks, which are geometric random walks, will decrease over long periods of time (Lewontin and Cohen, 1969), this was not thought to be an issue since the data should overcome these prior assumptions. No distributions were assumed for the initial states for all 3 processes (B_1, R_1 and m_1) and were all left free to be predicted from the data.

In summary, FMA contains the observed states $\mathbf{Y}_t = (I_t, I^R_t, L_t)^T$, the unobserved states $\mathbf{X}_t = (B_t, R_t, m_t)^T$, the fixed covariates $\mathbf{z}_t = (N_t, C_t, g_t, g^R_t)^T$ and the parameters $\boldsymbol{\theta} = (q_I, q_R, S, \sigma^2_\epsilon, \sigma^2_\upsilon, \sigma^2_\kappa, \sigma^2_\tau, \sigma^2_\phi, \sigma^2_\eta)^T$.

FMB

Preliminary analyses using FMA on the SPA 3 dataset identified issues related to the estimation of variance and catchability parameters, which prompted the development of a new approach. The simplest fix concerned the problematic use of a single data point per year described earlier. Problems with variance estimation and simulations done for FMA (Yin et al., 2019) indicated that the model was likely struggling due to the short length of the time-series. An approach that could account for every observations should be able to solve these issues.

Some survey tows caught no scallops at all, which led to zero-inflation issues during preliminary analyses. A delta approach was therefore implemented to account for this. While it does not separate "true" and "false" zeroes like other zero-inflated models do, the output would be exactly identical since this portion is essentially an intercept-only model (Thorson, 2018). This simply means that the observation stage of this state-space model is split into 2 components: predicting the probability of catching scallops, then linking the positive catches to the underlying biomass.

Therefore, the first part of the hierarchical structure is split into two, with the first equations modeling the survey positive catch probabilities for commercial size

and recruit biomass:

$$P_t^I \overset{Ind}{\sim} Bin(n_t^{tows}, p_I) \tag{2.15}$$

$$P_t^R \overset{Ind}{\sim} Bin(n_t^{tows}, p_I^R) \tag{2.16}$$

Here, both p_I and p_I^R are probabilities estimated using a binomial distribution where P_t^I is the number of tows with positive commercial size catches and P_t^R is the number of tows with positive recruit catches. They are both assumed independently distributed based on the number of tows n_t^{tows} in each year t for $t = 1, ..., T$. The probabilities are also defined as $P(I_t > 0) = p_I$ and $P(I_t^R > 0) = p_I^R$ and represent the probability of a positive survey catch for commercial and recruit biomass respectively. Once this step is taken, the modified observation equations are the following:

$$I_{i,t} = q_I B_t^\star \epsilon_{i,t}, \quad \epsilon_{i,t} \overset{Ind}{\sim} u\ell N(\sigma_\epsilon^2) \tag{2.17}$$

$$I_{i,t}^R = q_R R_t^\star \upsilon_{i,t}, \quad \upsilon_{i,t} \overset{Ind}{\sim} u\ell N(\sigma_\upsilon^2) \tag{2.18}$$

$$L_{i,t} \overset{Ind}{\sim} Bin(L_{i,t} + N_{i,t}, m_t S) \tag{2.19}$$

Equation 2.17 is very close to Equation 2.9 with a few additions. Instead of having a single data point for each year $t = 1, ..., T$, each observed commercial size biomass $I_{i,t}$ in each tow i in year t is treated as an independent representation of the underlying biomass $B_t^\star$ with constant catchability q_I and log-normal errors $\epsilon_{i,t}$ with a constant variance of σ_ϵ^2. $B_t^\star$ is not the true underlying biomass, rather it is the predicted biomass if $p_I = 1$, meaning that it represents the biomass if every survey tow had positive catches. Equation 2.18 is modified the same way relative to equation 2.10 where each individual survey observation for recruitment $I_{i,t}^R$ linked to recruitment biomass $R_t^\star$ if $p_R = 1$, with catchability q_R and log-normal error terms $\upsilon_{i,t}$ and associated variance σ_υ^2.

Equation 2.11 has been dramatically simplified. Although conceptually interesting, the "popcorn" model is not easy to fit and hard to generalize. A much simpler approach was taken instead, where it is assumed that the proportion $m_t S$ is bounded

Table 2.1: Parameters for all 3 models with description.

Parameter	Model	Description
K	BM	Scaling constant
q	BM	Catchability
q_I	FMA, FMB	Commercial Size Catchability
q_R	FMA, FMB	Recruit Size Catchability
S	BM, FMA, FMB	Clapper hinge dissolution rate (BM, FMA)/Clapper catchability (FMB)
σ_τ	BM, FMA, FMB	Commercial size biomass process error
σ_ϕ	FMA, FMB	Recruitment process error
σ_η	FMA, FMB	Natural mortality process error
σ_ϵ	FMA, FMB	Commercial size index observation error
σ_υ	FMA, FMB	Recruitment index observation error
σ_κ	BM, FMA	Clapper index observation error
p_I	FMB	Probability of positive commercial size survey tow
p_I^R	FMB	Probability of positive recruit survey tow

between 0 and 1. This means that each individual shell in a tow i in year t can be seen as having the same probability $m_t S$ of being a clapper $L_{i,t}$ with the total number of shells caught being the number of clappers plus the number of live scallops $N_{i,t}$. The parameter S, instead of representing hinge dissolution rate, becomes akin to a catchability parameter specific to clappers.

Since $B_t^\star$ and $R_t^\star$ do not account for zeroes, the real underlying biomass and recruitment is obtained using the estimated probability of capturing scallops:

$$B_t^\star = p_I B_t \tag{2.20}$$

$$R_t^\star = p_I^R R_t \tag{2.21}$$

Here, B_t is the real underlying biomass in year t while R_t is the real underlying recruitment after accounting for probability of zeroes. The process equations for this model are identical to Equations 2.12 to 2.14, so they are not reported again.

In summary, FMB contains the observed states $\mathbf{Y}_t = (I_{i,t}, I_{i,t}^R, L_{i,t})^T$, the unobserved states $\mathbf{X}_t = (B_t, R_t, m_t)^T$, the fixed covariates $\mathbf{z}_t = (N_{i,t}, C_t, g_t, g_t^R)^T$ and the parameters $\boldsymbol{\theta} = (p_I, p_I^R, q_I, q_R, S, \sigma_\epsilon^2, \sigma_\upsilon^2, \sigma_\tau^2, \sigma_\phi^2, \sigma_\eta^2)^T$. Table 2.1 shows all parameters used in all models and their descriptions.

Table 2.2: Difference between setups for each experiment.

Experiment	Status of q_I	Time-Series Length
1	Estimated	22 Years
2	Fixed	22 Years
3	Estimated	50 Years
4	Fixed	50 Years

2.3 Simulation Study

Four simulation experiments were done to assess the estimability and identifiability of the proposed FMB with the focus on parameter estimation and random effects prediction. The simulation design is inspired by that presented in Yin et al. (2019). Both data simulation and model fit is done using TMB. Preliminary analyses identified q_I as one of the most difficult parameter to reliably estimate. Due to this, the first experiment estimated q_I normally while the second fixed it at the simulated real value. The motivation for this was to identify how much improvement would be gained by fixing this parameter, given that it was fixed to the correct value. These first two experiments simulated data of the same time length as the SPA 3 data at 22 years. The last two experiments replicated the design and approach of the first two but extended the simulated time series to 50 years.

2.3.1 Simulation Design

Equations 2.12 to 2.21 were used to simulate $\mathbf{Y}_{1:T}$ and $\mathbf{X}_{1:T}$ 1000 times. Fixed covariates $\mathbf{z}_t$ needed to be directly specified. Since the growth rates g_t and g_t^R are fixed, they are made constant and set at 1.1 and 1.5 for simplicity's sake. Other elements that are necessary but cannot be simulated through equations are the following: the number of tows n_t^{tows} is set to 100 every year, the total number of live and dead scallops caught $(L_{i,t} + N_{i,t})$ is also set to 100 in every tow. This last element needs to be simulated separately because, as was done for N_t in Yin et al. (2019), the number of shell caught is not a response but is part of fixed covariates $\mathbf{z}_t$, and is essential to fitting a binomial distribution. The initial states for the processes are set to the following: B_0 is set to 1000 metric tons, R_0 is set to 100 metric tons and m_0 is set at 0.1.

Table 2.3: Parameters used for simulation experiment and their respective optimization starting values.

Parameter	True Value	Starting Value
σ_τ	0.1	$exp(-1)$
σ_ϕ	0.1	$exp(-1)$
σ_η	0.1	$exp(-1)$
σ_ϵ	0.1	$exp(-1)$
σ_υ	0.1	$exp(-1)$
q_I	0.3	$exp(-1)$
q_R	0.1	$exp(-1)$
S	0.2	$exp(-1)$
p_I	0.8	0.5
p_I^R	0.4	0.5

Since the commercial catch is not modeled, it was therefore set as a log-normal distribution with a mean of 20% of B_t for every year with a variance of 0.1 on the log scale. Simulating the commercial catch as a direct proportion of the biomass was chosen to avoid the possibility of simulating negative biomass, which is a common issue in this type of models (Yin et al., 2019; Best and Punt, 2020).

The true values for the parameters $\boldsymbol{\theta}$ and their optimization starting values can be seen in Table 2.3. Optimization starting values for the random effects, chosen to be much larger than realistically expected, are 2000 metric tons for B_t, 200 metric tons for R_t and 0.3 for m_t. The maximization of the likelihood was done using the quasi-Newton optimizer *nlminb* in R. The design for the simulations where q_I is fixed at 0.3 are identical aside from the obvious change.

2.3.2 Simulation Results

For all 4 experiments, all simulations converged. However, quite a few did not succeed in reliably estimating certain parameters (q_I, q_R and S). These would be estimated at nonsensical values with standard errors that were orders of magnitudes larger than their point estimates. A more stringent definition of success therefore needed to be developed, since convergence did not appear to be sufficient. Simulations where any of these 3 parameters were estimated at values larger than 2 were rejected. For a tow to capture 200% of the available biomass, it would require capturing every single

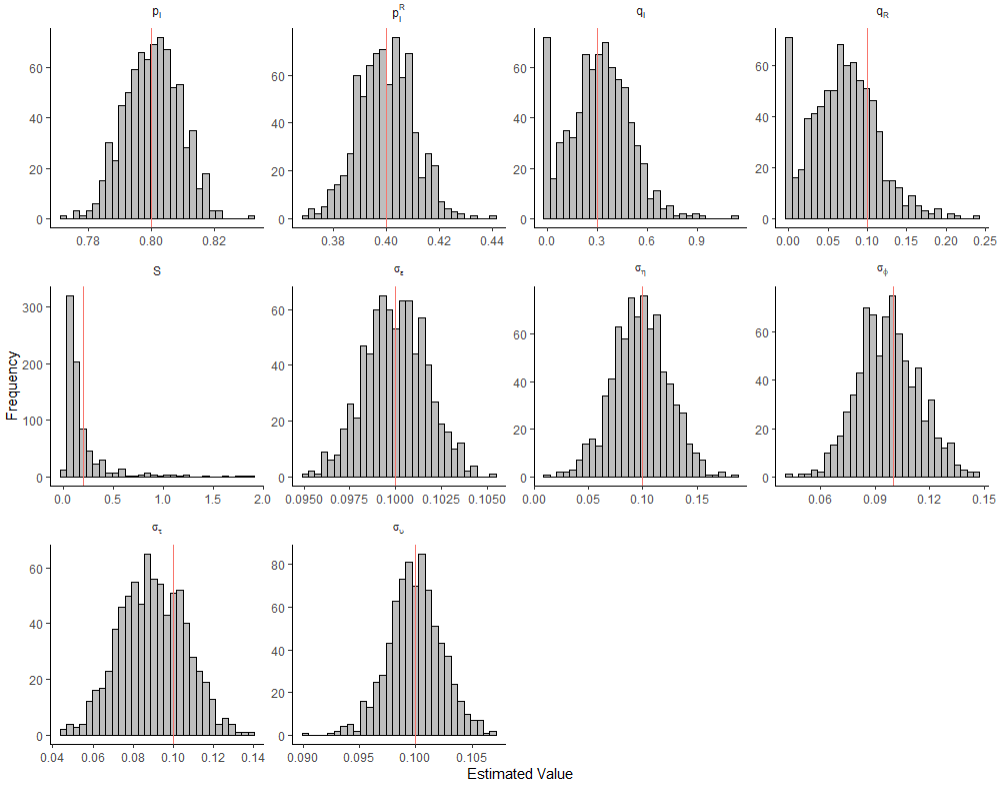

Figure 2.2: Distribution of parameter estimates from first experiment (778 simulations of 22 years). Red line denotes true value.

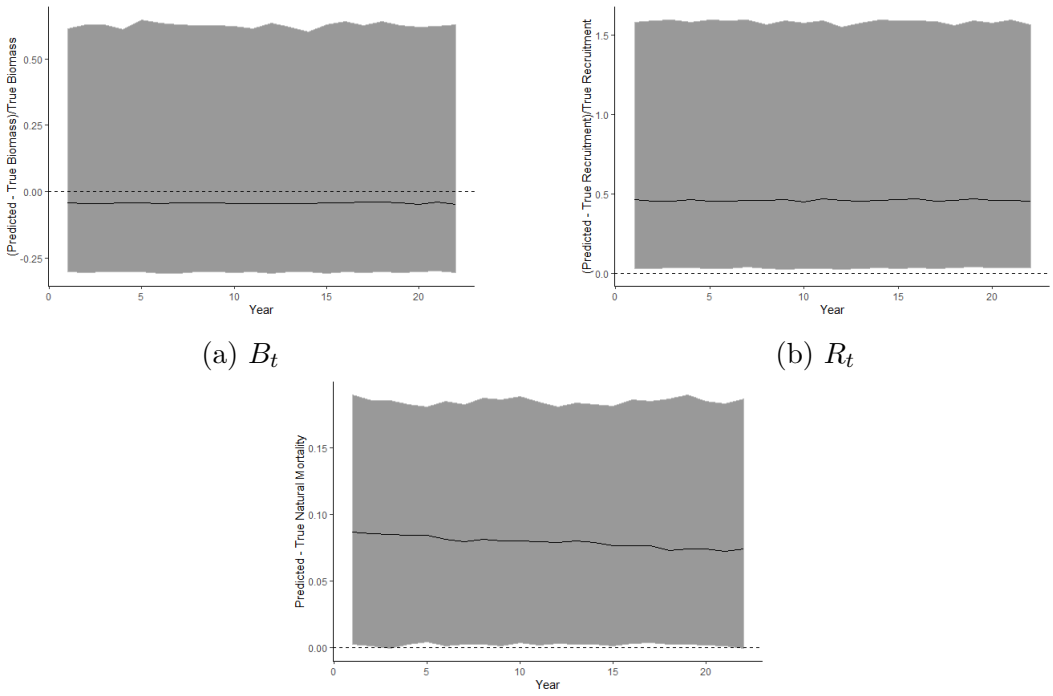

(a) B_t

(b) R_t

(c) m_t

Figure 2.3: Functional boxplots (without whiskers) for Experiment 1 of the difference of the predicted processes and their true value with horizontal dotted line at 0 and median difference shown by solid black line. 2.3a and 2.3b show the difference as a percentage of the true value (predicted - true / true) while 2.3c simply shows the net difference (predicted - true).

scallop in the towed area while also attracting the same number from neighboring areas, which seems highly unrealistic for a mostly sedentary species (Hart and Chute, 2004). There is clear evidence of avoidance behavior for scallops (Caddy, 1968), so it would be highly unlikely for a catchability larger than 2 to happen. Furthermore, every simulation where a catchability was estimated at a value larger than 2 was always associated with a massive standard error, indicating that it should not be trusted.

For the first 2 experiments, the number of successful simulations using this definition was 778 when q_I is estimated and 922 when q_I is fixed. For the last two experiments, the number of successes when q_I is fixed was 983 and 918 when q_I is estimated. Rejecting these unsuccessful simulations implies that simple convergence is not a sufficient criteria for the applicability of this model, and that the user must pay particular attention to the parameter estimates to validate it.

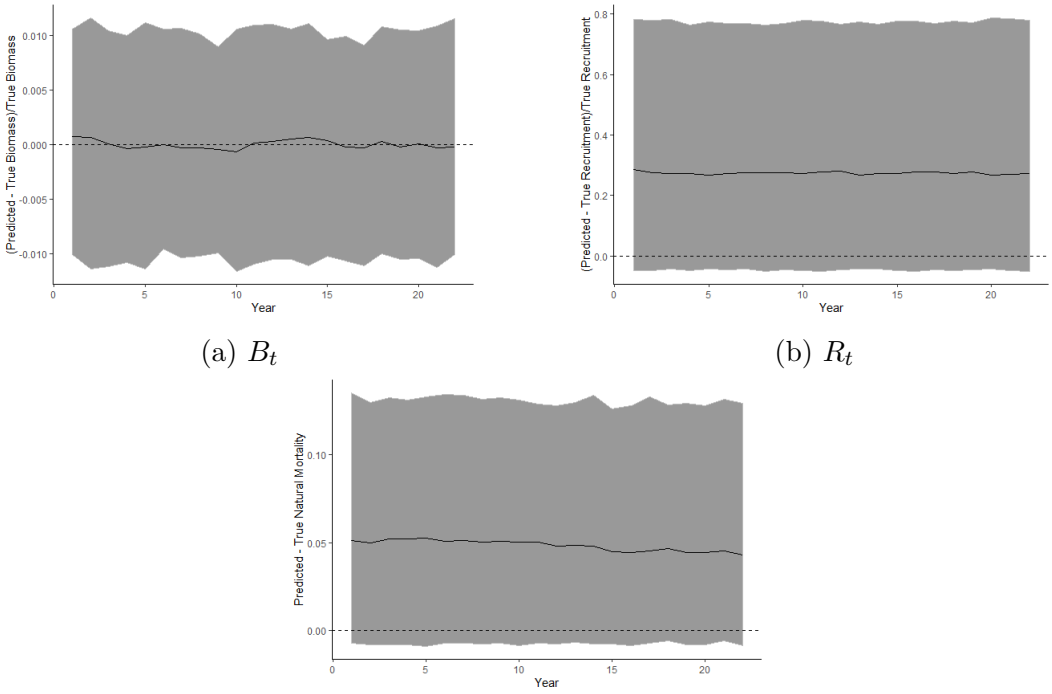

(a) B_t

(b) R_t

(c) m_t

Figure 2.4: Functional boxplots (without whiskers) for Experiment 2 of the difference of the predicted processes and their true value with horizontal dotted line at 0 and median difference shown by solid black line when q_I is fixed. 2.4a and 2.4b show the difference as a percentage of the true value (predicted - true / true) while 2.4c simply shows the net difference (predicted - true).

Figure 2.2 shows the histogram of parameter estimates for the 778 successful simulations of the first experiment. All variance parameters are on average well recovered without noticeable bias. A non-negligible number of simulations have had estimates of q_I and q_R arbitrarily close to 0. However, it is easy to identify these as erroneous since they all came with standard errors larger than their point estimates, indicating that the model did not reliably estimate them. q_R and S appear to be underestimated on average. Since both of these parameters are related to the productivity of the system (recruitment and mortality), it is likely that they are confounded together. This points to potential identifiability issues where FMB might not be able to reliably separate the recruitment and mortality parameters, but is able to reliably estimate and predict their combined effect on the biomass. There are clear cases where the model is able to capture patterns appropriately (since all variances are estimated mostly correctly), but struggles to find the true magnitude.

Parameter estimation behaved extremely similarly when q_I is fixed (see Appendix A for corresponding figure), with the exception that q_R was never estimated arbitrarily close to 0.

Figure 2.3 shows the functional boxplot (Sun and Genton, 2011) without whiskers of the difference between the predicted processes and their simulated true value, with B_t and R_t shown as a percentage of the true simulated value and m_t as the point-wise difference. Since the biomass is generally very well predicted but the recruitment and natural mortality are both positively biased, the model can accurately capture the true productivity but it cannot separate them consistently, leading to confounding of the recruitment and natural mortality. However, even by leaving the initial state free, the drastic change in the number of data points used here (from 1 a year to 100 a year) seems to have completely removed the slight initial bias seen in Yin et al. (2019). The model is also extremely consistent, wherein if the actual biomass magnitude is slightly off, it seems to be off by the same factor for the entirety of the time-series. This seems to be entirely driven by issues with the estimation of q_I, since Figure 2.4 shows that fixing q_I at the correct value captures the biomass almost perfectly.

The effects of extending the simulated time-series to 50 years in experiments 3 and 4 was to stabilize the estimation of q_I (Figures in Appendix A). This indicates that having more yearly commercial catch data would increase the ability of this model to estimate q_I reliably. One caveat that should be mentioned is that the simulated populations tended to decrease over time, as expected from the use of log-normal random walks (Lewontin and Cohen, 1969). However, population biomass only reached unrealistic numbers on much longer time scales than analyzed for real data (around 200 years), so are not expected to have caused any issues in these simulations (Figures in Appendix A).

2.4 Application to Nova Scotia Inshore Scallop Fishery

A request was made to obtain the commercial logbook data between 1995 and 2018 from DFO, but since location data for these logbooks was only available from 1998 onwards, 1995 to 1997 were not obtained. Therefore, FMA and FMB fit show the output from 1997 to 2018, while only the output between 1996 and 2017 was available for BM. BM had been fit using the R package SSModel, which runs WinBUGS in the

Table 2.4: Parameter estimates for BM, FMA and FMB fit to Scallop Production Area 3 (standard error in parentheses).

Bayesian Approach		Frequentist Approach			
BM		FMA		FMB	
Parameter	Estimate	Parameter	Estimate	Parameter	Estimate
K	746.19(234.681)	σ_τ	0.232(0.080)	σ_τ	0.212(0.058)
q	0.307(0.073)	σ_ϕ	$4.14X10^{-5}$(0.004)	σ_ϕ	0.345(0.082)
S	0.261(0.065)	σ_η	$3.73X10^{-5}$(0.005)	σ_η	0.680(0.097)
σ_κ	0.260(0.059)	σ_ϵ	0.213(0.064)	σ_ϵ	1.000(0.019)
σ_τ	0.252(0.189)	σ_υ	1.123(0.173)	σ_υ	1.069(0.028)
		σ_κ	0.568(0.088)	q_I	0.212(0.301)
		q_I	$3.45X10^{-8}(NaN)$	q_R	0.048(0.050)
		q_R	$2.57X10^{-7}(NaN)$	S	0.221(0.099)
		S	0.948(0.543)	p_I	0.913(0.007)
				p_I^R	0.491(0.013)

background, while FMA and FMB were both fit using the Template Model Builder (TMB) package in R using the *nlminb* optimizer with the same starting values shown in Table 2.3 and random effects starting values set to $10 * max(I_t)$ or $10max(I_{i,t})$ for B_t, $10max(I_t^R)$ or $10max(I_{i,t}^R)$ for R_t and 0.3 for m_t. Every model converged successfully.

Table 2.4 shows that aside from σ_τ, the few directly comparable parameters can have different behaviors depending on which parameter is examined. σ_τ appears highly consistent between all three models, the FMB estimate of q_I seems somewhat consistent with the BM estimate, albeit with a very wide standard error, while the estimates of σ_κ from BM and FMA greatly differ. FMA has clear problems in estimating σ_ϕ, σ_ϕ, q_I and q_R, which are all arbitrarily close to 0 with either no standard errors or standard errors orders of magnitude larger than their point estimates.

Estimates of variances, S and both probabilities of capturing live scallops are all in reasonable spaces with small standard errors for FMB. The model can clearly identify two separate catchabilities, but both of them have standard errors larger than their point estimates. σ_τ and σ_ϕ are reasonably small, indicating that the commercial size biomass and the recruit biomass have a rather steady behavior, while σ_η indicates that natural mortality varies quite a bit. σ_ϵ and σ_υ have large values consistent with the large variability present in the data.

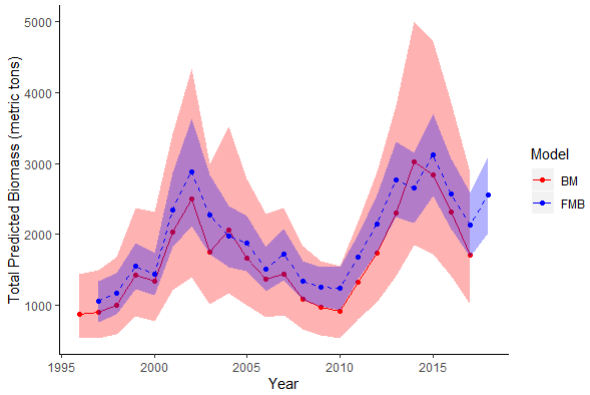

(a) Predicted Biomass (metric ton)

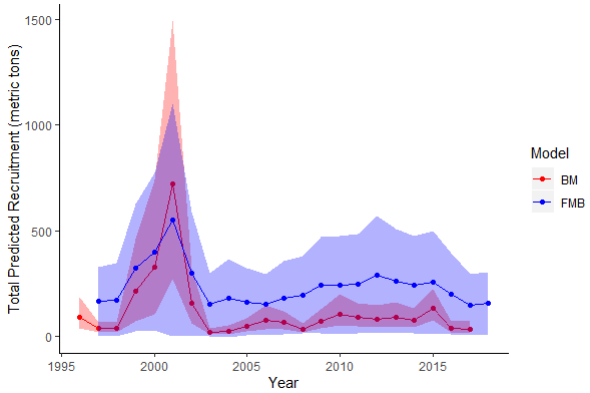

(b) Predicted Recruitment (metric ton)

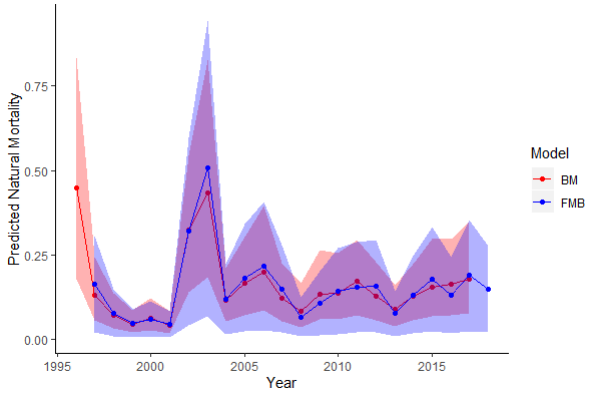

(c) Predicted Natural Mortality

Figure 2.5: Predicted random effects on the SPA 3 scallop data from BM (red) and FMB (blue). Envelopes represent interpolated point-wise 95% credible intervals and 95% confidence intervals respectively.

Table 2.5: Parameter estimates for FMB fit to Scallop Production Area 3 (standard error in parentheses).

Parameter	Estimates
σ_τ	0.211(0.058)
σ_ϕ	0.344(0.081)
σ_η	0.661(0.095)
σ_ϵ	0.998(0.019)
σ_υ	1.069(0.028)
q_R	0.056(0.026)
S	0.222(0.098)
p_I	0.913(0.007)
p_I^R	0.491(0.013)

Since the catchability parameters could be not be confidently captured, the decision was made to fix q_I at 0.3. This value was chosen since most issues related to the Bayesian framework were related to variance estimates and not catchability (Yin et al., 2019). While estimates of gear efficiency with typical scallop fishing gear is usually higher in the open ocean (Gedamke et al., 2004; Miller et al., 2019), they are relatively close and it is likely that nearshore areas would have slightly different catchabilities. Furthermore, preliminary analyses had shown that while biomass predictions were very sensitive to catchabilities below 0.3, the effect was not very strong at and above 0.3. This approach successfully converged with the estimates presented in Table 2.5. All other parameters have almost identical estimates and standard errors aside from the standard error of q_R which has noticeably shrinked.

Figure 2.5 shows the predicted random effects for all 3 underlying processes for both BM and FMB with fixed q_I. For BM, the lines represent the posterior mean and the envelope represents the interpolated point-wise 95% credible interval, while for FMB the solid line represents the predicted value given the optimized $\boldsymbol{\theta}$ and the envelope is based on the exponentiated bounds constructed on the log scale (prediction $\pm$ 1.96 standard error). These last are not as rigorous as other methods (e.g. bootstrapped standard errors) and are simply meant to give a general idea of the variability of these predictions. The recruitment predicted by FMB looks like a smoothed version of the one predicted by BM with a larger uncertainty, stemming from the large standard error associated with q_R. The mortality predicted by both

models are almost identical aside from the larger uncertainty associated with FMB. The commercial size biomass is highly consistent between both models, with very few cases where the posterior mean obtained by BM is outside of the confidence interval for the predictions from FMB. The confidence interval for the predicted biomass from FMB is much smaller than the credible interval for BM, likely due to a fixed q_I. Lastly, the same model was tested replacing the delta-approach with a zero-inflated poisson distribution and the outputs were, as expected (Thorson, 2018), exactly identical (Figures in Appendix A).

2.5 Discussion

Given the rigorous testing of FMA for SPA 4 (Yin et al., 2019), its inability to properly estimate some variance parameters for SPA 3 suggests that it is not flexible enough to fit this area well. The simulation study done by Yin et al. (2019) demonstrated that it became more reliable the longer the time series. Therefore, if more data were available, FMA would likely be able to account for the increased variability in SPA 3 (as compared to SPA 4) and reliably estimate variance parameters. However, our new approach suggests that waiting several years to obtain more data may not be necessary. The simulations in Section 3 demonstrated the reliability with which trends in population changes are estimated with the data currently available. Our new model retains all the advantages of using a frequentist SSM framework, amply demonstrated by Yin et al. (2019), while increasing its reliability and accuracy with the available time series.

Directly incorporating each individual survey tow as an individual observation brings forward a significant improvement to the estimation of the variance parameters, which results in accurate and reliable predictions of population trends. The information required to reliably estimate trends in populations already exist in most stock assessment data, but many standard approaches fail to harness this information fully. While it does not posit whether the empty tows are "true" or "false" zeroes (Martin et al., 2005), the implemented delta approach is able to incorporate the information they contain and use it to capture changes in scallop adult and recruit populations. Furthermore, the simplified natural mortality model is flexible enough to capture both yearly changes, like the "popcorn" model did (Nasmith et al., 2016; Yin

et al., 2019), while making fewer assumptions and predicting the long-term average for this species (Merrill and Posgay, 1964). Stock assessment models, and the subsequent advice provided to fisheries management, should incorporate as much available information as possible while accounting for every potential sources of uncertainty.

While patterns of population change are reliably estimated using this approach, the actual population magnitude (through the catchability parameters) is more difficult to assess. Simulations have shown that having a longer time series would alleviate this issue, but many fisheries do not have access such long term and high quality data (Costello et al., 2012). Particular attention therefore needs to be paid by the user to their uncertainty to properly assess the appropriateness of the model. In some cases, it becomes necessary to include external information to reliably predict the magnitude of the commercial size biomass and recruitment. This could be done successfully by adapting our novel approach to a Bayesian framework, which would only require the addition of prior distributions. If a frequentist framework is preferred, the easiest solution would be to fix a parameter as was done here. This has the advantage of making any assumptions explicit and thus easier to replicate, but requires validation of the values chosen for parameters that have to be fixed.

There remain ways in which this model could be improved. The underlying processes for recruitment and natural mortality do not have any biological basis and any number of different, more realistic models could replace the relatively straightforward random walks. Other information, such as habitat suitability, could be used to properly understand the sources of zeroes. Furthermore, the model does not account for the spatial patterns present in the SPA 3 sea scallop populations.

Spatial autocorrelation, wherein observations are correlated according to the distance between them instead of randomly, is intrinsic to a large proportion of ecological data (Legendre, 1993), including the SPA 3 data. Ignoring these spatial patterns may misrepresent the underlying mechanisms (Ciannelli et al., 2008) and can have serious consequences in regards to fisheries management (Carson et al., 2017). Furthermore, the spatial aggregation of the fishing effort for this species (Caddy, 1975; Nasmith et al., 2016; Smith et al., 2017) can also lead to serious modeling issues. For example, aggregating over space can result in only a few tows dragging the biomass and recruitment predictions up, when in reality these outliers only represent a local event.

While it may be true that the population in a specific sub-area boomed, extrapolating from that to the entire population can potentially result in mismanagement and overfishing. We expect that accounting for these spatial issues will lead to further improvement of this model and any resulting stock assessment.

Explicitly modeling each individual tow instead of a single index of abundance per year takes the first step into explicitly incorporating spatial information into the sea scallop stock assessment model. Directly modeling each individual observation represents the mid-point between a single data point a year to modeling the location of each individual data point to explicitly incorporate the effect of space (e.g. Kristensen et al., 2014; Thorson et al., 2015c). This novel model demonstrates how general stock assessments across the world can better harness their own existing data in a simple and straightforward manner. Expanding pre-existing models to properly account for the true variability and zero-inflation instead of averaging over everything promises to improve the ability to appropriately track changes in populations over time without requiring new investments or difficult conceptual tools. Proper use of this type of approach should increase the confidence that fisheries managers and stakeholders have in the predictions used to manage important fish stocks.

Chapter 3

Applying a new spatio-temporal state-space stock assessment model for the Nova Scotia Inshore Sea Scallop (*Placopecten magellanicus*) Fishery

Abstract

Traditional stock assessment models have tended to focus on temporal variations in productivity. These models assume the area of interest to be homogeneous with respect to both the recruitment and mortality of the fish stock. However, strong spatial patterns in fisheries data have been shown to cause issues when fitting strictly temporal models. Recent technological and statistical improvements have provided modelers with the capacity to incorporate spatial variability into the stock assessment framework. Here, we propose a spatio-temporal state-space delay-difference stock assessment model for the Nova Scotia Inshore Sea Scallop Fishery. Results demonstrate that this framework can predict the distribution and abundance of scallops at a much finer spatial scale than previously available. Simulations show how the spatial coverage of fishing effort can introduce bias in predictions from the temporal model unlike the proposed spatio-temporal model which reliably captures strong anisotropic behavior, predicts biomass in both space and time and retains the ability to scale back up to predictions for the entire area.

3.1 Introduction

An over-arching objective of fisheries science is to explain and predict the variability in population abundance of important fish stocks. Strong spatial patterns in fishing pressure (Baranov, 1918; Beverton and Holt, 1957; Caddy, 1975) and biological characteristics (e.g. Smith and Rago, 2004) have long been known to exist, and ignoring these patterns has been shown to result in serious issues for the management of these stocks (Carson et al., 2017). Spatial methods have only recently seen

widespread use because of improvements in statistical approaches and computational capacities. Utilizing either geostatistical approaches or generalizations of common regression techniques (Ciannelli et al., 2008), the implementation of spatial statistics into fisheries stock assessment has greatly improved our ability to model fine-scale changes in population abundance and distribution (e.g. Cadigan et al., 2017; Kai et al., 2017).

Regression-based methods focus on modeling the mean effect, often through generalized additive frameworks (Ciannelli et al., 2008; Pedersen et al., 2018). These typically require high quality information on both environmental variables (temperature, nutrient availability, etc.) and the fish population, and tend to not be available for many fisheries (Costello et al., 2012). Alternatives such as geostatistics account for spatial patterns by incorporating spatial autocorrelation into the residual structure of a model (Ciannelli et al., 2008). This has been done in generalized linear model frameworks by splitting the error structure into its spatial and non-spatial components (e.g. Thorson et al., 2015c, 2019) or by explicitly modeling a single spatial error structure to capture the latent spatial variability (e.g. Cadigan et al., 2017; Stock et al., 2020). These methods allow the mean effect to be specified by other components, including traditional stock assessment models such as biomass dynamics models.

Biomass dynamics models only require two inputs per year: an index of population abundance, and commercial landings (Hilborn, 1992). While there are many formulations, a common example is the delay-difference model (Deriso, 1980; Schnute, 1985). Modern applications often involve the use of a state-space framework (e.g. Smith and Hubley, 2014; Xu et al., 2019; Best and Punt, 2020), which allows the separation of observation errors (from the measurement itself) and process errors (from the imperfect knowledge of the underlying dynamical process) (Cressie et al., 2009; Aeberhard et al., 2018). These approaches tend to be strictly temporal, and only recently has there been increased interest in incorporating spatial information (e.g. Thorson et al., 2015b; Cadigan et al., 2017).

While a significant proportion of fisheries are likely to benefit from the inclusion of spatial information in their assessment (Berger et al., 2017), some species lend themselves more intuitively to these approaches. Sea scallops (*Placopecten magellanicus*) are a shellfish species that inhabit the Western North Atlantic from Cape Hatteras

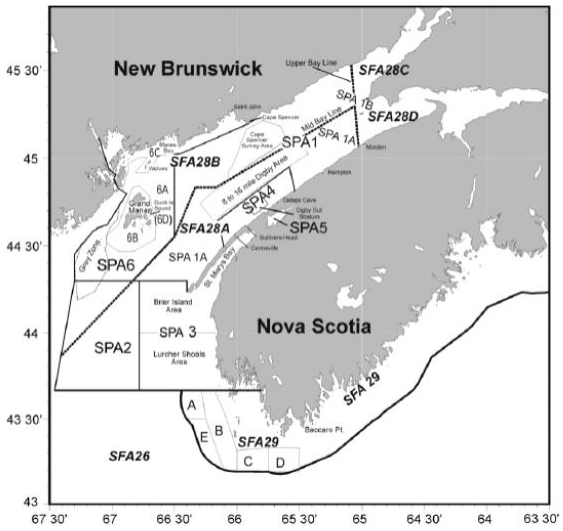

Figure 3.1: Map of Scallop Production Areas (SPA) and Scallop Fishing Areas (SFA) in Bay of Fundy and surroundings (taken from Nasmith et al., 2016). SPAs and SFAs are regulated differently, hence the difference in labeling.

to Labrador (Smith and Rago, 2004). These animals are characterized by strong spatial patterns in growth rates and egg production, minimal dispersal as adults, and recurring aggregation in scallop beds (Smith and Rago, 2004). Furthermore, the fishing effort for this species tends to be strongly linked to higher habitat suitability (Smith and Rago, 2004; Smith et al., 2017). This spatially aggregated fishing mortality has been identified as a potential issue when assessing the stock status for these animals (Caddy, 1975; Smith and Rago, 2004; Smith et al., 2017). Explicitly modeling this spatial variability should improve the advice given to fisheries managers and stakeholders, increasing the likelihood that sea scallops remain ecologically viable and commercially sustainable.

The fishery of concern here is the Nova Scotia Inshore Sea Scallop Fishery, particularly the areas in and around the Bay of Fundy seen in Figure 3.1. Extensive efforts have gone into describing the impact of spatially aggregated commercial fishing and habitat suitability on scallop populations and model predictions (Caddy, 1975; Smith et al., 2017). The recent focus has been on two different areas: Scallop Production Area (SPA) 4, and the Scallop Fishing Area (SFA) 29. The analysis of SPA 4 focused on issues related to the use of a Bayesian model framework (Yin et al., 2019), while a clear link between habitat suitability and fishing effort was identified for the western

part of SFA 29 (Smith et al., 2017). This can lead to the spatial aggregation of fishing effort, which impacts model predictions (Caddy, 1975; Smith et al., 2017).

Data from SPA 3, north-west of SFA 29, have exhibited strong spatial variations in population abundance and commercial fishing effort, which has resulted in serious modeling issues. These issues are likely caused by these strong spatial patterns, which the strictly temporal biomass dynamics model used for the area ignores (Nasmith et al., 2016). Because of this, Fisheries and Oceans Canada (DFO) recently restratified SPA 3 based on recurrent commercial fishing locations through the implementation of a Vessel Monitor System (VMS) on each ship, and only the regularly exploited strata (St-Mary's Bay and the Inside VMS strata) are modeled while the rest (Outside VMS stratum) is ignored (Nasmith et al., 2016). These factors identified SPA 3 as a strong candidate area to incorporate the existing spatial information into its stock assessment model, and will be the focus of our efforts.

The current stock assessment model used by DFO is a type of delay-difference model described in detail in both Nasmith et al. (2016) and Yin et al. (2019). Due to identifiability issues associated with its use of a Bayesian framework, an alternative frequentist framework was proposed (Yin et al., 2019). We developed a hybrid between a strictly temporal model and a spatio-temporal model (Chapter 2). However, this was done only for St-Mary's Bay and the Inside VMS strata and its applicability for the entirety of SPA 3 was not tested. Furthermore, the heterogeneity of the area is likely to be obfuscated by a strictly temporal model. We propose two closely related spatio-temporal models to incorporate fine-scale spatial information into the stock assessment for SPA 3 and test them to see if their local predictions are reliable with the broad goal of reliably estimating the current status of the SPA 3 stock. The output from these explicitly spatial models will be compared to the temporal model to test their ability to capture population trends for the whole area. We also aim to examine the effect of fitting a strictly temporal model to variable spatial data through simulation studies.

Section 3.2 describes SPA 3 data and introduces the notation and structure of the three models of interest: a strictly temporal state-space model (TM) which treats each survey tow as an independent observation and tracks the total biomass over

time, a spatio-temporal model (STM1) where recruitment and mortality are spatially-autocorrelated but the commercial size biomass is considered spatially independent, and a spatio-temporal model (STM2) where recruitment, mortality and commercial size biomass are all spatially-autocorrelated. Section 3.3 presents two simulation studies, where the first demonstrates the reliability and identifiability of the spatio-temporal models developed in Section 2, while the second demonstrates the effects of fitting a strictly temporal model to data simulated from a spatio-temporal model. This second study aims to demonstrate the effect of spatially uneven fishing pressure on the strictly temporal predictions. Section 3.4 presents the results of fitting all three models to SPA 3, with Section 3.5 discussing key findings.

3.2 Model and Data Descriptions

3.2.1 SPA 3 Data

SPA 3 is surveyed annually using a stratified random sampling design with partial replacement. A subset of the survey fishing gear is lined with a mesh of 38mm to capture recruit-sized scallops, while the rest is left as is (Nasmith et al., 2016). All scallops and clappers are counted and binned by size (5mm bins). Scallops with shells larger than 80mm are classified as commercial size, scallops between 65mm and 79mm are classified as recruits while scallops smaller than 65mm are classified as pre-recruits. The data for the recruits are taken from the lined gear, while the commercial size data are obtained from the unlined gear. Out of the scallops larger than 50mm, a subset is set aside (3 per 5mm bins) to record individual shell height, meat weight and age in order to estimate a shell height to meat weight relationship (as it would be impossible to measure them all). The approach taken here follows a simple cube law (Froese, 2006):

$$w_i = A h_i^3 d_i^b \epsilon_i, \quad \epsilon_i \overset{Ind}{\sim} u\ell N(\sigma_\epsilon^2) \tag{3.1}$$

where w_i is the meat weight of scallop i, A is the intercept on the log-scale, h_i is the shell height of scallop i, d_i is the depth where it was caught with associated slope b on the log-scale, and ϵ_i is a log-normally distributed error term. This model is fit separately for each year. Once estimates of A and b are obtained, the equation

is applied deterministically (i.e. without error) to all live scallops in every tow. This is done by applying Equation 3.1 to the midpoint of each size bin in each tow (e.g. 42.5mm for bin 40-45mm), at which point the observed commercial size biomass and recruit size biomass can be summed up in every tow.

Some portions of SPA 3 were removed from the modeled area. A large portion in the north-west of SPA 3 contains very few scallops due to its different composition of glaciomarine mud (Shaw et al., 2012, 2014). The south-easternmost portion of the area was also removed from the modeled area due to the absence of any observations, either survey tows or commercial fishing. For the coastline, the commercial fishing data showed that over 99% of the fishing was done at depths deeper than 7m, so the modeled area was cut off at this depth.

The spatial approaches involve setting up a grid over the area. Due to the large number of random fields involved in the spatio-temporal models described here, the "predictive" approach described in Thorson et al. (2015c) was adopted. This means that instead of modeling a given random field over every possible location, its value is approximated as being piece-wise constant. The user must specify the number of locations, called "knots", at which the model will track the value of the random fields. This choice drives both the resolution of the model predictions and the computational load, since more knots will lead to higher resolution but the fitting process will be slower. The decision concerning the number of knots used should be based on the spatial coverage of the data to control the accuracy of the piece-wise approximation. This means that having more knots than data is likely to lead to a less accurate approximation, since the model will have to predict the values at certain knots exclusively based on the values in neighboring cells. The locations of these knots are obtained by applying a k-means clustering algorithm on the location of all survey tows. The number and location of knots is held constant for model fitting and all observations (both survey tows and commercial catches) are attributed to their respective closest knot.

Preliminary tests were done with different numbers of knots (20, and 30 and 40) to find the best resolution that the data allowed. Serious convergence issues were identified when fitting to 30 or more knots. These issues appeared to be caused by the survey spatial cover. Higher numbers of knots resulted in a grid in which the first

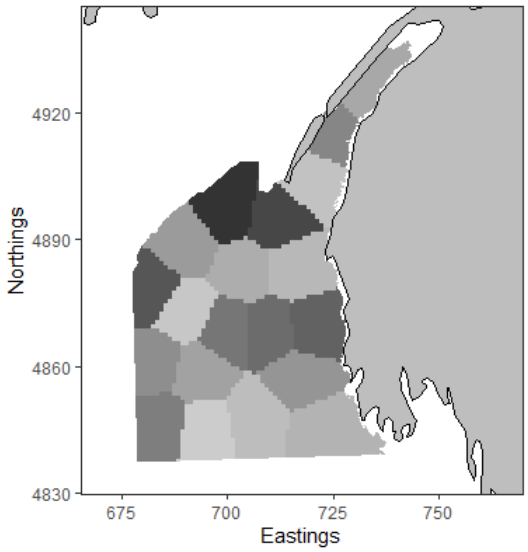

Figure 3.2: Modeled area of SPA 3 with grid obtained from knots based on survey tow locations. Greyscale used to delineate grid cells.

ten years did not have complete spatial cover (defined as each grid cell having at least one positive survey tow), while fewer knots usually had complete cover in the first or second year. It is also possible that these issues were caused by overparameterization, since each additional knot meant an additional 60 random effects. To avoid these convergence issues, the chosen number of knots was 20. The resulting grid is shown in Figure 3.2.

To obtain the survey observations for TM, the observed commercial size and recruit biomass of each individual tow is multiplied by the number of towable units (total modeled area divided by area covered by a standard tow). The number of clappers and live scallops in each tow is taken as is.

To obtain the survey observations for STM1 and STM2, the commercial size and recruit biomass of each tow is divided by the area covered by a standard tow (scaling it to 1km^2) and attributed to the closest knot. Visualizations of the data are available in Appendix B. The number of clappers and live scallops is once more taken as is and attributed to the closest knot.

Commercial landings are obtained by summing up all landings reported in fishing logbooks for each separate fishing year. The model assumes that all commercial fishing is done after a given survey, but there is a mismatch between survey years, which are from June to May since the surveys are done between June and August (Nasmith

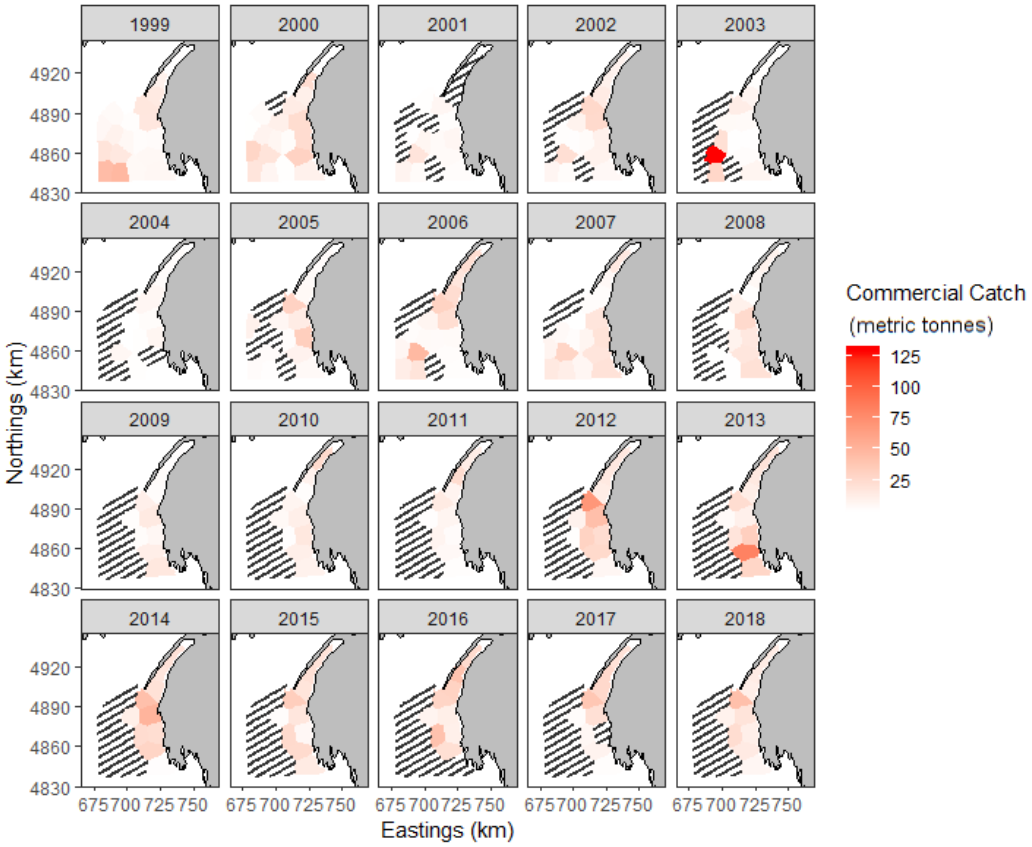

Figure 3.3: Spatial distribution of commercial catch (metric tonnes) between 1999 and 2018. Striped grid cells represent areas where the number of licenses operating was beneath 5, so cannot be reported.

et al., 2016), and fishing years, which are from October to September. This is fixed by temporally aligning the commercial fishing data appropriately by assigning each individual logbook to the appropriate survey year instead of their respective fishing year. For example, a logbook detailing landings from a fishing trip done in September 2002 should be assigned to the survey year of 2002-2003, even if it is in the fishing year of 2001-2002.

Furthermore, there is a mismatch between the annual official landings and the annual sums obtained from the logbooks. The official landings have been deemed a more accurate representation of the total landings in a fishing year, so the difference between the two sources must be added onto the logbook data. This difference must also be prorated into the appropriate survey years. For example, if this difference is 10 tonnes in the 2002-2003 fishing year and 70% of the landings in that fishing period were done before the survey, then 7 tonnes are attributed to the 2001-2002 survey year and 3 tonnes to the 2002-2003 survey year. This can then be used directly by TM.

The logbooks from which the commercial landings are obtained contain a unique location for each fishing trip. For STM1 and STM2, the landings from each individual trip is attributed to the closest knot. The commercial catch is then summed up in each cell. The previously mentioned difference between the official landings and the yearly sums from the logbooks is proportionally added to each cell (e.g. if a given cell contains 10% of the total catch, 10% of the difference is added to that cell). Afterwards, the total landings for each cell is scaled down to represent 1km^2 (e.g. if 100 tonnes was caught in a cell covering 100km^2, it is scaled down to 1 ton). A key difficulty in modeling SPA 3 is the spatial aggregation of commercial catch in the near shore areas seen in Figure 3.3. This has been identified as a potential issue by previous work (Caddy, 1975; Smith et al., 2017) and its effect will be examined in simulation studies.

3.2.2 Model Descriptions

State-space models (SSMs) are hierarchical models defined by two stochastic processes: $\mathbf{X}_t$ represents the unobserved dynamic state process describing population

abundance and productivity in year $t = 1, ..., T$, and $\mathbf{Y}_t$ represents the directly observed variables linked to the true underlying dynamical processes of interest (Aeberhard et al., 2018). The model parameters are contained in a p-vector $\boldsymbol{\theta} \in \boldsymbol{\Theta} \subseteq \mathbb{R}^p$, with fixed covariates $\mathbf{z}_t$. A frequentist perspective is taken wherein $\boldsymbol{\theta}$ is considered a vector of fixed effects and $\mathbf{X}_t$ a vector of random effects predicted from estimates of $\boldsymbol{\theta}$. Both $\mathbf{Y}_t$ and $\mathbf{z}_t$ are directly observed.

These models focuses on maximizing the following marginal log-likelihood:

$$\mathscr{L}(\boldsymbol{\theta}, \mathbf{Y}_{1:T}) = log \int L(\boldsymbol{\theta}, \mathbf{Y}_{1:T}, \mathbf{X}_{1:T}) d\mathbf{X}_{1:T} \tag{3.2}$$

These intractable high-dimensional integrals are approximated using the Laplace method through the TMB package in R (Kristensen et al., 2016). TMB's use of Automatic Differentiation, which keeps track of higher order derivatives for all modeled functions, has been shown to be computationally more efficient than most other packages without loss of accuracy (Kristensen et al., 2016; Auger-Méthé et al., 2017). Furthermore, it has been successfully used to fit similarly complex spatial models (e.g. Thorson et al., 2015c; Cadigan et al., 2017; Thorson et al., 2019).

Temporal Model (TM)

Based on the state-space model described in (Yin et al., 2019), itself based on DFO's Bayesian model first presented in (Smith and Lundy, 2002) and more recently in (Nasmith et al., 2016), the temporal model described here was developed to solve issues with parameter estimation associated with the highly variable SPA 3 (Chapter 2). The first level of the hierarchical structure follows a delta approach, which models the zeroes separately from the positive observations (Thorson et al., 2015c). The first part (Equations 3.3 to 3.4) uses the number of tows where no scallops were caught to estimate the probability of capturing scallops (either commercial or recruit size). The second part (Equations 3.5 and 3.6) focuses on the tows where scallops were caught and relates them to the underlying commercial and recruit biomass. Finally, they are recombined together so that the predicted processes (commercial biomass and recruitment) account for both empty and positive tows. The observation equation for the natural mortality (Equation 3.7) can account for zeroes, so does not use a delta-approach.

The zeroes are modeled the following way:

$$P_t^I \overset{Ind}{\sim} Bin(n_t^{tows}, p_I) \tag{3.3}$$

$$P_t^R \overset{Ind}{\sim} Bin(n_t^{tows}, p_I^R) \tag{3.4}$$

Here, both p_I and p_I^R are probabilities estimated using a binomial distribution where P_t^I is the number of tows with positive commercial size catches and P_t^R is the number of tows with positive recruit catches. They are both assumed independently distributed based on the number of tows n_t^{tows} in each year t for $t = 1, ..., T$.

The positive observations are then modeled the following way:

$$I_{i,t} = q_I B_t^\star \epsilon_{i,t}, \quad \epsilon_{i,t} \overset{Ind}{\sim} u\ell N(\sigma_\epsilon^2) \tag{3.5}$$

$$I_{i,t}^R = q_R R_t^\star \upsilon_{i,t}, \quad \upsilon_{i,t} \overset{Ind}{\sim} u\ell N(\sigma_\upsilon^2) \tag{3.6}$$

$$L_{i,t} \overset{Ind}{\sim} Bin(L_{i,t} + N_{i,t}, m_t S) \tag{3.7}$$

All variables are indexed by a discrete time index for each year t with $t = 1, ..., T$, and $u\ell N(\sigma^2)$ denotes a log-normal distribution with unit mean on the natural scale ($\mu_l = -0.5\sigma^2$ on the log scale) and variance σ^2 on the log scale. $B_t^\star = p_I B_t$ where B_t is the underlying commercial biomass, and $R_t^\star = p_I^R R_t$ where R_t is the underlying recruit biomass. Equation 3.5 links each observed commercial size biomass $I_{i,t}$ as independent observations of the underlying biomass B_t while accounting for zeroes through p_I. q_I is the catchability parameter for the commercial size biomass, and $\epsilon_{i,t}$ are log-normal error terms with associated variance σ_ϵ^2. Equation 3.6 links recruit size biomass $I_{i,t}^R$ to the underlying recruitment R_t after accounting for zeroes through p_I^R, scaled with recruit catchability q_R, and with log-normal error term $\upsilon_{i,t}$ with associated variance σ_υ^2. Equation 3.7 links the number of clappers $L_{i,t}$ (empty shells with their hinge still present) to the natural mortality m_t, scaled by a clapper catchability S through a binomial distribution with the size being the total number of shells caught (clappers plus live scallops $N_{i,t}$). This assumes that each shell caught has an equal probability of dying between each surveys.

The second level of the hierarchical structure, which models the latent population dynamics, is the following:

$$B_t = [e^{-m_t} g_{t-1}(B_{t-1} - C_{t-1}) + e^{-m_t} g^R_{t-1} R_{t-1}]\tau_t \tag{3.8}$$

$$R_t = R_{t-1}\phi_t, \quad \phi_t \overset{Ind}{\sim} u\ell N(\sigma^2_\phi) \tag{3.9}$$

$$m_t = m_{t-1}\eta_t, \quad \eta_t \overset{Ind}{\sim} u\ell N(\sigma^2_\eta) \tag{3.10}$$

Here, $\tau_t \overset{Ind}{\sim} u\ell N(\sigma^2_\tau)$ for $t = 2, ..., T$. Equation 3.8 moves the biomass B_t from one year to the next after removing the commercial catch C_t, removing those that died from natural mortality m_t, and growing the surviving scallop biomass by growth g_{t-1}. The natural mortality is afterwards applied to the recruitment biomass R_t, which is grown by recruit growth g^R_{t-1} and added to the biomass to obtain the final value, which is then associated with error term τ_t and log-normal variance σ^2_τ. Yearly growth rates are obtained from separate work and are considered fixed.

Equation 3.9 and 3.10 are both simple random walks on the log scale with error terms ϕ_t and η_t, with associated variances σ^2_ϕ and σ^2_η. While these do not incorporate realistic dynamics for these processes, they were added as a way of incorporating more variability in their predictions (Yin et al., 2019). The data was assumed more than sufficient to overcome the expected long-term population decrease inherent to geometric random walks such as log-normal ones (Lewontin and Cohen, 1969). Predictions well into the future would decrease steadily, but this should not unduly affect predictions a single year ahead. The initial state for all processes are left free to be predicted.

In summary, TM contains the observed states $\mathbf{Y}_t = (I_{i,t}, I^R_{i,t}, L_{i,t})^T$, the unobserved states $\mathbf{X}_t = (B_t, R_t, m_t)^T$, the fixed covariates $\mathbf{z}_t = (N_{i,t}, C_t,\ g_t, g^R_t)^T$ and the parameters $\boldsymbol{\theta} = (p_I, p^R_I, q_I, q_R, S, \sigma^2_\epsilon, \sigma^2_\upsilon, \sigma^2_\tau, \sigma^2_\phi, \sigma^2_\eta)^T$.

Spatial Approach

The state-space framework described earlier has to be modified to incorporate the location of every knot. Therefore, the unobserved dynamic state process describing population abundance and productivity in year $t = 1, ..., T$ and knot location

$s = 1, ..., S$ is now $\mathbf{X}_{s,t}$, while the directly observed variables are now $\mathbf{Y}_{s,t}$. Model parameters are still contained in a p-vector $\theta \in \Theta \subseteq \mathbb{R}^p$ with fixed covariates $\mathbf{z}_{s,t}$. The frequentist perspective is retained where $\boldsymbol{\theta}$ is still a vector of fixed effects, $\mathbf{X}_{s,t}$ is a vector of random effects predicted from estimates of $\boldsymbol{\theta}$, while both $\mathbf{Y}_{s,t}$ and $\mathbf{z}_{s,t}$ are directly observed.

This results in a modified marginal log-likelihood:

$$\mathscr{L}(\boldsymbol{\theta}, \mathbf{Y}_{1:S,1:T}) = log \int L(\boldsymbol{\theta}, \mathbf{Y}_{1:S,1:T}, \mathbf{X}_{1:S,1:T}) d\mathbf{X}_{1:S,1:T} \tag{3.11}$$

Since each knot covers a different area, the model was set up to predict biomass and recruit density, meaning that each data point has to be scaled to 1km^2. This can later be scaled back up to represent the whole area covered by a given knot and then combined into a total prediction of biomass for all of SPA 3.

The incorporation of spatial statistics is done through the use of Gaussian Markov Random Fields (GMRFs), which models spatial autocorrelation at discrete locations (Zimmerman and Stein, 2010). This assumes that a continuous underlying Gaussian Random Field (GRF) exists that can be represented by a discrete GMRF (Lindgren and Rue, 2011). When implemented with constant discrete locations $\mathbf{s}$ in year t, a GMRF can be reduced to a multivariate Gaussian distribution:

$$\boldsymbol{\Omega}_t \sim MVN(\boldsymbol{\mu}, \boldsymbol{\Sigma}_t) \tag{3.12}$$

Here, GMRF $\boldsymbol{\Omega}_t$ follows a multivariate normal distribution with mean $\boldsymbol{\mu}$ and explicitly spatial covariance matrix $\boldsymbol{\Sigma}_t$ in year t. For this application, the mean is set to 0 everywhere. This covariance matrix is set to follow a stationary Matérn distribution that can account for geometric anisotropy in the following way:

$$Matérn(s, s') = \tau^2 \frac{1}{\Gamma(\nu) 2^{\nu-1}} (\kappa d(s, s'))^{\nu} K_{\nu}(\kappa d(s, s')) \tag{3.13}$$

$$\boldsymbol{\Sigma}(s, s') = Matérn(||\mathbf{H}(s - s')||) \tag{3.14}$$

Equation 3.13 shows the Matérn covariance function where τ^2 is the spatial variance, ν determines smoothness and is fixed at 1 (e.g. Thorson et al., 2015c; Carson et al., 2017), κ is the range parameter which determines the distance at which two

locations are effectively uncorrelated, $\Gamma(\cdot)$ is the gamma function, $K(\cdot)$ is the Bessel function of the second kind and $d(s, s')$ is the Euclidean distance between two points ($d(s, s') = \sqrt{(x - x')^2 + (y - y')^2}$ with x and y being coordinates). Equation 3.14 shows the covariance function itself, where $\mathbf{H}$ is a linear transformation (similar to a rotation matrix) to account for anisotropy. $\mathbf{H}$ is parameterized to preserve volume with two unique parameters following the approach taken by Thorson et al. (2015c). Incorporating anisotropy is extremely important for near-shore fisheries since their distribution often follows depth profiles (Thorson et al., 2015c).

Although there are methods to apply GMRFs on a sphere (Lindgren and Rue, 2011), it is computationally easier and more interpretable if the surface is flat. To accomplish this, the locations are projected onto the Universal Transverse Mercator (UTM) system. This has the added advantage of making spatial parameters more interpretable, since the UTM coordinate units are in meters (rescaled into kilometers for numerical stability).

Spatio-Temporal Model 1 (STM1)

Following the same hierarchical framework as TM, the initial step to estimate the probability of having positive survey observations are identical between TM and STM1 and are not reported again. The second part of the first hierarchical level modeling the observations are the following:

$$I_{i,s,t} = q_I B^{\star}_{s,t} \epsilon_{i,s,t}, \quad \epsilon_{i,s,t} \overset{Ind}{\sim} u\ell N(\sigma^2_{\epsilon}) \tag{3.15}$$

$$I^R_{i,s,t} = q_R R^{\star}_{s,t} \upsilon_{i,s,t}, \quad \nu_{i,s,t} \overset{Ind}{\sim} u\ell N(\sigma^2_{\upsilon}) \tag{3.16}$$

$$L_{i,s,t} \overset{Ind}{\sim} Bin(L_{i,s,t} + N_{i,s,t}, m_{s,t} S) \tag{3.17}$$

where $B^{\star}_{s,t} = p_I B_{s,t}$ and $R^{\star}_{s,t} = p^R_I R_{s,t}$. These equations are almost identical to Equations 3.5, 3.6 and 3.7 except that each observed density in tow i in year t is modeled separately at each knot s. This assumes that the observations are conditionally independent of one another given the underlying spatial patterns, and further assumes that all 3 catchabilities are constant across space and time.

The second hierarchical level that models the process dynamics is the following:

$$B_{s,t} = [e^{-m_{s,t}} g_{t-1}(B_{s,t-1} - C_{s,t-1}) + e^{-m_{s,t}} g_{t-1}^{R} R_{s,t-1}]\tau_{s,t} \tag{3.18}$$

$$R_{s,t} = R_{s,t-1} e^{\Omega_{s,t}^{R}} \tag{3.19}$$

$$m_{s,t} = m_{s,t-1} e^{\Omega_{s,t}^{m}} \tag{3.20}$$

Equation 3.18 is the same as Equation 3.8 but is done separately at each knot s in year t with $t = 2, ..., T$, assuming that each knot is independent of one another. There is biological evidence that commercial size scallops are mostly sedentary (Smith and Rago, 2004) and, since each area covers over 100km^2, it appears to be a reasonable assumption. Recruitment and mortality, however, directly incorporate spatial autocorrelation by constructing their error structures $\mathbf{\Omega}^R$ and $\mathbf{\Omega}^m$ as GMRFs on the log scale. Each year has its respective GMRF, indicating that the error structure can vary every year. These are based on their respective constant spatial variance τ_R and τ_m and their respective range parameters κ_R and κ_m, which are constant over time. Furthermore, each process has their respective anisotropy matrices $\mathbf{H}_R$ and $\mathbf{H}_m$. The initial value at every knot in year 1 for Equation 3.18 is left open to be predicted.

For Equations 3.19 and 3.20, since the GMRFs are set up as error structures with mean 0, the first year must be initialized. To minimize the number of random effects and parameters, this is done by simply specifying a single mean parameter to give some mean value in the following way:

$$R_{s,1} = R_0 e^{\Omega_{s,1}^{R}} \tag{3.21}$$

$$m_{s,1} = m_0 e^{\Omega_{s,1}^{m}} \tag{3.22}$$

Here, R_0 and m_0 represent an overall mean value that is then modified by the first year's GMRF. This initializes each knot with a different spatially autocorrelated value based on the patterns seen in the observations without having to fix the starting values.

The total recruitment and biomass can then be derived by multiplying $B_{s,t}$ and $R_{s,t}$ by the area covered by their respective knots, then summing up over all knots s to obtain a single B_t and R_t per year t.

In summary, STM1 contains the observed states $\mathbf{Y}_{s,t} = (I_{i,s,t}, I^R_{i,s,t}, L_{i,s,t})^T$, the unobserved states $\mathbf{X}_{s,t} = (B_{s,t}, R_{s,t}, m_{s,t})^T$, the fixed covariates $\mathbf{z}_{s,t} = (N_{i,s,t}, C_{s,t}, g_t, g^R_t)^T$ and the parameters $\boldsymbol{\theta} = (p_I, p^R_I, q_I, q_R, S, \sigma^2_\epsilon, \sigma^2_\upsilon, \sigma^2_\tau, R_0, m_0, \tau_R, \tau_m, \kappa_R, \kappa_m, \mathbf{H}^R_{input}, \mathbf{H}^m_{input})^T$.

Spatio-Temporal Model 2 (STM2)

The first hierarchical level of STM1 and STM2 is identical, so is not reported again. The second hierarchical level is very similar, with the processes for recruitment and mortality being identical and initialized the same way. However, the biomass process in Equation 3.18 is replaced by the following:

$$B_{s,t} = [e^{-m_{s,t}} g_{t-1}(B_{s,t-1} - C_{s,t-1}) + e^{-m_{s,t}} g^R_{t-1} R_{t-1}] e^{\Omega^B_{s,t}} \tag{3.23}$$

The error term τ_t is replaced by $\Omega^B_{s,t}$, which represents a GMRF calculated the same way as the ones described previously, with separate spatial parameters (τ_B and κ_B) and anisotropy matrix $\mathbf{H}_B$ from the other processes. The initial states for every knot is furthermore set as the following:

$$B_{s,1} = B_0 e^{\Omega^B_{s,1}} \tag{3.24}$$

The only difference between STM1 and STM2 is the removal of the independence assumption between each knot for the commercial size biomass. In summary, STM2 contains the observed states $\mathbf{Y}_{s,t} = (I_{i,s,t}, I^R_{i,s,t}, L_{i,s,t})^T$, the unobserved states $\mathbf{X}_{s,t} = (B_{s,t}, R_{s,t}, m_{s,t})^T$, the fixed covariates $\mathbf{z}_{s,t} = (N_{i,s,t}, C_{s,t}, g_t, g^R_t)^T$ and the parameters $\boldsymbol{\theta} = (p_I, p^R_I, q_I, q_R, S, \sigma^2_\epsilon, \sigma^2_\upsilon, B_0, R_0, m_0, \tau_B, \tau_R, \tau_m, \kappa_B, \kappa_R, \kappa_m, \mathbf{H}^B_{input}, \mathbf{H}^R_{input}, \mathbf{H}^m_{input})^T$. Table 3.1 summarizes and describes all parameters for all three models.

3.3 Simulation Studies

Two simulation studies were performed. The first, consisting of 4 different settings (A to D) as shown in Table 3.2, was to assess the identifiability and estimability of the proposed spatio-temporal models. The second, with three different settings (E

Table 3.1: Parameters for all 3 models with description.

Parameter	Model	Description
q_I	TM, STM1, STM2	Commercial Size Catchability
q_R	TM, STM1, STM2	Recruit Size Catchability
S	TM, STM1, STM2	Clapper catchability (FMB)
σ_τ	TM, STM1	Commercial size biomass process error
σ_ϕ	TM	Recruitment process error
σ_η	TM	Natural mortality process error
σ_ϵ	TM, STM1, STM2	Commercial size index observation error
σ_υ	TM, STM1, STM2	Recruitment index observation error
p_I	TM, STM1, STM2	Probability of positive commercial size survey tow
p_I^R	TM, STM1, STM2	Probability of positive recruit survey tow
κ_B	STM2	Biomass range parameter
κ_R	STM1, STM2	Recruitment range parameter
κ_m	STM1, STM2	Natural mortality range parameter
τ_B	STM2	Biomass spatial variation parameter
τ_R	STM1, STM2	Recruitment spatial variation parameter
τ_m	STM1, STM2	Natural mortality spatial variation parameter
$\mathbf{H}_B$	STM2	Biomass anisotropy matrix
$\mathbf{H}_R$	STM1, STM2	Recruitment anisotropy matrix
$\mathbf{H}_m$	STM1, STM2	Natural mortality anisotropy matrix
B_0	STM2	Biomass initial mean parameter
R_0	STM1, STM2	Recruitment initial mean parameter
m_0	STM1, STM2	Natural mortality initial mean parameter

Table 3.2: Difference between settings for first simulation study.

Setting	Simulating Model	Fitting Model	Status of q_I	Simulated Fishing Cover
A	STM1	STM1	Estimated	Constant Partial
B	STM1	STM1	Fixed	Constant Partial
C	STM2	STM2	Estimated	Constant Partial
D	STM2	STM2	Fixed	Constant Partial
E	STM1	TM	Fixed	Constant Partial
F	STM1	TM	Fixed	Complete
G	STM1	TM	Fixed	Moving Partial

to G) as shown in Table 3.2, aimed to test the effect of uneven spatial coverage on temporal model predictions.

3.3.1 Simulation Design

For the first study, settings A and B concerned STM1, wherein Equations 3.15 to 3.22 were used to simulate and fit data using the TMB package in R. Previous work (Chapter 2) identified q_I as one of the most difficult parameters to reliably estimate. In the first setting, q_I was estimated, while in the second it was fixed at its real value in order to identify how much improvement would be achieved by doing so. Settings C and D explored the same for STM2, replacing Equation 3.18 by Equation 3.23 and adding Equation 3.24.

For the second simulation study, settings E to G assessed the effect of commercial catch aggregation. STM1 was used to simulate data with Equations 3.15 to 3.22. After modifying the data to be on the scale for the entire area, TM was then fit using Equations 3.5 to 3.10. Setting E simulated commercial catch in a constant subset of knots, setting F simulated complete spatial coverage of the commercial catch (i.e. commercial catch at every knot), while setting G simulated commercial catch in a variable subset of knots.

Aside from commercial catch, all seven settings follow the same simulation design. The simulated area was a 50km by 50km square shown in Figure 3.4. 20 years of data with $n_t^{tows} = 100$ each year were simulated. The locations of these 2000 data points were randomly assigned across the space. The knots were then obtained based on those random locations following the same approach as with the real data. g_t and

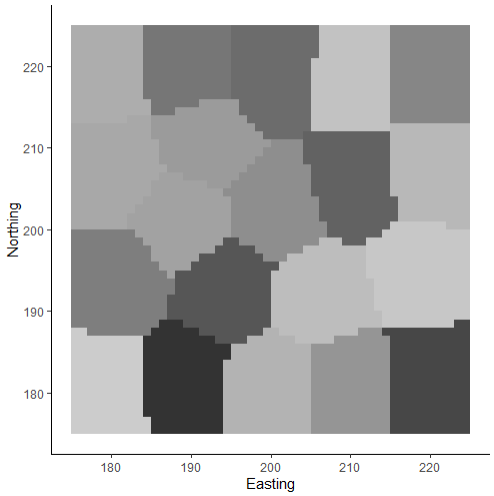

Figure 3.4: Grid for simulation experiments based on simulated locations, greyscale used simply to delineate cells and does not represent simulated value.

g_t^R were assumed constant and set at 1.1 and 1.5. The total number of live and dead scallops ($L_{i,t} + N_{i,t}$) is set to 120 in every tow. The initial states at each knot for the biomass in year 1 are left open to be predicted and are thus not obtained from the equations directly. Therefore, the initial value at each knot was simulated from a log-normal distribution with a mean of 400kg per km^2 on the natural scale with a variance of 0.1 on the log scale. The low biomass value was chosen to reduce the chance of having the population increase exponentially, while the low variance was chosen to reduce the chance of simulating strong outliers as initial states.

The parameter values chosen for the simulations along with the starting values used during optimization are shown in Table 3.3. The anisotropy parameters ($\mathbf{H}_{input}$) were chosen to simulate strong anisotropy where the decorrelation range going north-south was much larger than east-west. The true values for the spatial variability parameters τ_B, τ_R and τ_m were obtained by setting the variance of the random fields at 0.1 and range parameters κ_B, κ_m and κ_R are obtained by setting the mean decorrelation ranges of the random fields at 50km for commercial size biomass, 40km for recruitment and 20km for mortality. For STM1, the optimization starting values for the random effects for were set to 3000 for $B_{s,t}$ and 0 for all random fields ($\mathbf{\Omega}_{s,t}^R$ and $\mathbf{\Omega}_{s,t}^m$). For STM2, the optimization starting values for the random fields ($\mathbf{\Omega}_{s,t}^B$,$\mathbf{\Omega}_{s,t}^R$ and $\mathbf{\Omega}_{s,t}^m$) in STM2 were also set to 0.

For settings A to D and to mimic the spatially uneven fishing pressure present in

Table 3.3: Parameters used for simulation study and their respective optimization starting values.

STM1			STM2		
Parameter	True Value	Starting Value	Parameter	True Value	Starting Value
σ_τ	0.1	$exp(-1)$	σ_ϵ	0.1	$exp(-1)$
σ_ϵ	0.1	$exp(-1)$	σ_υ	0.1	$exp(-1)$
σ_υ	0.1	$exp(-1)$	q_I	0.3	$exp(-1)$
q_I	0.3	$exp(-1)$	q_R	0.2	$exp(-1)$
q_R	0.2	$exp(-1)$	S	0.5	$exp(-1)$
S	0.5	$exp(-1)$	p_I	0.8	$exp(-1)$
p_I	0.8	$exp(-1)$	p_I^R	0.4	$exp(-1)$
p_I^R	0.4	$exp(-1)$	B_0	400	1000
R_0	50	150	R_0	50	150
m_0	0.1	0.3	m_0	0.1	0.3
κ_R	0.0707	1	κ_B	0.0566	1
τ_R	39.8942	1	τ_B	49.8678	1
κ_m	0.1414	1	κ_R	0.0707	1
τ_m	19.9471	1	τ_R	39.8942	1
H_{input}^R	$-1.83, -0.24$	$0, 0$	κ_m	0.1414	1
H_{input}^m	$-0.56, 0.12$	$0, 0$	τ_m	19.9471	1
			H_{input}^B	$-1.23, -0.54$	$0, 0$
			H_{input}^R	$-1.83, -0.24$	$0, 0$
			H_{input}^m	$-0.56, 0.12$	$0, 0$

the SPA 3 data, presence of commercial catch was simulated as Bernoulli process with probability of 0.6 at every knot s. If commercial catch was present, each year's catch was simulated from a log-normal distribution with the mean of 20% of the biomass on the natural scale at knot s in year s and a variance of 0.1 on the log scale. This was done to simulate an overall exploitation rate a little higher than 10% every year and avoid simulating negative biomass, a common issue for these types of models (Yin et al., 2019; Best and Punt, 2020). If there was no catch present in the first year at a knot, commercial catch was kept at 0 there for the rest of the simulation.

The starting values for TM used in setting E to G are shown in Table 3.4. Setting E simulated an uneven spatial distribution of catch, with the presence of catch simulated as Bernoulli process with probability of 0.6 at each knot s. This was only done in the first year, meaning that knots with simulated fishing effort were fished across the entire time lapse while other knots were never fished. If commercial catch was present, each year's catch in knot s was simulated from a log-normal distribution with the mean at 10% of the biomass on the natural scale at that knot in year t and a variance of 0.5 on the log scale. Setting F simulated a complete spatial coverage of the commercial catch with each knot's catch simulated from log-normal distribution with the mean at 20% of the biomass on the natural scale at that knot in that year and a variance of 0.5 on the log scale. Setting G simulated the presence of catch through a Bernoulli process with probability of 0.6. This was done separately for every year, simulating a partial spatial cover of fishing effort but one that moved every year. If commercial catch was present, each year's catch in a knot was simulated from a log-normal distribution with the mean at 20% of the biomass on the natural scale at that knot in that year and a variance of 0.5 on the log scale. This way, all of them had an overall exploitation rate around 10%, but only the spatial coverage of it differed. The catchability q_I was fixed at 0.3 for the estimation process using TM for all three experiments.

Simulation Results

Since both STM1 (settings A and B) and STM 2 (settings C and D) behaved similarly, only the results from settings A and B are presented here with Figures for settings C and D shown in Appendix B.

Table 3.4: Parameter optimization starting values set for TM before model fitting attempts.

Parameter	Starting Value
σ_τ	$exp(-1)$
σ_ϕ	$exp(-1)$
σ_η	$exp(-1)$
σ_ϵ	$exp(-1)$
σ_υ	$exp(-1)$
q_I	$exp(-1)$
q_R	$exp(-1)$
S	$exp(-1)$
p_I	0.5
p_I^R	0.5

For settings A to D, 200 simulations were run for each and every single run converged. Some fits were unsuccessful in estimating the spatial parameters correctly and would estimate them at non-sensical values with massive standard errors. Due to this, any simulations where the anisotropy parameters were estimated below -5 or above 5 (which are already unrealistic bounds) were not included in the results. Using this new definition, 36 simulations were rejected for setting A, 24 for setting B, 37 for setting C, and 54 for setting D. This implies that convergence is not a sufficient criterion to assess fitting success when applied to real data and closer examination is necessary. However, it is easy to identify parameter estimates far from their true value since they were all associated with standard errors larger than their point estimates, indicating that the model did not reliably estimate them.

Figure 3.5 shows the distribution of parameter estimates for simulations from setting A where q_I is estimated. Variance, probability and catchability parameters are recovered with high accuracy. The spatial parameters appear more difficult to estimate, but are still generally well recovered. Fixing q_I does not show any clear improvement in parameter estimations as seen in Figure 3.6.

The median difference at every knot in every year for the biomass density shown in Figure 3.7 is very small and does not show any particular pattern. STM1 is able to recapture the true values very well with minimal errors. The positive bias, wherein the biomass is too high everywhere, is driven by issues estimating q_I since it disappears

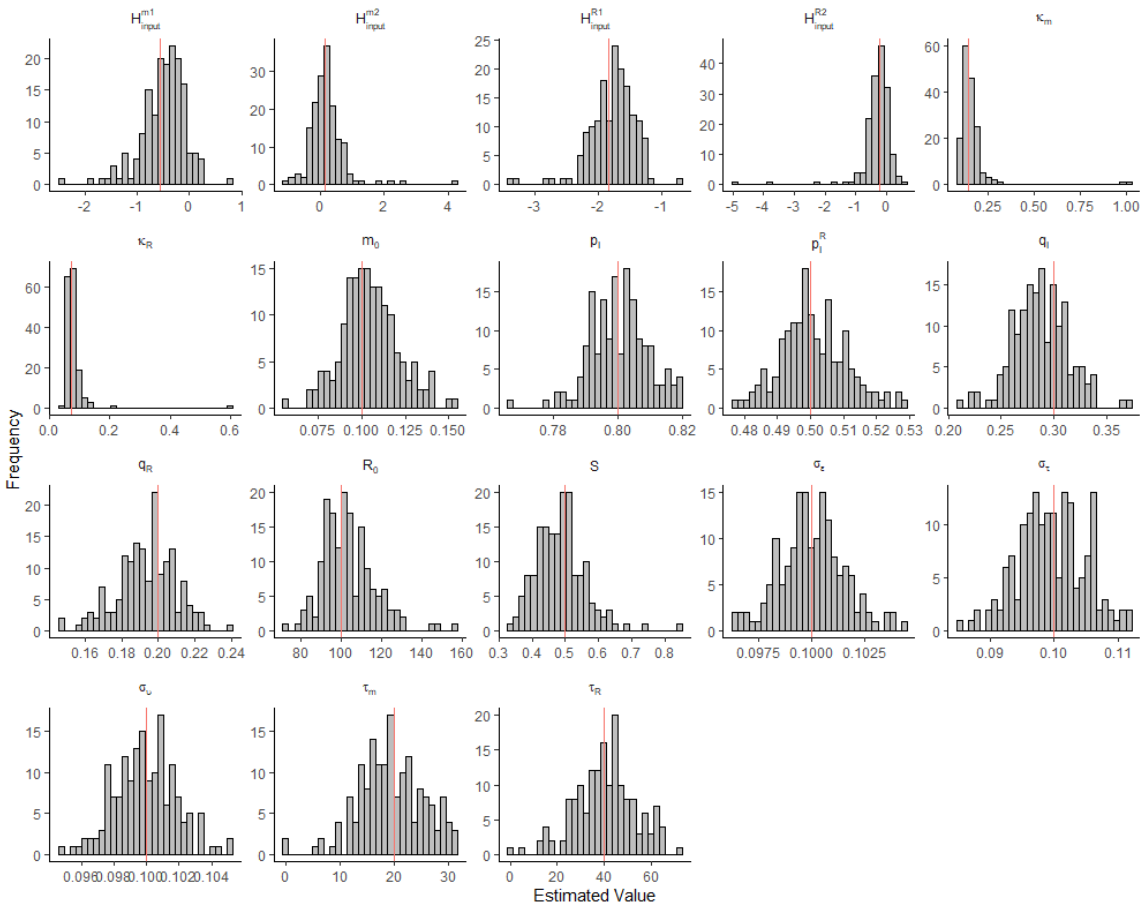

Figure 3.5: Histograms of parameter estimates from successful simulations from setting A. Red line denotes true value.

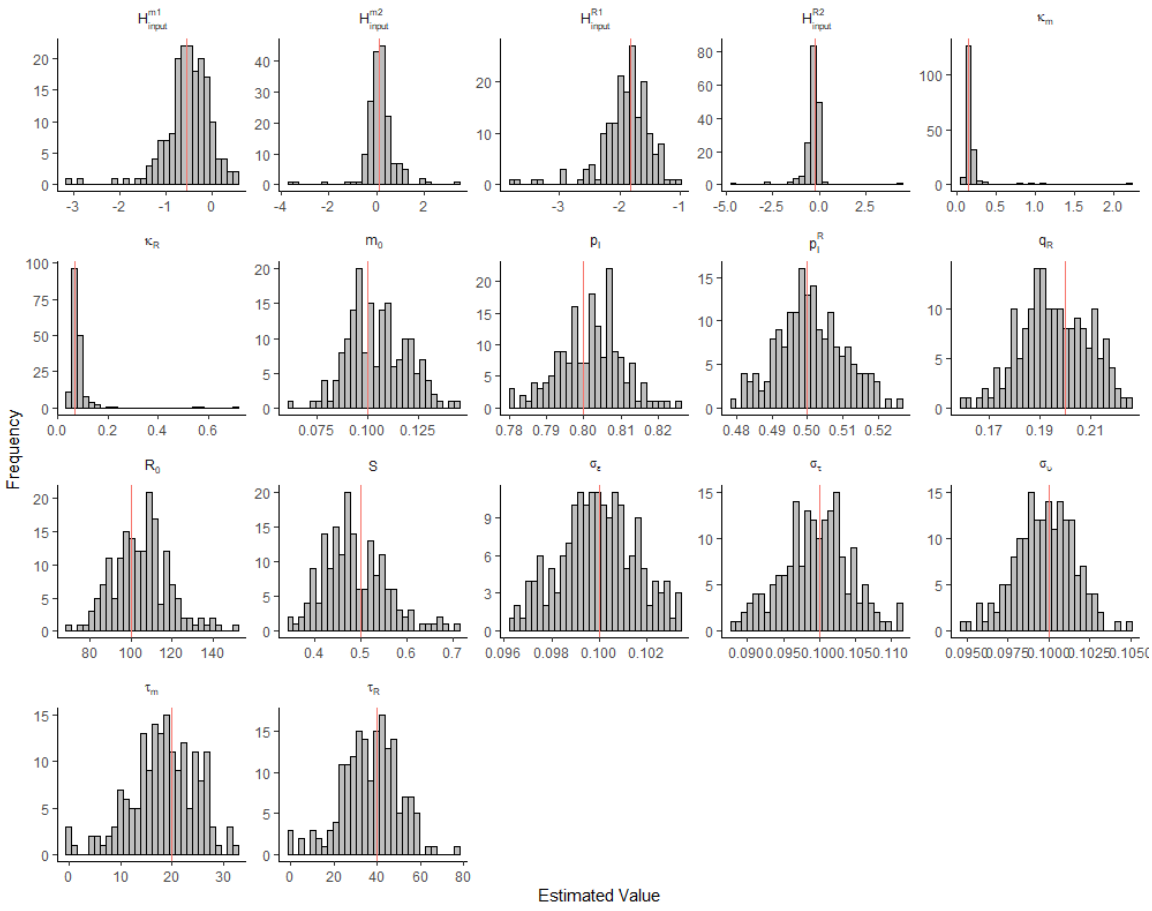

Figure 3.6: Histograms of parameter estimates from successful simulations from setting B. Red line denotes true value.

Figure 3.7: Median percent difference biomass density ((predicted-true)/true) at every knot for every year for successful simulations of setting A.

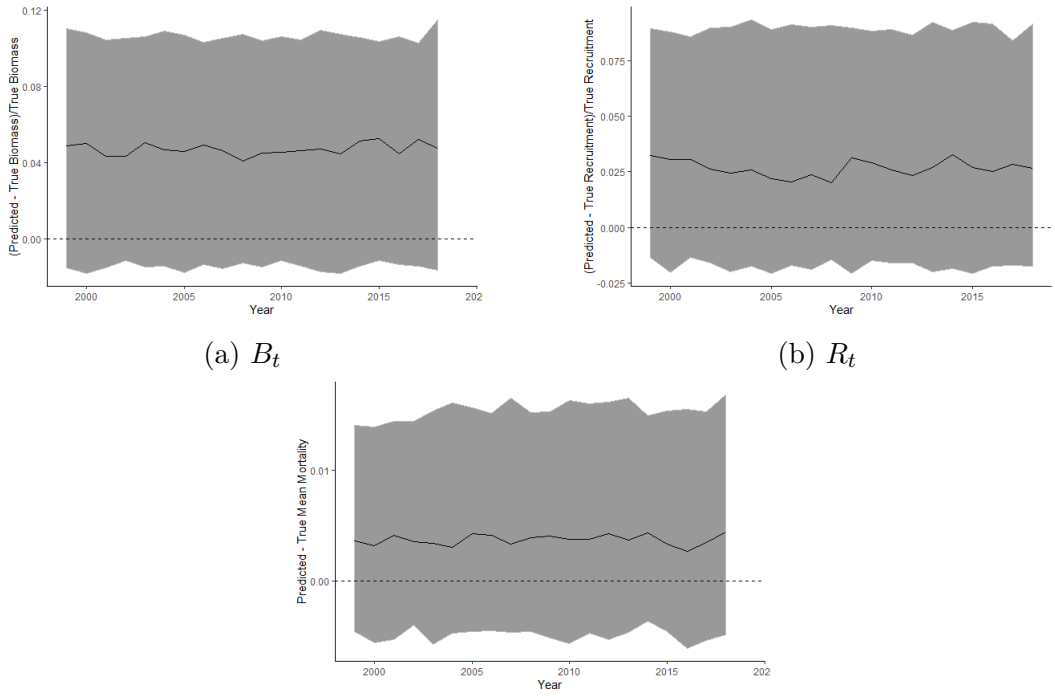

(a) B_t

(b) R_t

(c) m_t

Figure 3.8: Functional boxplots (without whiskers) of the difference of the predicted processes and their true value with horizontal dotted line at 0 and median difference shown by solid black line from setting A. 3.8a and 3.8b show the difference as a percentage of the true value (predicted - true / true) while 3.8c simply shows the net difference (predicted - true).

when it is fixed (figures in Appendix B). The results are consistent for the recruitment and mortality, and for STM2. These figures are shown in Appendix B.

The Nova Scotia scallop fishery uses a management approach based on a Total Allowable Catch (TAC), which sets the maximum amount of landings that the commercial fleets are allowed to catch in a given year (Nasmith et al., 2016). This type of approach currently requires a single prediction for the total amount of biomass over the entire area. It is therefore essential that the spatial models can reliably predict the population biomass for the entire area, which is what we focused on for these simulations.

Figure 3.8 shows the functional boxplots (Sun and Genton, 2011) without whiskers of the difference between the predicted processes (biomass, recruitment and natural mortality) and their simulated true value. B_t and R_t are obtained by multiplying each $B_{s,t}$ and $R_{s,t}$ by the area covered by their respective knot s before summing

across all knots. m_t is obtained by simply taking the mean of all $m_{s,t}$ across knots s. All 3 processes exhibit slight positive bias, most likely driven by the catchability estimates since this bias consistent over time. The second simulation experiment (Figures in Appendix B), where the bias for B_t is completely eliminated, supports this. Both models fully capture the temporal trends for all three processes. Unlike the strictly temporal random walks studied in Chapter 2, the populations simulated through log-normal random walks did not show any tendency to decrease Lewontin and Cohen (1969) on the time scales analyzed here, but only when they were simulated on significantly longer and unrealistic time scales (e.g. 200 years). Figures showing examples of these simulated populations are shown in Appendix B.

For settings E to G, 200 simulations were also run for each. For setting E, all of them converged. For setting F, 11 runs could not work because the simulated catch was too high for the optimization starting values to run the initial step. All simulations converged for setting G. However, a significant amount of simulations led to non-sensical parameter estimates, often arbitrarily close to 0 and with standard errors orders of magnitude larger than their point estimates. Since the goal of this study was to examine the effect of the spatial cover of fishing effort and not the estimability of the models, successful simulations were therefore defined as those that contained no standard errors larger than 1.2 times their point estimate. We chose this much narrower definition of success to only examine the ones where the model gives the impression that it captured the trends reliably. The value of 1.2, while somewhat arbitrary, was chosen since it would only include the simulations where the model was highly confident in its estimates. Using this more stringent definition of success, 26 models were considered successful for settings E, 8 for setting F, and 26 were successful for setting G.

Figure 3.9 shows the difference between the predicted processes and their true value when fitting TM to explicitly spatial data when the commercial catch only covers a constant portion of the area, while Figure 3.10 shows the same variables when the simulated commercial catch covers the entirety of the space. Figure 3.11 shows the same variables when the simulated commercial catch covers a variable portion of the area. Since all experiments followed an identical design except for the commercial catch, it stands to reason that the differences seen in Figures 3.9 to 3.11

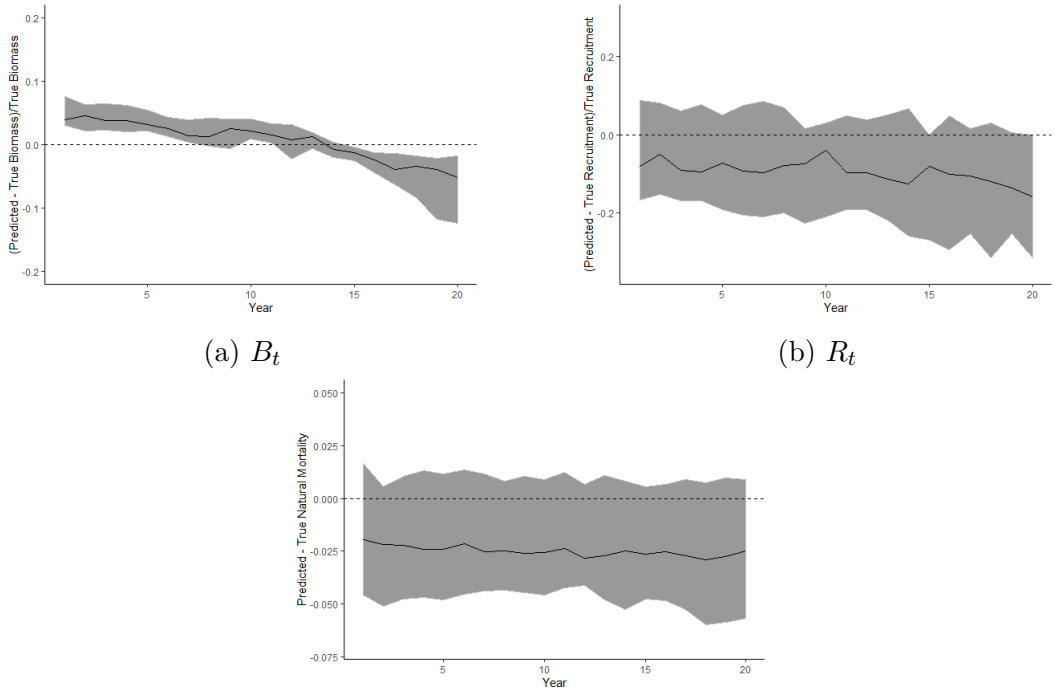

(a) B_t

(b) R_t

(c) m_t

Figure 3.9: Functional boxplots (without whiskers) of the difference of the predicted processes and their true value for setting E, with horizontal dotted line at 0 and median difference shown by solid black line. All panels simply show the difference between the predicted process and the true value.

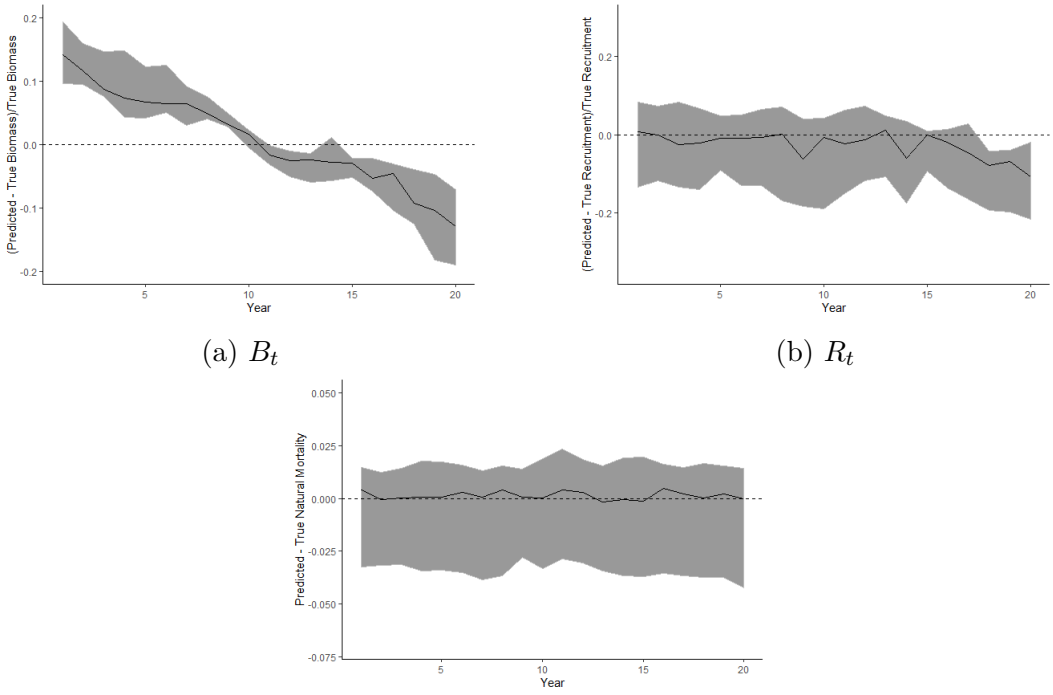

(a) B_t

(b) R_t

(c) m_t

Figure 3.10: Functional boxplots (without whiskers) of the difference of the predicted processes and their true value for setting F, with horizontal dotted line at 0 and median difference shown by solid black line. All panels simply show the difference between the predicted random effect and the true value.

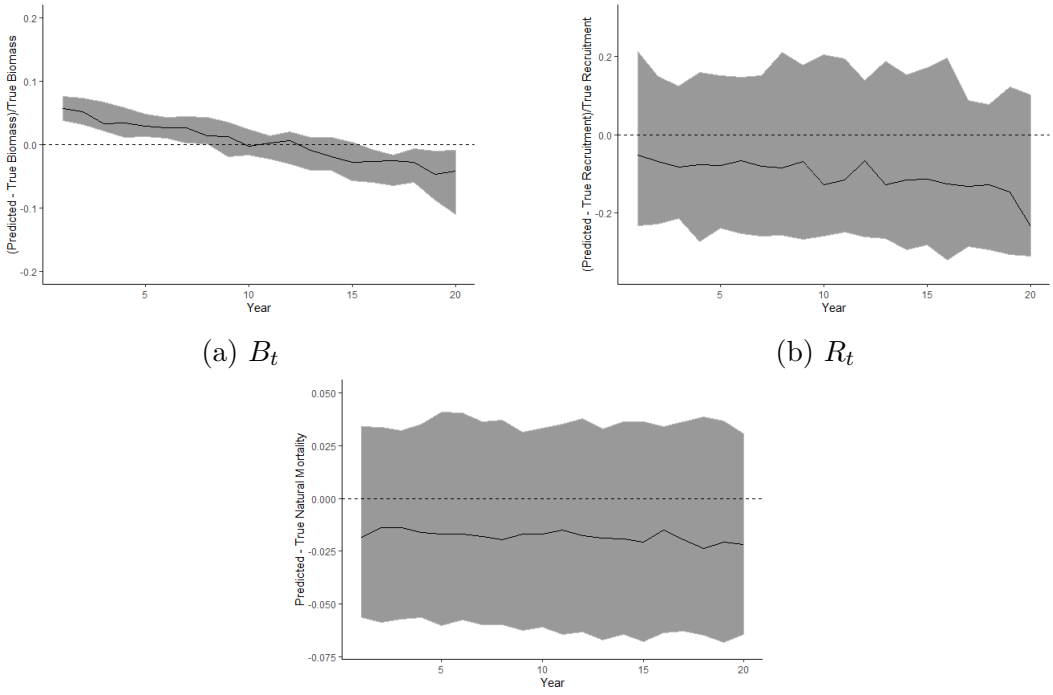

(a) B_t

(b) R_t

(c) m_t

Figure 3.11: Functional boxplots (without whiskers) of the difference of the predicted processes and their true value for setting G, with horizontal dotted line at 0 and median difference shown by solid black line. All panels simply show the difference between the predicted random effect and the true value.

are only caused by differences in commercial catch.

The trend in the predicted biomass bias is worrying since its cause is not clear. The predicted biomass is positively biased at the start of the time-series, but this bias steadily decreases until it flips into the negative as time goes on. Preliminary runs with different simulation values of different parameters or fixed covariates did not help elucidate why this is happening. Furthermore, other tests with longer time-series presented an identical pattern where the lack of bias would appear at the midpoint. This hints that fitting a temporal model to explicitly spatial data might result in persistent bias in future predictions, but that adding years does not strongly impact the amount of bias.

The impact of the spatial coverage of fishing effort is of great interest. Having a complete spatial coverage reduces the persistent bias in predicted biomass by an order of magnitude. This indicates that predictions from an aggregated temporal model over spatial data might not be too far off the mark as long as it only models the area covered by the commercial catch, such as is currently done in the SPA 3 stock assessment (Nasmith et al., 2016). This complete coverage of commercial catch appears to cause the natural mortality and the recruitment to become confounded. Interestingly, if the spatial coverage of the fishing effort moves around, the bias is also dramatically reduced, albeit to a slightly lesser extent than consistent partial coverage. It appears that it is not the percent coverage of the fishing effort that matters most, it is its temporal persistence that impacts the bias of the temporal model output.

3.4 Application to Scallop Data

Since the survey data was available from 1996 to 2018, a request was made to obtain spatially indexed fishing logbooks from 1995 to 2018, but the locations of these fishing trips were only available from 1998 to 2018. Furthermore, it was discovered during preliminary analyses that an almost complete spatial coverage of the area by the survey data in the initial year was necessary for STM1 and STM2 to converge. Since there were no tows in St-Mary's Bay between 1996 and 1998, the fishery was only modeled from 1999 to 2018. All 3 models were fit twice using the Template Model Builder (TMB) package in R using the *nlminb* optimizer, once with q_I fixed at 0.3

Table 3.5: Parameter estimates for TM, STM1 and STM2 fit to Scallop Production Area 3 (standard error in parentheses).

TM		STM1		STM2	
Parameter	Estimate	Parameter	Estimate	Parameter	Estimate
σ_τ	0.234(0.051)	κ_R	0.070(0.019)	κ_B	0.068(0.013)
σ_ϕ	0.241(0.062)	τ_R	17.047(7.185)	τ_B	18.571(5.072)
σ_η	0.553(0.085)	κ_m	0.141(0.018)	κ_R	0.070(0.020)
σ_ϵ	1.176(0.016)	τ_m	2.329(0.382)	τ_R	16.641(7.202)
σ_υ	1.078(0.024)	σ_τ	0.265(0.030)	κ_m	0.142(0.018)
q_I	$1.25X10^{-7}(3.25X10^{-5})$	σ_ϵ	1.050(0.015)	τ_m	2.311(0.377)
q_R	$2.95X10^{-10}(7.68X10^{-6})$	σ_υ	0.924(0.022)	σ_ϵ	1.059(0.015)
S	0.242(0.138)	S	0.571(0.105)	σ_υ	0.924(0.022)
p_I	0.910(0.005)	q_R	0.146(0.224)	S	0.628(0.121)
p_I^R	0.358(0.009)	q_I	0.087(0.124)	q_R	$42.952(1.198X10^6)$
		R_0	47.847(74.252)	q_I	$8.57X10^8(7.29X10^5)$
		m_0	0.029(0.013)	R_0	$0.1627(4.54eX10^3)$
		p_I	0.913(0.005)	B_0	$3.76X10^9(3.20X10^{12})$
		p_I^R	0.359(0.009)	m_0	0.029(0.013)
		H_{input}^{R1}	−1.83(0.585)	p_I	0.913(0.005)
		H_{input}^{R2}	−0.237(0.440)	p_I^R	0.359(0.009)
		H_{input}^{m1}	−0.561(0.228)	H_{input}^{B1}	−0.854(0.447)
		H_{input}^{m2}	0.118(0.214)	H_{input}^{B2}	−0.779(0.525)
				H_{input}^{R1}	−1.871(0.599)
				H_{input}^{R2}	−0.244(0.449)
				H_{input}^{m1}	−0.563(0.227)
				H_{input}^{m2}	0.124(0.213)

and once estimating q_I. The choice of 0.3 was made because it matched the original best estimate of the Bayesian model (Chapter 2) and was also reasonably close to the estimated efficiency of similar types of gear to the same species, albeit out in the open ocean (Gedamke et al., 2004; Miller et al., 2019). Unlike previous work (Chapter 2), all models are fit to the entirety of the area instead of strictly St-Mary's Bay and the Inside VMS strata (Nasmith et al., 2016).

For TM, the same starting values shown in Table 3.4 were used, with optimization starting values set to $10max(I_{i,t})$ for B_t, $10max(I_{i,t}^R)$ for R_t and 0.3 for m_t. For STM1, the optimization starting values shown in Table 3.3 were used, with optimization starting values set to 3000 everywhere for B_t and the starting values for all random fields ($\mathbf{\Omega}_{s,t}^R$ and $\mathbf{\Omega}_{s,t}^m$) set to 0. STM2 also uses the optimization starting values shown in Table 3.3 with the optimization starting values for all random fields ($\mathbf{\Omega}_{s,t}^B$,$\mathbf{\Omega}_{s,t}^R$ and $\mathbf{\Omega}_{s,t}^m$) set to 0. Every model converged successfully.

Table 3.6: Parameter estimates for TM, STM1 and STM2 fit to Scallop Production Area 3 when q_I is fixed to 0.3 (standard error in parentheses).

TM		STM1		STM2	
Parameter	Estimate	Parameter	Estimate	Parameter	Estimate
σ_τ	0.242(0.052)	κ_R	0.069(0.018)	κ_B	0.081(0.015)
σ_ϕ	0.240(0.062)	τ_R	17.591(6.922)	τ_B	13.575(3.499)
σ_η	0.553(0.085)	κ_m	0.141(0.018)	κ_R	0.074(0.022)
σ_ϵ	1.176(0.016)	τ_m	2.327(0.382)	τ_R	15.598(6.743)
σ_υ	1.078(0.024)	σ_τ	0.263(0.030)	κ_m	0.141(0.018)
q_R	0.060(0.058)	σ_ϵ	1.051(0.015)	τ_m	2.321(0.382)
S	0.246(0.148)	σ_υ	0.925(0.022)	σ_ϵ	1.058(0.016)
p_I	0.910(0.005)	S	0.541(0.093)	σ_υ	0.922(0.022)
p_I^R	0.358(0.009)	q_R	0.164(0.083)	S	0.555(0.131)
		R_0	42.104(23.058)	q_R	0.099(0.103)
		m_0	0.025(0.011)	R_0	68.981(71.483)
		p_I	0.914(0.005)	B_0	1069.17(210.65)
		p_I^R	0.359(0.009)	m_0	0.024(0.011)
		H_{input}^{R1}	−1.714(0.535)	p_I	0.914(0.005)
		H_{input}^{R2}	−0.230(0.427)	p_I^R	0.359(0.009)
		H_{input}^{m1}	−0.563(0.229)	H_{input}^{B1}	−0.984(0.475)
		H_{input}^{m2}	0.116(0.214)	H_{input}^{B2}	−0.324(0.387)
				H_{input}^{R1}	−1.772(0.594)
				H_{input}^{R2}	−0.246(0.440)
				H_{input}^{m1}	−0.563(0.227)
				H_{input}^{m2}	0.122(0.213)

For the fits estimating q_I, all variance and spatial parameters shown in Table 3.5 are estimated reliably for all models, but none of them are able to get reliable estimates of q_I or q_R. The q_I estimate from TM is significantly worse than shown during the temporal analysis (Chapter 2), with the only differences being spatial coverage and length of time series. Anisotropy parameters are difficult to interpret on their own, but the estimated standard errors are in reasonable spaces.

As seen in Table 3.6, fixing q_I to 0.3 only impacts parameters related to the magnitude of commercial size biomass and recruit such as q_R, B_0 and R_0. All other parameters are almost identical.

Figure 3.12 shows that natural mortality is not correlated at very high distances,

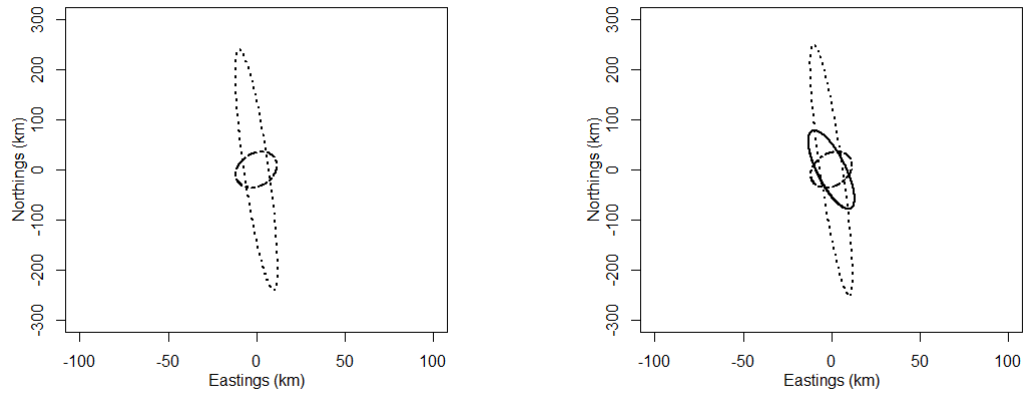

(a) STM1 (b) STM2

Figure 3.12: Decorrelation ranges in all directions for biomass (solid line), recruitment (dotted line) and natural mortality (dashed line) processes for both STM1 and STM2.

while recruitment is very highly correlated following the bathymetry of SPA 3 at ranges larger than the area itself, but decorrelates rapidly from east to west. Biomass presents a similar pattern to recruitment but decorrelates more rapidly when it is explicitly modeled spatially.

Figures 3.13 to 3.15 shows the predicted biomass density $B_{s,t}$, recruitment density $R_{s,t}$ and survival $e^{-m_{s,t}}$ at all knots between 1999 and 2018, with their respective predictions for 2019 for the biomass and natural mortality using STM1 with q_I fixed at 0.3. Due to the absence of any data in 2019, the predicted mortality is identical to 2018. The patterns predicted by STM2 are extremely similar and are not reported here (Figures in Appendix B). The figures showing the standard errors for Figures 3.13 to 3.15 are all presented in Appendix B.

The knots with a high commercial size biomass density are generally the same knots that are more intensely fished, as seen in Figure 3.3. There are three recurring hot spots of biomass: a specific section in the south-west, the nearshore areas and the tip of St-Mary's Bay. Recruitment is sparse and patchy aside from two notable events, the first in the south-west in 2000-2001 and one at the tip of St-Mary's bay in 2015. Outer sections of the area consistently show lower survival, with the rest of the knots presenting patchy but generally high survival.

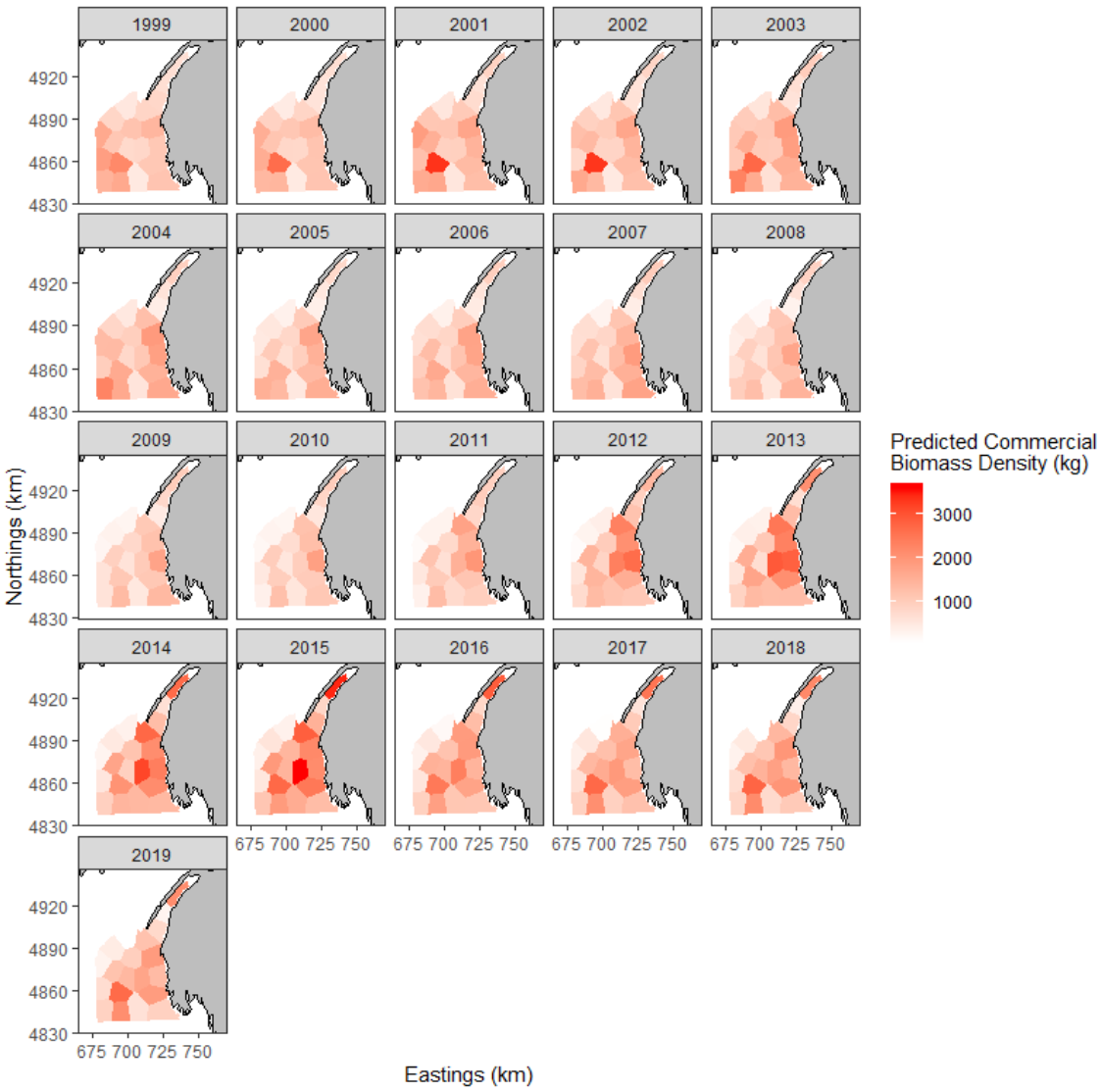

Figure 3.13: Predicted commercial size biomass density (kg/km^2) at each knot between 1999 and 2019.

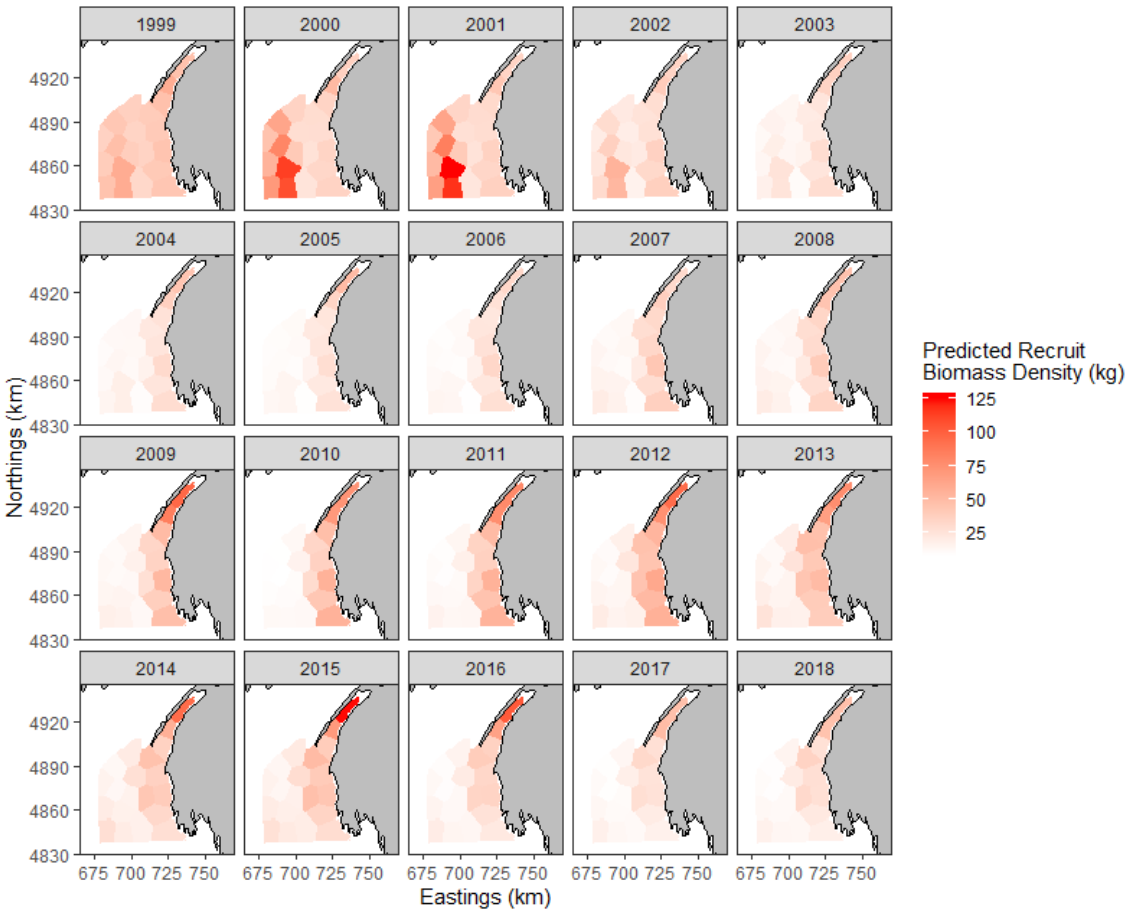

Figure 3.14: Predicted recruit biomass density (kg/km^2) at each knot between 1999 and 2018.

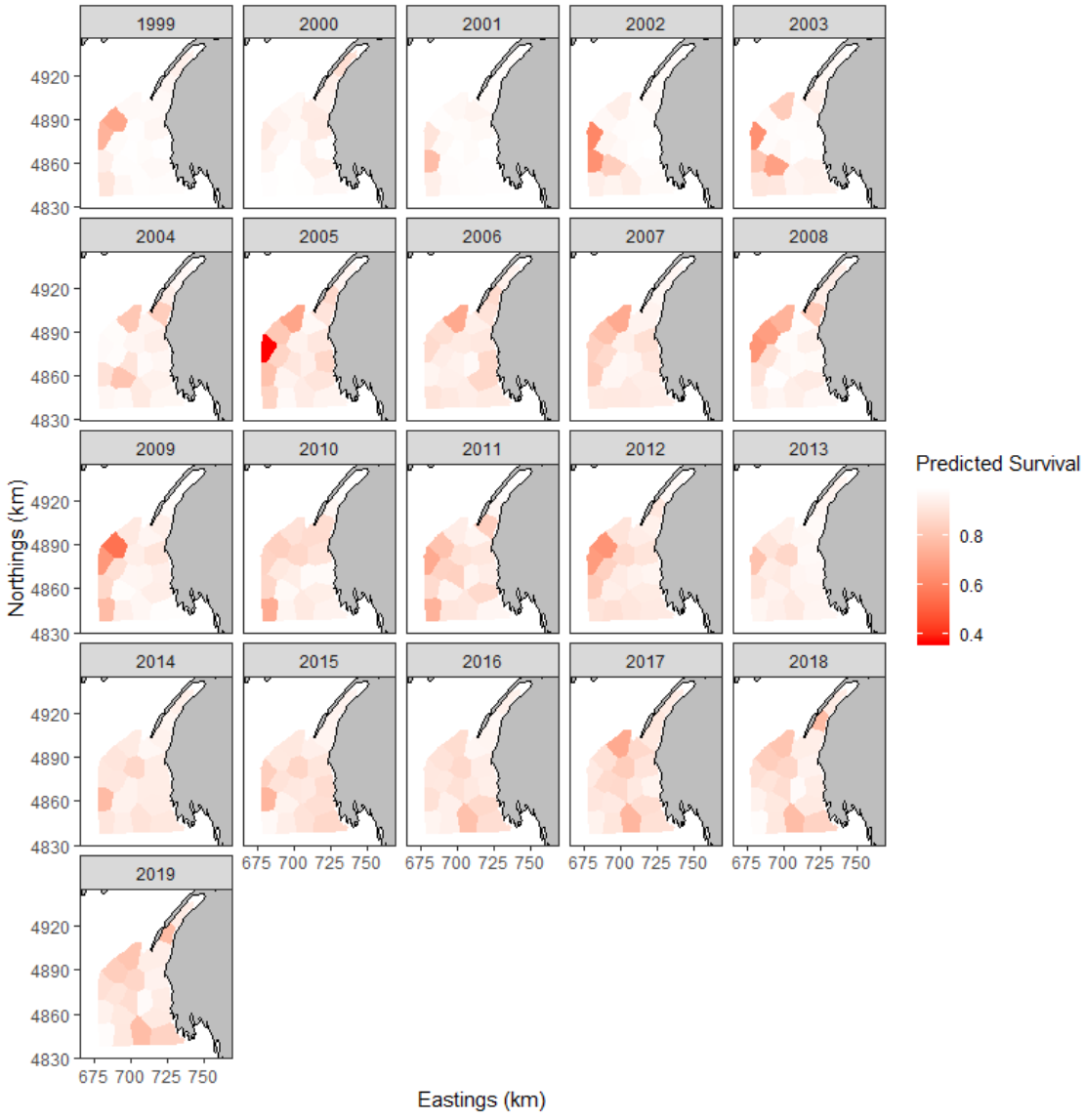

Figure 3.15: Predicted survival at each knot between 1999 and 2019.

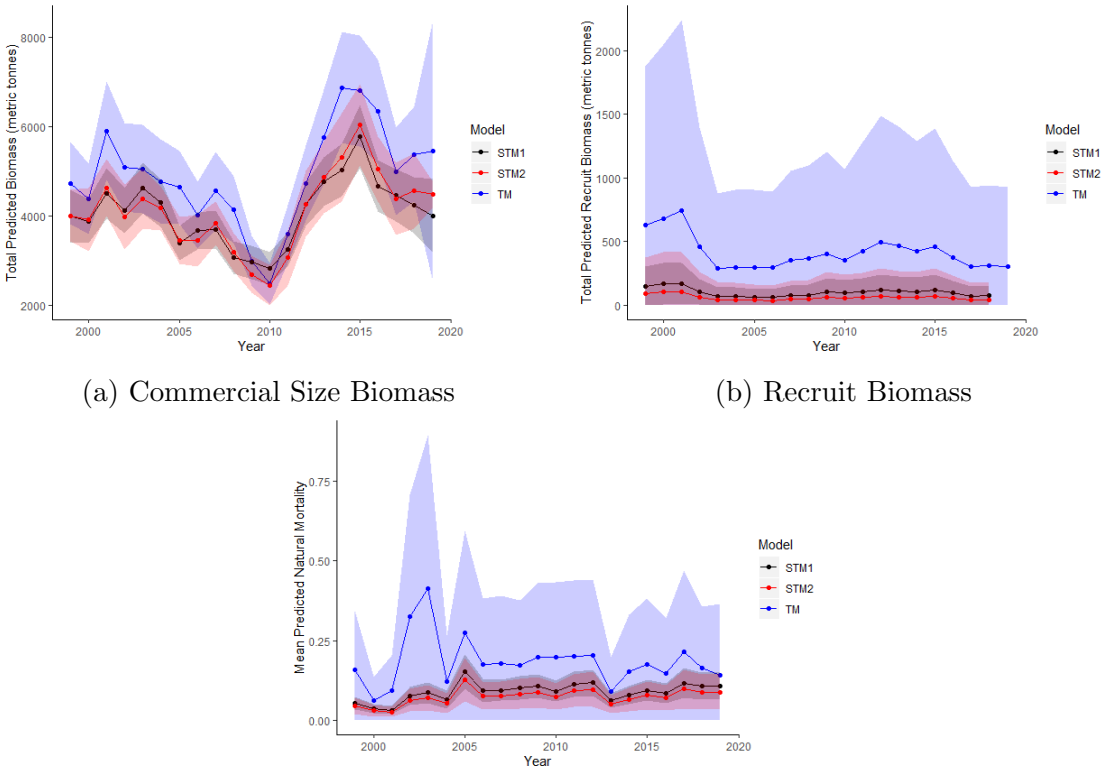

(a) Commercial Size Biomass

(b) Recruit Biomass

(c) Natural Mortality

Figure 3.16: Predicted total biomass, total recruitment and mean natural mortality for SPA 3 from TM (blue), STM1 (red) and STM2 (black). Envelopes represent interpolated point-wise 95% confidence intervals.

Figure 3.16 shows the predicted total biomass, recruitment and the mean natural mortality for SPA 3. The envelopes represent the 95% confidence interval based on the exponentiated bounds constructed on the log scale (prediction $\pm$ 1.96 standard error). While not as rigorous as other methods (e.g. bootstrapped standard errors) these intervals simply aim to give an idea of the variability of these predictions.

All three models are extremely similar in their prediction for total biomass with highly similar uncertainties. The general pattern of population change is captured well by all three models. Both spatio-temporal models predict drastically lower recruitment and natural mortality than TM, which consistently captures a higher temporal variability than either STM1 or STM2. STM1 and STM2 indicate that population changes are mostly related to growth of adult size scallops instead of the productivity, which seems to drive TM. The recruitment predicted by STM2 has a much larger uncertainty, which is caused by the large uncertainty around the estimate of q_R. However, although they both present relatively smooth lines for recruitment and mortality, both of these processes have a clear spatial structure. While the recruitment event in 2000-2001 is clearly reflected in the prediction for TM, it is restricted to a couple grid cells in both STM1 and STM2 and is not strongly affecting the total recruitment. A similar pattern is exhibited by the natural mortality, but the overall mean mortality stays near 0.1. This is consistent with what is known of this species (Merrill and Posgay, 1964).

The uncertainty for TM expands greatly when predicting 1 year forward into 2019, while the uncertainty predicted by STM2 shrinks. Since the random fields between years are not correlated in any way, the model simply assumes that the error structure in 2019 is identical to 2018 without error, which arbitrarily shrinks the uncertainty around the biomass. The uncertainty predicted by STM1 expands slightly, but nowhere near as much as TM. This makes sense since STM1 predicts the uncertainty of a derived quantity obtained from 20 predicted points, while TM has to predict the uncertainty of a single point which has to be more variable.

3.5 Discussion

A clear relation between the bathymetry and the abundance of scallops is apparent, with both spatio-temporal models predicting higher biomass in nearshore areas and

St-Mary's Bay. Furthermore, these areas generally line up with areas that are under a much higher fishing pressure. This demonstrates the reliability of STM1 and STM2, since fishing effort tends to focus on areas of higher density (Smith et al., 2017), therefore the areas with highest biomass are expected to be under the highest fishing pressure. While STM2 was expected to be successful at modeling SPA 3, it is likely that the similar success of STM1, which has no spatial structure on the commercial biomass, is caused by the sedentary nature of scallops.

It is surprising, given the results of the simulation study, just how closely the three models concur in their predictions of biomass. It appears that, although fishing effort is highly aggregated, it does not completely ignore certain areas and has moved around over time. It therefore seems likely that the bias present in the temporal predictions is minimal. All of them indicate that the population across the entirety of SPA 3 has been relatively stable over time. However, the spatial models clearly show how the distribution and areas of peak density have shifted over time. Nearshore areas have always tended towards higher abundances, but a specific spot in the south-west has gone from extremely high density (from an extreme recruitment event in 2000-2001) to relatively low, before increasing again in recent years. These clearly appear to be the most important scallop beds for the area, and coincide with the area that is currently modeled by DFO for the stock assessment. Since that model (described in Chapter 2) does not account for any spatial information, subsetting the area with the populations of highest interest appears to have been an enlightened decision and highlights why this stock has been managed so successfully.

While TM might capture the temporal population changes well, it does not predict the productivity of the whole area to be anywhere near the same as the spatio-temporal models. Both STM1 and STM2 predict a low, relatively constant recruitment over time when taken across the entire space accompanied with a low, steady natural mortality. TM, on the other hand, predicts wildly variable recruitment and natural mortality. The large spikes predicted by TM can be seen from the STM1 and STM2 results, but only if one looks at individual areas. The massive recruitment spike in 2000-2001 was a local spike in the south-west portion of SPA 3, but was not reflected elsewhere. The spikes in natural mortality further match up with larger death events on the margins of SPA 3, which were also localized events. Just a few

outlying observations appear to be enough to pull TM in strong directions, while they are appropriately attributed to only local areas for the spatio-temporal models. It seems unreasonable to extrapolate from these localized events to the whole area, but non-spatial models have no easy way of avoiding this extrapolation. However, these outliers are very useful to identify productivity hot spots. Fishing pressure also responds to these events rapidly, which is reflected by the vast majority of the commercial catch in 2003 being localized to the same area as the recruitment spike 2 years prior.

The key factor here is that these spatio-temporal models are fully able to track local changes in population abundance without the presence of any covariates or predictors. Incorporating spatial-autocorrelation in the productivity processes or in all of the processes appears to capture the underlying spatial pattern. This pattern could be related to habitat suitability (Smith et al., 2017), growth rates (Smith and Rago, 2004) or larval retention (Tremblay and Sinclair, 1988), all of which would require extensive work and investment to obtain reliable information about them. While including them in a model would likely improve its accuracy, these models show that one can harness these latent spatial patterns without extensive information about the ecosystem in which these populations evolve.

The main lingering issues are the estimability of the parameters related to the population magnitude (q_I and q_R, which lead to issues with B_0 and R_0). While fixing a parameter based on sensible values has the advantage of making any assumption explicitly clear, it removes any uncertainty around these parameters. Many other approaches could be used to deal with this estimability issue, such as priors in a Bayesian framework. There were attempts, in preliminary model formulations, to explicitly model the catchability spatially, temporally or spatio-temporally, but these approaches were all unsuccessful in improving catchability estimates. The information to estimate these parameters in the temporal version of this model usually comes from the interplay between the index of abundance and the commercial landings (Chapter 2). Given that more information on this interplay became available, it was thought that splitting up the area would facilitate the estimation of these catchabilities. This has instead introduced much more variability into this relationship, which the models are unable to deal with. The simulation experiments, where the commercial landings

do not vary as much as the real data, were able to reliably recapture them. It is possible, since adding random fields to the biomass hindered the estimation of catchabilities, that the model is slightly overparameterized in this case. It is also likely that having data for a longer time-frame would help stabilize these estimates, especially for STM1. However, the vast majority of fisheries do not have the extensive time-series and data to reliably do so (Costello et al., 2012).

To help improve the estimability of the catchability parameters, the first thought would be to attempt to explicitly model the commercial landings. For example, one could implement an observation equation to model the catch through some form of the Baranov catch equation or based on effort dynamics (e.g. Thorson et al., 2013; Yin et al., 2019). Unfortunately, this did not help the TM fit in this area (Chapter 2). Furthermore, modeling the commercial catch would likely involve incorporating uncertainty in the landings reported, which can be unnecessary in a fishery where the reported landings are considered highly reliable (Nasmith et al., 2016). However, that is not to say that there is no uncertainty associated to them, especially in this spatio-temporal setting. Each logbook record represents an individual trip from an individual fishing vessel, and only has a single location associated with it. That does not mean that every single scallop caught on this fishing trip was caught at that location, it instead represents an area that was covered during this trip. The actual spatial cover of each trip is unknown, and while the resolution chosen here likely accounts for this in some way, fishing trips near the edges of the grid cells likely captured some scallops in neighboring cells. It is therefore possible that explicitly modeling this might help catchability estimates. Since it has been shown that spatial coverage of fishing effort is related to the productivity of the local area (Caddy, 1998; Smith et al., 2017), placing some constraint or structure on this commercial catch to explicitly link it to the recruitment process might also be an avenue worth exploring.

STM1 and STM2 are very similar, which begs the question as to why two models were created. The initial setup mostly focused on STM2, but its issues with the catchability parameters prompted the creation of STM1 to see if fewer parameters might realistically improve these estimates. While it wasn't fully successful in that endeavor, the estimate of q_I obtained by STM1 was not as biologically unreasonable as the estimate from STM2, which seemed to indicate that STM2 might be suffering

from overparameterization when it comes to fitting SPA 3. While fixing q_I solves that issue, including both models seemed advisable for a couple reasons. First, as stated before, a lot of fisheries do not have access to long time-series so a simpler model with fewer parameters might be more practical. Second, it suggested the reliability of both models since they both predicted similar patterns. Finally, while STM1 is clearly applicable to sedentary shellfish species or groundfish species whose distribution is relatively constant, its applicability to motile fish species is less clear. Therefore, we felt that STM1 would be great to assess the status of more sedentary species when fewer years of data are available, but that STM2 is a better model for non-sedentary species and overall better if one has enough data or low variability in commercial catch.

While they successfully model the highly variable SPA 3, there are multiple ways in which STM1 and STM2 could be modified to incorporate other important factors related to scallop biology. Specifically for STM2, some reasonable correlation between the random fields in each year would need to be implemented for its predictions a year forward to be reliable. For both STM1 and STM2, more realistic processes for the natural mortality or the recruitment could be examined. A stock-recruitment relationship could be incorporated, which has been done to some success with other stocks of the same species (McGarvey et al., 1993). Given more environmental information, it would be possible to explicitly model the environmental effects on natural mortality. Furthermore, the probability of capturing commercial size or recruit scallops could be modified using similar spatial methods to explicitly predict a different probability at each knot based on these same environmental variables. The effect of habitat suitability on the scallop themselves and on the fishing pressure, which have been clearly demonstrated (Smith et al., 2017), could be incorporated. This could be related directly to the probability of capturing scallops, to the commercial fishing and to the catchabilities. Finally, having constant growth parameters across the entirety of SPA 3 seems unreasonable, since it has been shown that the biomass growth is affected by environmental factors that change over space (Smith et al., 2001). Since these are not taken into account, it is possible that the models overestimate the biomass in poorer habitats. The common trend here is that extensive work needs to be done to obtain information related to most of these variables for them to be

included in SPA 3 and its resulting management.

The regulations and management of the scallop population of SPA 3 is already implicitly spatial, in that decisions are based on strictly modeling the areas where fishing pressure is or has been highest (Nasmith et al., 2016). While questionable on a surface level, this work demonstrates how this approach has likely led to high-quality and reliable predictions and has led to the sustainability and health of the scallop population in the area (Nasmith et al., 2016). However, this geographic approach is somewhat inflexible, and extensive work and analysis will be required to modify the modeled strata if the fishing pressure ever moves or extends outside of the modeled bounds. Adopting a spatio-temporal stock assessment approach, such as the one shown here with STM1 and STM2, will provide invaluable flexiblity necessary to deal with potential changes in spatial fishing pressure. It would also allow DFO to track local changes in population abundance and distribution. This increased knowledge could be harnessed directly into the mandated Precautionary Approach, wherein reference points based on biological characteristics are set to determine the health of a population (Hilborn et al., 2001; Smith and Rago, 2004; Nasmith et al., 2016), to determine local reference points. These could then be used to reliably manage local trends and ensure the biological and commercial sustainability of this fishery for the foreseeable future.

Chapter 4

Conclusion

In this thesis, we examined ways of modeling the highly variable and spatially explicit data available for Scallop Production Area (SPA) 3 of the Nova Scotia Inshore Sea Scallop (*Placopecten magellanicus*) Fishery for the purposes of better predicting changes in scallop abundance and biomass. In Chapter 2 we showed how explicitly modeling the intra-annual variability in the survey tows improved the estimation of variance parameters, which led to more reliable predictions of population change. This approach removed the need to aggregate all intra-annual observations into a single index of abundance. It also introduced the requirement to account for zero-inflation in the survey tows.

In Chapter 3 we expanded the model framework further to incorporate spatial autocorrelation into the dynamical processes for commercial biomass, recruit biomass and natural mortality. This was performed using Gaussian Markov Random Fields (GMRF) without requiring extensive information about environmental covariates. Results showed that while a strictly temporal approach was appropriate for capturing changes in population for SPA 3 as a whole, it inflated estimates of natural mortality and recruitment. This was driven by large outliers including the recruitment spike in 2001. On the other hand, our spatio-temporal model framework was able to attribute these spikes to their local areas while reliably tracking the rest of the population. Our approach of simultaneously predicting both the total biomass and its distribution across space is highly appropriate for various management approaches, from the implementation of quotas for the entire area to explicitly spatial management.

Thorough examination of SPA 3 demonstrates the importance of modeling the spatial characteristics of fish stocks. Even if a temporal model can reliably capture the total biomass, key information that may impact management decisions is missed. For example, the SPA 3 sea scallop population was seen to have been relatively stable on a temporal scale, but the distribution of scallops and of fishing effort has

undergone great shifts in space over time. Since heavily fished areas are most likely the most productive scallop beds (Smith et al., 2017), ignoring local changes could endanger the biological and economical sustainability of this area. While the current assessment compensates by exclusively modeling areas under high fishing pressure (Nasmith et al., 2016), it cannot guarantee that the fishing effort or areas of high biomass will not shift in the future. Our spatio-temporal model framework helps future-proof assessments against these unforeseen circumstances.

Spatio-temporal stock assessment models can be fully embedded into the Precautionary Approach used by DFO. Not only can these models provide reference points for total population biomass, they also open up the possibility of setting spatially-explicit reference points. For example, one could set reference points for different subareas that could be adjusted according to an area's productivity. These types of assessments promise to improve the economical and biological sustainability of any fisheries that make the effort to incorporate them.

4.1 Future Directions

The most obvious future direction is to incorporate environmental covariates. This could be done in a fairly straightforward manner by modifying the observation equations for survey tows to include environmental covariate information by way of a regression framework. However, this would require obtaining explicit information on these covariates through substantial time and expense, such as putting instruments to record temperature or other variables on the survey gear.

Other research directions include modifying the underlying structure of these spatio-temporal models. For example, one could examine the effect of having a Gaussian or exponential correlation structure instead of a Matérn structure for spatial autocorrelation. Furthermore, implementing potentially more realistic formulations for natural mortality and recruitment may be fruitful. These could take the form of a stock-recruit relationship for recruitment, while the popcorn model described in Chapter 2 could be reworked into one that incorporates spatial structure directly.

It would be very interesting to see how effective our spatio-temporal models are when applied to different areas or fisheries that are more or less variable than SPA 3. If they could be successfully fit to multiple areas of the same fishery, one could

even try to fit these models to the entire inshore fishery. While this would require modifications so that correlation does not extend across land (see Bakka et al., 2016), it may well result in a unified assessment instead of having to fit multiple models, all the while maintaining the ability to manage them separately.

While the applicability of these models to populations of relatively sedentary species is clear, generalizing them to other fisheries might require some more work. For motile species, it would be interesting to implement some form of movement model to track the movement between subareas of interest. The inclusion of large-scale population movements, such as salmon migrations, could also be beneficial to the assessments of certain stocks.

Finally, it will be important to assess the effect of processing the locations of commercial landings data. These landings represent the total catches from a single trip, whose lengths can vary greatly, and are only associated with a single location. This introduces uncertainty regarding the true locations of these removals which our current models ignore. Obtaining more information about the length and area covered by a particular fishing trip could help. Alternatively, one could also try to explicitly model the potential area covered by a single fishing trip (e.g. fuzzy clustering, spatial approaches, etc.) and split up each fishing trip into the appropriate subareas. Regardless of what remains, it seems abundantly clear that the future of stock assessments is necessarily spatial.

Bibliography

Aeberhard, W. H., Flemming, J. M., and Nielsen, A. (2018). Review of State-Space Models for Fisheries Science. *Annu. Rev. Stat. Its Appl.*, 5:215–235.

Albertsen, C. M., Nielsen, A., and Thygesen, U. H. (2017). Choosing the observational likelihood in state-space stock assessment models. *Can. J. Fish. Aquat. Sci.*, 74(5):779–789.

Angelini, R. and Moloney, C. L. (2007). Fisheries, ecology and modelling: An historical perspective. *Panam. J. Aquat. Sci.*, 2(2):75–85.

Auger-Méthé, M., Albertsen, C. M., Jonsen, I. D., Derocher, A. E., Lidgard, D. C., Studholme, K. R., Bowen, W. D., Crossin, G. T., and Flemming, J. M. (2017). Spatiotemporal modelling of marine movement data using Template Model Builder (TMB). *Mar. Ecol. Prog. Ser.*, 565:237–249.

Auger-Méthé, M., Field, C., Albertsen, C. M., Derocher, A. E., Lewis, M. A., Jonsen, I. D., and Flemming, J. M. (2016). State-space models' dirty little secrets: Even simple linear Gaussian models can have estimation problems. *Sci. Rep.*, 6(December 2015):1–10.

Bakka, H., Vanhatalo, J., Illian, J., Simpson, D., and Rue, H. (2016). Non-stationary Gaussian models with physical barriers.

Banerjee, S., Gelfand, A. E., Finley, A. O., and Sang, H. (2008). Gaussian predictive process models for large spatial data sets. *J R Stat Soc Ser. B Stat Methodol.*, 70(4):825–848.

Baranov, T. (1918). On the question of the biological basis of fisheries. *Proc. Inst. Ichthyol. Investments*, 1:81–128.

Berger, A. M., Goethel, D. R., Lynch, P. D., Quinn, T., Mormede, S., McKenzie, J., and Dunn, A. (2017). Space oddity: The mission for spatial integration. *Can. J. Fish. Aquat. Sci.*, 1716:1–19.

Besag, J. (1974). Spatial Interaction and the Statistical Analysis of Lattice Systems. *J. R. Stat. Soc. Ser. B*, 36(2):192–236.

Besag, J. (1975). Statistical Analysis of Non-Lattice Data. *J. R. Stat. Soc. Ser. D (The Stat.*, 24(3):179–195.

Best, J. K. and Punt, A. E. (2020). Parameterizations for Bayesian state-space surplus production models. *Fish. Res.*, 222(105411):1–9.

Beverton, R. J. H. and Holt, S. J. (1957). *On the dynamics of exploited fish populations*. Ministry of Agriculture, Fisheries and Food, London (Great Britain).

Bolker, B. M., Brooks, M. E., Clark, C. J., Geange, S. W., Poulsen, J. R., Stevens, M. H. H., and White, J. S. S. (2009). Generalized linear mixed models: a practical guide for ecology and evolution. *Trends Ecol. Evol.*, 24(3):127–135.

Caddy, J. F. (1968). Underwater Observations on Scallop (*Placopecten magellanicus*) Behaviour and Drag Efficiency . *J. Fish. Res. Board Canada*, 25(10):2123–2141.

Caddy, J. F. (1975). Spatial Model for an Exploited Shellfish Population, and its Application to the Georges Bank Scallop Fishery. *J. Fish. Res. Board Canada*, 32(8):1305–1328.

Caddy, J. F. (1998). A short review of precautionary reference points and some proposals for their use in data-poor situations. Technical report, FAO, Rome.

Caddy, J. F. and Chandler, R. A. (1968). Lurcher Scallop Survey , March 1967. *Fish. Res. Board Canada*, (965):1–5.

Cadigan, N. G., Wade, E., and Nielsen, A. (2017). A spatiotemporal model for snow crab (Chionoecetes opilio) stock size in the southern Gulf of St. Lawrence. *Can. J. Fish. Aquat. Sci.*, 74:1808–1820.

Callihan, J. L., Godwin, C. H., and Buckel, J. A. (2014). Effect of demography on spatial distribution: Movement patterns of the Albemarle sound-Roanoke river stock of striped bass (*Morone saxatilis*) in relation to their recovery. *Fish. Bull.*, 112(2-3):131–143.

Carson, S., Shackell, N., and Mills Flemming, J. (2017). Local overfishing may be avoided by examining parameters of a spatio-temporal model. *PLoS One*, 12(9):1–21.

Casella, G., George, E. I., Casella, G., and George, E. I. (1992). Explaining the Gibbs Sampler. *Am. Stat.*, 3:167–174.

Ciannelli, L., Fauchald, P., Chan, K. S., Agostini, V. N., and Dingsør, G. E. (2008). Spatial fisheries ecology: Recent progress and future prospects. *J. Mar. Syst.*, 71(3-4):223–236.

Costello, C., Ovando, D., Hilborn, R., Gaines, S. D., Deschenes, O., and Lester, S. E. (2012). Status and Solutions for the World ' s Unassessed Fisheries. *Science (80-.).*, 338(6106):517–520.

Cressie, N. A., Calder, C., Clark, J., Hoef, J., and Wikle, C. (2009). Accounting for uncertainty in ecological analysis: the strengths and limitations of hierachical modeling. *Ecol. Appl.*, 19(3):553–570.

De Valpine, P. (2002). Review of methods for fitting time-series models with process and observation error and likelihood calculations for nonlinear, non-Gaussian state-space models. *Bull. Mar. Sci.*, 70(2):455–471.

Deriso, R. B. (1980). Harvesting Strategies and Parameter Estimation for an Age-Structured Model. *Can. J. Fish. Aquat. Sci.*, 37:268–282.

FAO (2018). *The State of World Fisheries and Aquaculture 2018 - Meeting the sustainable development goals*, volume 35. Food and Agriculture Organization of the United Nations.

Fletcher, D., MacKenzie, D., and Villouta, E. (2005). Modelling skewed data with many zeros: A simple approach combining ordinary and logistic regression. *Environ. Ecol. Stat.*, 12(1):45–54.

Froese, R. (2006). Cube law, condition factor and weight-length relationships: History, meta-analysis and recommendations. *J. Appl. Ichthyol.*, 22(4):241–253.

Gedamke, T., DuPaul, W. D., and Hoenig, J. M. (2004). A Spatially Explicit Open-Ocean DeLury Analysis to Estimate Gear Efficiency in the Dredge Fishery for Sea Scallop *Placopecten magellanicus* . *North Am. J. Fish. Manag.*, 24(2):335–351.

Gelfand, A. E., Schmidt, A. M., Wu, S., Silander, J. A., Latimer, A., and Rebelo, A. G. (2005). Modelling species diversity through species level hierarchical modelling. *J. R. Stat. Soc. Ser. C Appl. Stat.*, 54(1):1–20.

Goethel, D. R., Quinn, T. J., and Cadrin, S. X. (2011). Incorporating spatial structure in stock assessment: Movement modeling in marine fish population dynamics. *Rev. Fish. Sci.*, 19(2):119–136.

Harley, S. J., Myers, R. A., and Dunn, A. (2001). Is catch-per-unit-effort proportional to abundance? *Can. J. Fish. Aquat. Sci.*, 58(9):1760–1772.

Hart, D. R. and Chute, a. S. (2004). Essential Fish Habitat Source Document: Sea Scallop, *Placopecten magellanicus*, Life History and Habitat Characteristics. Technical Report September.

Hilborn, R. (1992). Current and future trends in fisheries stock assessment and management. *South African J. Mar. Sci.*, 12(1):975–988.

Hilborn, R. (2007). Reinterpreting the state of fisheries and their management. *Ecosystems*, 10(8):1362–1369.

Hilborn, R., Maguire, J. J., Parma, A. M., and Rosenberg, A. A. (2001). The precautionary approach and risk management: Can they increase the probability of successes in fishery management? *Can. J. Fish. Aquat. Sci.*, 58(1):99–107.

Hooten, M. B., Larsen, D. R., and Wikle, C. K. (2003). Predicting the spatial distribution of ground flora on large domains using a hierarchical Bayesian model. *Landsc. Ecol.*, 18(5):487–502.

Houde, E. D. (2008). Emerging from Hjort's shadow. *J. Northwest Atl. Fish. Sci.*, 41:53–70.

Hutchings, J. A. and Myers, R. A. (1994). What Can Be Learned from the Collapse of a Renewable Resource? Atlantic Cod, *Gadus morhua*, of Newfoundland and Labrador. *Can. J. Fish. Aquat. Sci.*, 51(9):2126–2146.

Jones, R. and Martin, J. H. A. (1981). The Relationship Between Demersal Fish Landings and Bottom Temperature. *Int. Counc. Explor. Sea*, 44:1–7.

Kai, M., Thorson, J. T., Piner, K. R., and Maunder, M. N. (2017). Predicting the spatio-temporal distributions of pelagic sharks in the western and central North Pacific. *Fish. Oceanogr.*, 26(5):569–582.

Kinas, P. G. (1996). Bayesian fishery stock assessment and decision making using adaptive importance sampling. *Can. J. Fish. Aquat. Sci.*, 53(2):414–423.

Kristensen, K., Nielsen, A., Berg, C. W., Skaug, H., and Bell, B. (2016). TMB: Automatic Differentiation and Laplace Approximation. *J. Stat. Softw.*, 70(5).

Kristensen, K., Thygesen, U. H., Andersen, K. H., and Beyer, J. E. (2014). Estimating spatio-temporal dynamics of size-structured populations. *Can. J. Fish. Aquat. Sci.*, 71(2):326–336.

Legendre, P. (1993). Spatial Autocorrelation : Trouble or New Paradigm ? *Ecology*, 74(6):1659–1673.

Lelièvre, M. A. (2017). Constructing a sacred chronology: How the Nova Scotian Institute of science made the Mi'kmaq a people without prehistory. *Ethnohistory*, 64(3):401–426.

Lewontin, R. C. and Cohen, D. (1969). On Population Growth in a Randomly Varying Environment. *Proc. Natl. Acad. Sci. United States Am.*, 62(4):1056–1060.

Lindgren, F. and Rue, H. (2011). An explicit link between Gaussian fields and Gaussian Markov random fields: the stochastic partial differential equation approach. *J. R. Stat. Soc. Ser. B*, 73:423–498.

Linton, B. C. and Bence, J. R. (2008). Evaluating methods for estimating process and observation error variances in statistical catch-at-age analysis. *Fish. Res.*, 94(1):26–35.

Lunn, D. J., Thomas, A., Best, N., and Spiegelhalter, D. (2000). WinBUGS - A Bayesian modelling framework: Concepts, structure, and extensibility. *Stat. Comput.*, 10:325–337.

Mackenzie, D. I., Nichols, J. D., Lachman, G. B., Droege, S., Andrew, J., Langtimm, C. A., and Langtimm, C. A. (2002). Estimating Site Occupancy Rates When Detection Probabilities Are Less Than One Stable. *Ecology*, 83(8):2248–2255.

Malthus, T. R. (1798). *An Essay on the Principle of Population, as it Affects the Future Improvement of Society, with Remarks on the Speculations of Mrs. Godwin, M. Condorcet and Others Writers.* V IX, London, U.K.

Martin, T. G., Wintle, B. A., Rhodes, J. R., Kuhnert, P. M., Field, S. A., Low-Choy, S. J., Tyre, A. J., and Possingham, H. P. (2005). Zero tolerance ecology: Improving ecological inference by modelling the source of zero observations. *Ecol. Lett.*, 8(11):1235–1246.

Matheron, G. and Krumbein, W. C. (1970). Structures aleatoires et geologie mathematique. *Rev. Int. Stat. Inst.*, 38(1):1–11.

Maunder, M. N. and Punt, A. E. (2004). Standardizing catch and effort data: A review of recent approaches. *Fish. Res.*, 70:141–159.

Maunder, M. N., Sibert, J. R., Fonteneau, A., Hampton, J., Kleiber, P., and Harley, S. J. (2006). Interpreting catch per unit effort data to assess the status of individual stocks and communities. *ICES J. Mar. Sci.*, 63(8):1373–1385.

McGarvey, R., Serchuk, F. M., and McLaren, I. A. (1993). Spatial and Parent-Age Analysis of Stock-Recruitment in the Georges Bank Sea Scallop (*Placopecten magellanicus*) Population. *Can. J. Fish. Aquat. Sci.*, 50:564–574.

Mello, L. G. and Rose, G. A. (2005). Using geostatistics to quantify seasonal distribution and aggregation patterns of fishes: An example of Atlantic cod (*Gadus morhua*). *Can. J. Fish. Aquat. Sci.*, 62(3):659–670.

Merrill, A. S. and Posgay, J. A. (1964). Estimating the Natural Mortality Rate of the Sea Scallop (*Placopecten magellanicus*). Technical Report NAFO SCS Doc. 14/023.

Meyer, R. and Millar, R. B. (1999). Bayesian stock assessment using a state–space implementation of the delay difference model. *Can. J. Fish. Aquat. Sci.*, 56(1):37–52.

Miller, T. J., Hart, D. R., Hopkins, K., Vine, N. H., Taylor, R., York, A. D., and Gallager, S. M. (2019). Estimation of the capture efficiency and abundance of atlantic sea scallops (*Placopecten magellanicus*) from paired photographic–dredge tows using hierarchical models. *Can. J. Fish. Aquat. Sci.*, 76(6):847–855.

Myers, R. A., Hutchings, J. A., and Barrowman, N. J. (1996). Hypotheses for the decline of cod in the North Atlantic. *Mar. Ecol. Prog. Ser.*, 138(1-3):293–308.

Myers, R. A. and Worm, B. (2003). Rapid worldwide depleation of predatory fish communities. *Nature*, 423:280–283.

Nasmith, L., Sameoto, J. A., and Glass, A. (2016). Scallop production areas in the Bay of Fundy: Stock status for 2015 and forecast for 2016. Technical Report 2016/021.

Paloheimo, J. E. and Dickie, L. M. (1964). Abundance and Fishing Success. *Rapp. Proces Verbaux des Reun. Cons. Int. pour l'Exploration la Mer*, pages 152–163.

Pedersen, E. J., Goto, D., Gaeta, J. W., Hansen, G., Sass, G., Vander Zanden, M. J., Cichosz, T., and Rypel, A. (2018). Long-term growth trends in northern Wisconsin walleye populations under changing biotic and abiotic conditions. *Can. J. Fish. Aquat. Sci.*, 75(5):733–745.

Petitgas, P. (1993). Geostatîstics for fish stock assessments: A review and an acoustic application.

Punt, A. E., Walker, T. I., Taylor, B. L., and Pribac, F. (2000). Standardization of catch and effort data in a spatially-structured shark fishery. *Fish. Res.*, 45(2):129–145.

Quinn, T. J. and Deriso, R. B. (1999). *Quantitative Fish Dynamics*. Press, Oxford University, New York, New York.

R Core Team (2020). The R Project for Statistical Computing.

Raitt, D. (1939). The Rate of Mortality of the Haddock of the North Sea Stock 1919-1938. *Rapp. Proces Verbaux des Reun. Cons. Int. pour l'Exploration la Mer*, pages 66–79.

Rue, H. and Held, L. (2010). Discrete Spatial Variation. In Gelfand, A. E., Diggle, P. J., Fuentes, M., and Guttorp, P., editors, *Handb. Spat. Stat.*, chapter 12, pages 172–198. CRC Press, Boca Raton, Florida.

Schnute, J. (1985). A General Theory for Analysis of Catch and Effort Data. *Can. J. Fish. Aquat. Sci.*, 42:414–429.

Schnute, J. T. (1994). A General Framework for Developing Sequential Fisheries Models. *Can. J. Fish. Aquat. Sci.*, 51(8):1676–1688.

Schnute, J. T. and Richards, L. J. (1995). The influence of error on population estimates from catch-age models. *Can. J. Fish. Aquat. Sci.*, 52(10):2063–2077.

Shaw, J., Todd, B. J., and Li, M. Z. (2014). Geologic insights from multibeam bathymetry and seascape maps of the Bay of Fundy, Canada. *Cont. Shelf Res.*, 83:53–63.

Shaw, J., Todd, B. J., Li, M. Z., and Wu, Y. (2012). Anatomy of the tidal scour system at Minas Passage, Bay of Fundy, Canada. *Mar. Geol.*, 323-325:123–134.

Sissenwine, M. P. (1984). Why Do Fish Populations Vary? *Exploit. Mar. Communities*, pages 59–94.

Skaug, H. J. and Fournier, D. A. (2006). Automatic approximation of the marginal likelihood in non-Gaussian hierarchical models. *Comput. Stat. Data Anal.*, 51(2):699–709.

Smith, F. E. (1961). Density Dependence in the Australian Thrips. *Ecology*, 42(2):403–407.

Smith, S. J. and Hubley, B. (2014). Impact of survey design changes on stock assessment advice: sea scallops. *ICES J. Mar. Sci.*, 72(2):82–92.

Smith, S. J., Hubley, B., Nasmith, L., Sameoto, J. A., Bourdages, H., and Glass, A. (2012). Scallop Production Areas in the Bay of Fundy: Stock Status for 2011 and Forecast for 2012. Technical report.

Smith, S. J., Kenchington, E. L., Lundy, M. J., Robert, G., and Roddick, D. (2001). Spatially Specific Growth Rates for Sea Scallops (*Placopecten magellanicus*). In Kruse, G. H., Bez, N., Booth, A., Dorn, M. W., Hills, S., Lipcius, R. N., Pelletier, D., Roy, C., Smith, S. J., and D., W., editors, *Spat. Process. Manag. Mar. Popul.*, pages 211–232. University of Alaska Sea Grant, Fairbanks, ak-sg-01-0 edition.

Smith, S. J. and Lundy, M. J. (2002). Scallop Production Area 4 in the Bay of Fundy: Stock status and forecast. Technical Report 2002/018.

Smith, S. J. and Rago, P. (2004). Biological reference points for sea scallops (*Placopecten Magellanicus*): the benefits and costs of being nearly sessile. *Can. J. Fish. Aquat. Sci.*, 61(8):1338–1354.

Smith, S. J., Sameoto, J. A., and Brown, C. J. (2017). Setting biological reference points for sea scallops (*Placopecten Magellanicus*) allowing for the spatial distribution of productivity and fishing effort. *Can. J. Fish. Aquat. Sci.*, 74(5):650–667.

Stock, B. C., Ward, E. J., Eguchi, T., Jannot, J. E., Thorson, J. T., Feist, B. E., and Semmens, B. X. (2020). Comparing predictions of fisheries bycatch using multiple spatiotemporal species distribution model frameworks. *Can. J. Fish. Aquat. Sci.*, 77(1):146–163.

Sun, Y. and Genton, M. G. (2011). Functional Boxplots. *J. Comput. Graph. Stat.*, 20(2):316–334.

Thorson, J. T. (2018). Three problems with the conventional delta-model for biomass sampling data, and a computationally efficient alternative. *Can. J. Fish. Aquat. Sci.*, 75(9):1369–1382.

Thorson, J. T. (2019). Guidance for decisions using the Vector Autoregressive Spatio-Temporal (VAST) package in stock, ecosystem, habitat and climate assessments. *Fish. Res.*, 210(October 2018):143–161.

Thorson, J. T., Adams, G., and Holsman, K. (2019). Spatio-temporal models of intermediate complexity for ecosystem assessments: A new tool for spatial fisheries management. *Fish Fish.*, 20(6):1083–1099.

Thorson, J. T. and Cope, J. M. (2017). Uniform, uninformed or misinformed?: The lingering challenge of minimally informative priors in data-limited Bayesian stock assessments. *Fish. Res.*, 194:164–172.

Thorson, J. T., Ianelli, J. N., Munch, S. B., Ono, K., Spencer, P. D., and Vinbrooke, R. (2015a). Spatial delay-difference models for estimating spatiotemporal variation in juvenile production and population abundance. *Can. J. Fish. Aquat. Sci.*, 72(12):1897–1915.

Thorson, J. T., Ianelli, J. N., Munch, S. B., Ono, K., Spencer, P. D., and Vinbrooke, R. (2015b). Spatial delay-difference models for estimating spatiotemporal variation in juvenile production and population abundance. *Can. J. Fish. Aquat. Sci.*, 72(12):1897–1915.

Thorson, J. T., Minto, C., Minte-Vera, C. V., Kleisner, K. M., and Longo, C. (2013). A new role for effort dynamics in the theory of harvested populations and data-poor stock assessment. *Can. J. Fish. Aquat. Sci.*, 70(12):1829–1844.

Thorson, J. T., Shelton, A. O., Ward, E. J., and Skaug, H. J. (2015c). Geostatistical delta-generalized linear mixed models improve precision for estimated abundance indices for West Coast groundfishes. *ICES J. Mar. Sci.*, 72(5):1297–1310.

Tremblay, A. M. J. and Sinclair, M. M. (1988). The Vertical and Horizontal Distribution of Sea Scallop (*Placopecten magellanicus*) Larvae in the Bay of Fundy in 1984 and 1985 . *J. Northwest Atl. Fish. Sci.*, 8:43–53.

Venables, W. N. and Dichmont, C. M. (2004). GLMs, GAMs and GLMMs: An overview of theory for applications in fisheries research. *Fish. Res.*, 70:319–337.

Worm, B., Barbier, E. B., Beaumont, N., Duffy, J., Folke, C., Halpern, B., Jackson, J., Lotze, H., Micheli, F., Palumbi, S., Sala, E., Selkoe, K. A., Stachowicz, J. J., and Watson, R. (2006). Impacts of biodiversity loss on ocean ecosystem services. *Science (80-.).*, 314(5800):787–790.

Xu, L., Li, B., Chen, X., and Chen, Y. (2019). A comparative study of observation-error estimators and state-space production models in fisheries assessment and management. *Fish. Res.*, 219(105322):1–7.

Yin, Y., Aeberhard, W. H., Smith, S. J., and Mills Flemming, J. (2019). Identifiable state-space models: A case study of the Bay of Fundy sea scallop fishery. *Can. J. Stat.*, 47(1):27–45.

Zimmerman, D. and Stein, M. (2010). Classical Geostatistical Methods. In Gelfand, A. E., Diggle, P. J., Fuentes, M., and Guttorp, P., editors, *Handb. Spat. Stat.*, chapter 3, pages 29–44. CRC Press, Boca Raton, Florida.

Appendix A

This appendix contains supplemental figures for Chapter 2. The discrepancies between the indices (I_t, I_t^R, L_t and N_t) are caused by slight differences between approaches taken in Chapter 2 and by DFO. DFO uses a linear model to correct the index in St-Mary's Bay when no survey tows are done there in a year, which was not the case for our approach. Furthermore, the repeated tows in the stratified random sampling design with partial replacement are slightly modified in the DFO approach to account for the previous year's abundance, which our approach also did not do. Discrepancies in the commercial catch (C_t) is caused by the temporal alignment described in Chapter 2, which was not the case for the DFO input.

The zero-inflated poisson approach replaced Equation 2.16 and 2.15 by the following:

$$P(y_i^I) = \begin{cases} \pi_B + (1-\pi_B)e^{-\lambda_B}, \text{if } y_i^I = 0 \\ (1-\pi_B)\frac{\lambda_B^{y_i^I} e^{-\lambda_B}}{y_i^I!}, \text{if } y_i^I > 0 \end{cases} \tag{A.1}$$

$$P(y_i^R) = \begin{cases} \pi_R + (1-\pi_R)e^{-\lambda_R}, \text{if } y_i^R = 0 \\ (1-\pi_R)\frac{\lambda_R^{y_i^R} e^{-\lambda_R}}{y_i^R!}, \text{if } y_i^R > 0 \end{cases} \tag{A.2}$$

where y_i^R and y_i^R are the number of commercial size and recruit size scallops caught in tow i, π_B and π_R are the respective probability of extra zeroes, and λ_B and λ_R are the respective Poisson expectations.

Figure A.1: Indices of Commercial Size Biomass (I_t) between 1996 and 2018 calculated by DFO (black) and from the raw survey data (red).

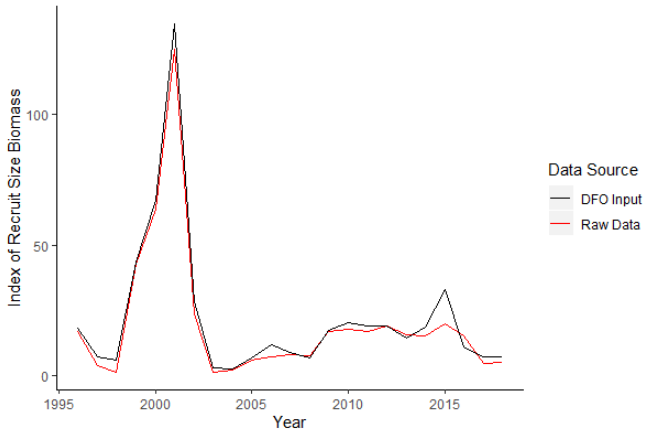

Figure A.2: Indices of Recruit Size Biomass (I_t^R) between 1996 and 2018 calculated by DFO (black) and from the raw survey data (red).

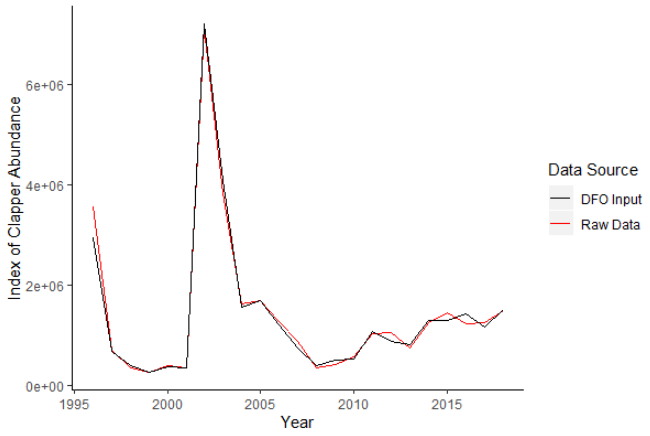

Figure A.3: Indices of Clapper Abundance (L_t) between 1996 and 2018 calculated by DFO (black) and from the raw survey data (red).

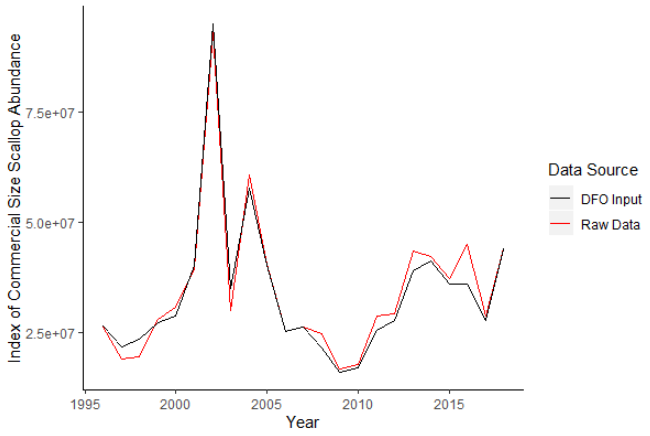

Figure A.4: Indices of Live Scallop Abundance (N_t) between 1996 and 2018 calculated by DFO (black) and from the raw survey data (red).

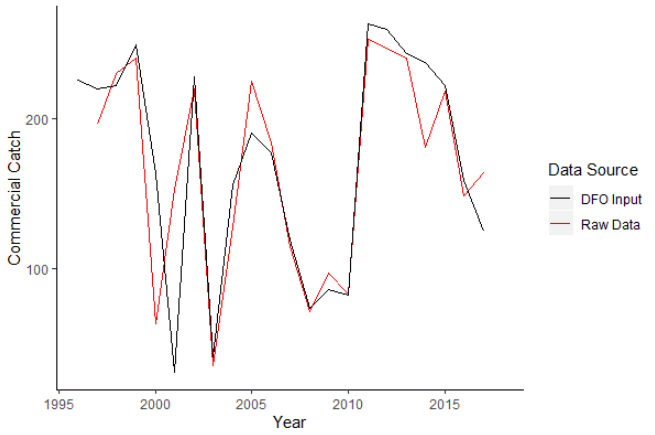

Figure A.5: Commercial Catch (C_t) between 1996 and 2018 calculated by DFO (black) and from the raw survey data (red).

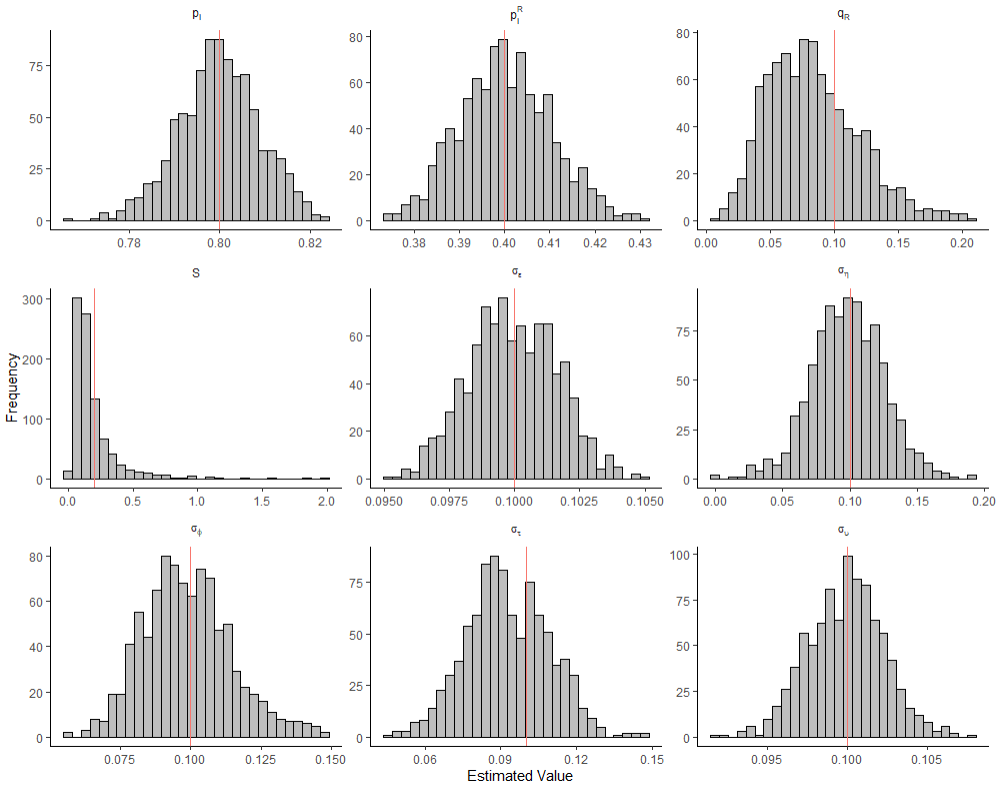

Figure A.6: Distribution of parameter estimates from second experiment experiment (922 simulations of 22 years). Red line denotes true value.

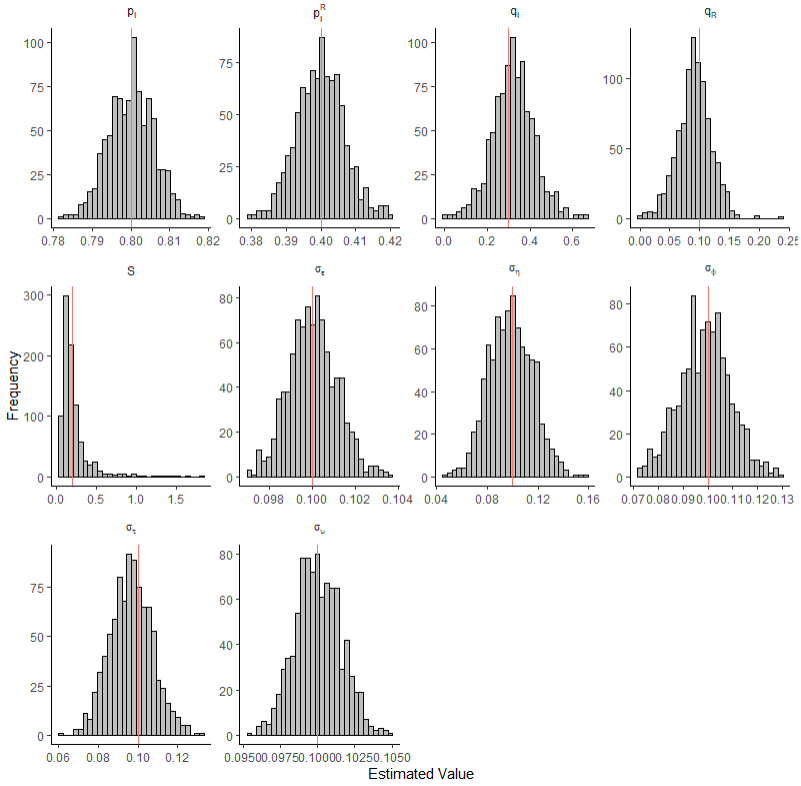

Figure A.7: Distribution of parameter estimates from third experiment (918 simulations of 50 years). Red line denotes true value.

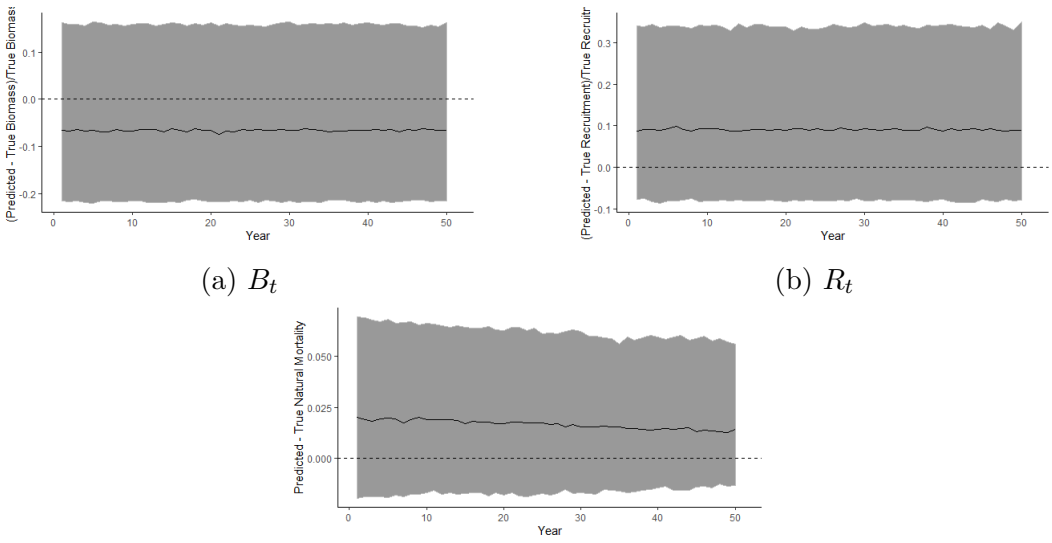

(a) B_t

(b) R_t

(c) m_t

Figure A.8: Functional boxplots (without whiskers) for Experiment 3 of the difference of the predicted random effects and their true value with horizontal dotted line at 0 and median difference shown by solid black line. 2.3a and 2.3b show the difference as a percentage of the true value (predicted - true / true) while 2.3c simply shows the net difference (predicted - true).

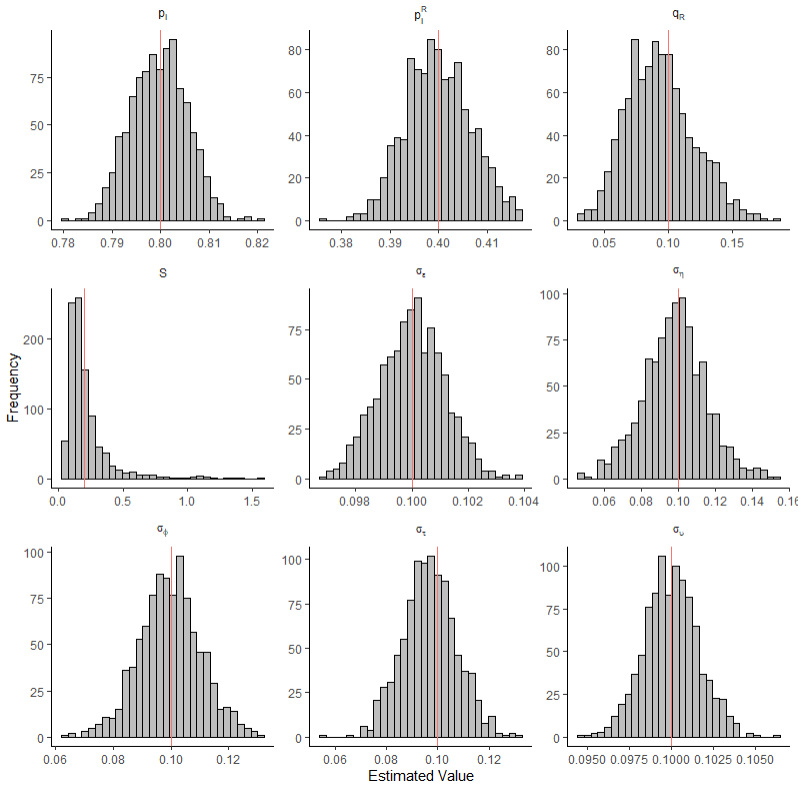

Figure A.9: Distribution of parameter estimates from fourth experiment (983 simulations of 50 years). Red line denotes true value.

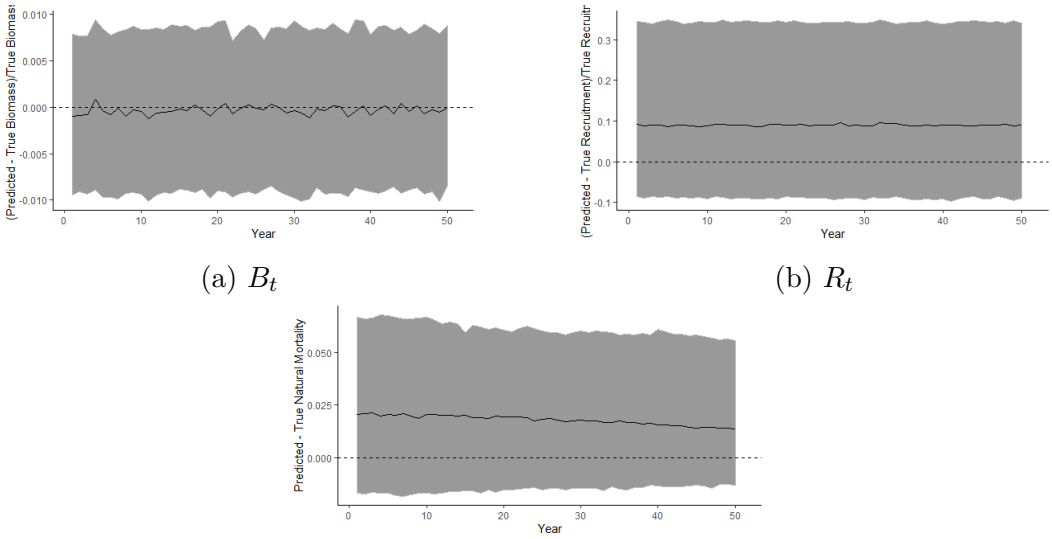

(a) B_t (b) R_t

(c) m_t

Figure A.10: Functional boxplots (without whiskers) for Experiment 4 of the difference of the predicted random effects and their true value with horizontal dotted line at 0 and median difference shown by solid black line. 2.3a and 2.3b show the difference as a percentage of the true value (predicted - true / true) while 2.3c simply shows the net difference (predicted - true).

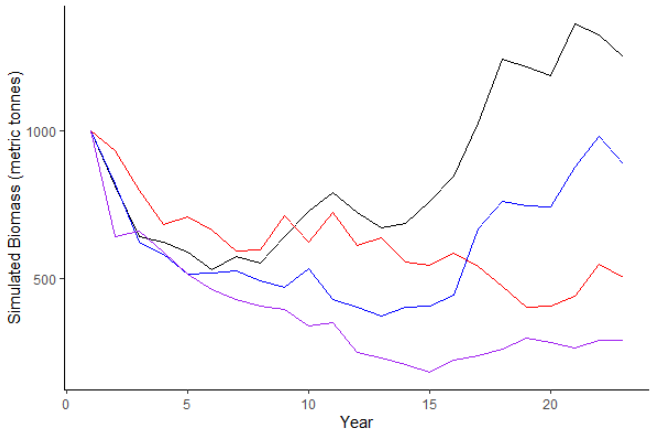

Figure A.11: Examples of simulated biomass over 22 years by FMB.

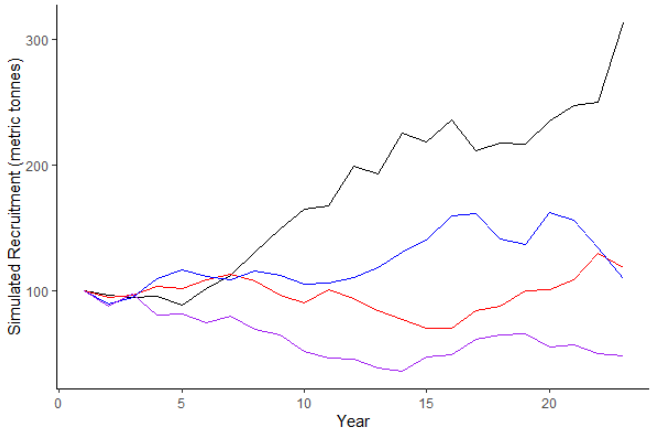

Figure A.12: Examples of simulated recruit biomass over 22 years by FMB.

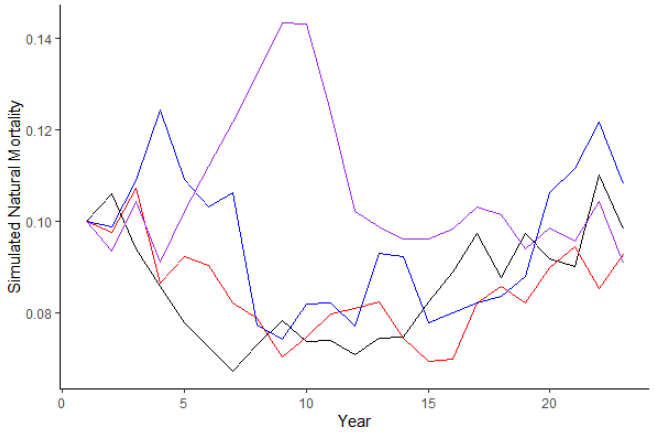

Figure A.13: Examples of simulated natural mortality over 22 years by FMB.

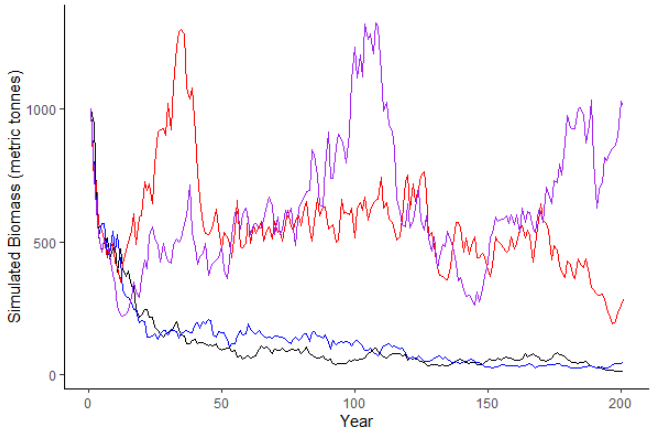

Figure A.14: Examples of simulated biomass over 200 years by FMB.

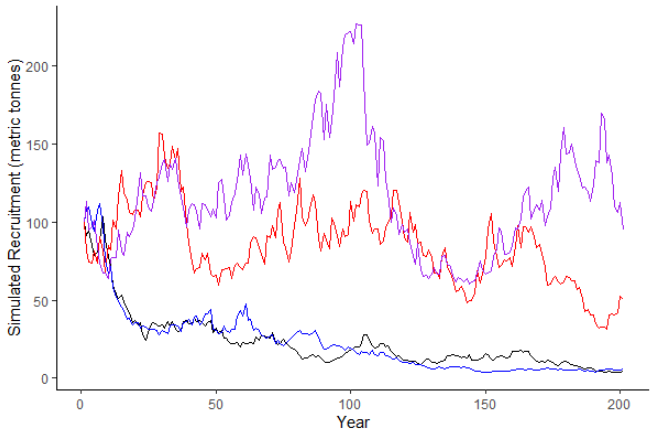

Figure A.15: Examples of simulated recruit biomass over 200 years by FMB.

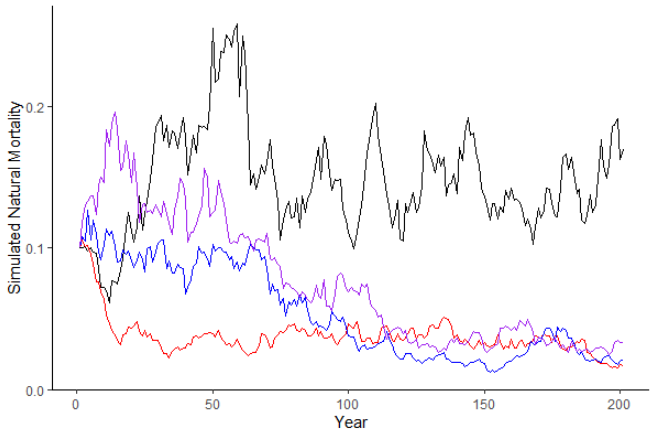

Figure A.16: Examples of simulated natural mortality over 200 years by FMB.

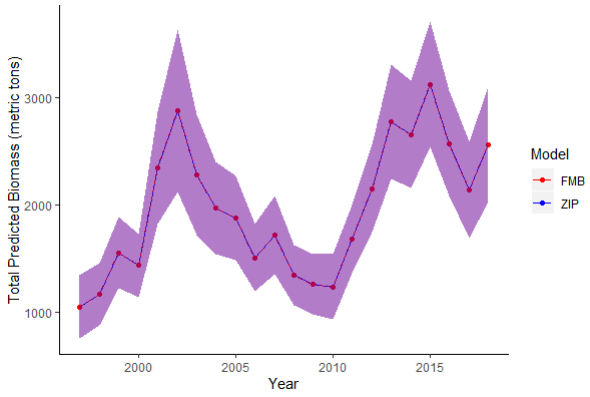

(a) Predicted Biomass (metric ton)

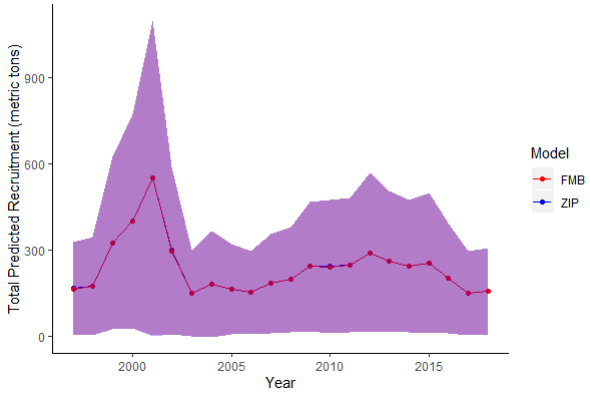

(b) Predicted Recruitment (metric ton)

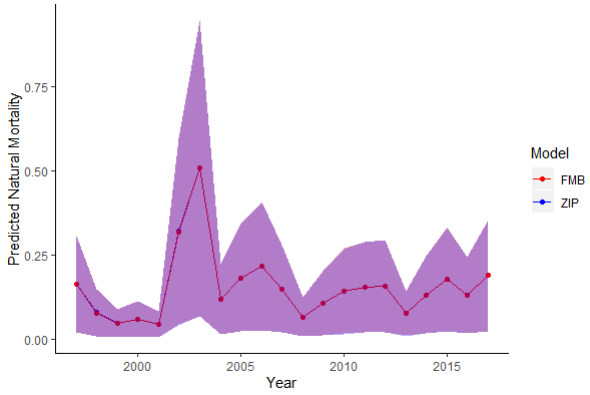

(c) Predicted Natural Mortality

Figure A.17: Predicted random effects on the SPA 3 scallop data from modified model using a zero-inflated poisson approach to zeroes (red) and FMB (blue). Envelopes represent interpolated point-wise 95% confidence intervals respectively.

Appendix B

This appendix contains supplemental figures for Chapter 3.

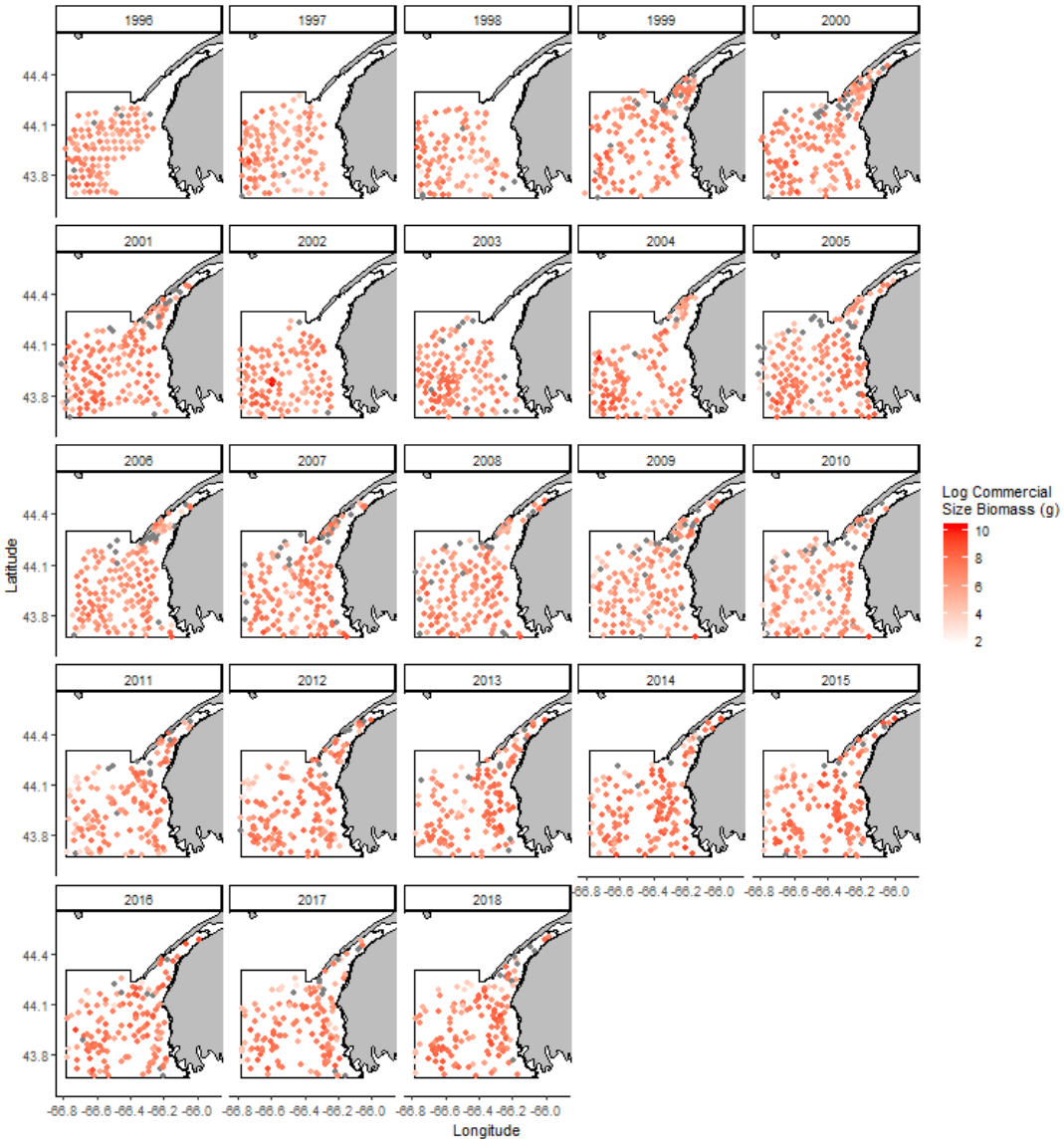

Figure B.1: Observed commercial size biomass at every survey tow between 1996 and 2018. Grey dots are tows where no commercial size scallops were caught.

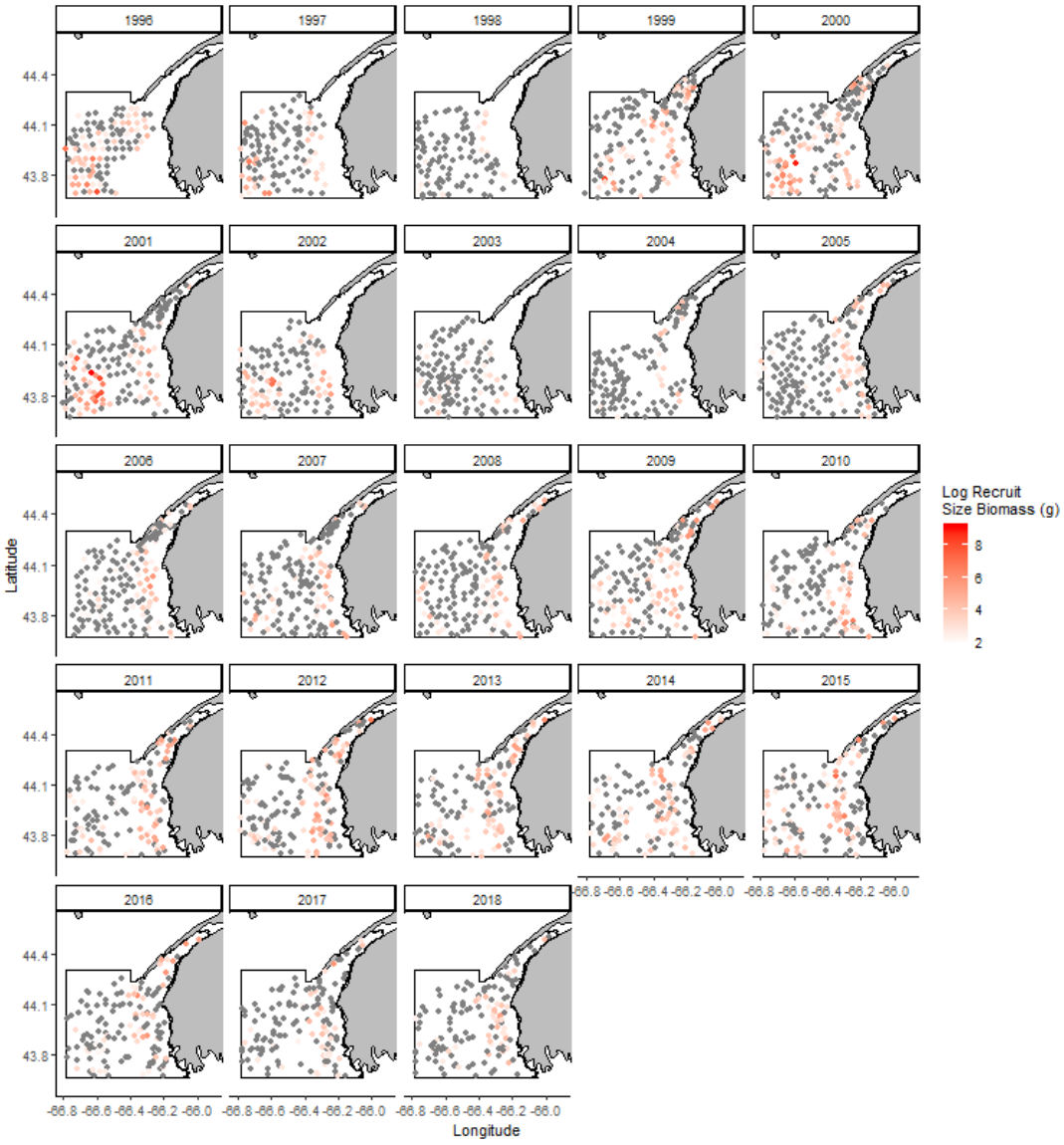

Figure B.2: Observed recruit size biomass at every survey tow between 1996 and 2018. Grey dots are tows where no recruit size scallops were caught.

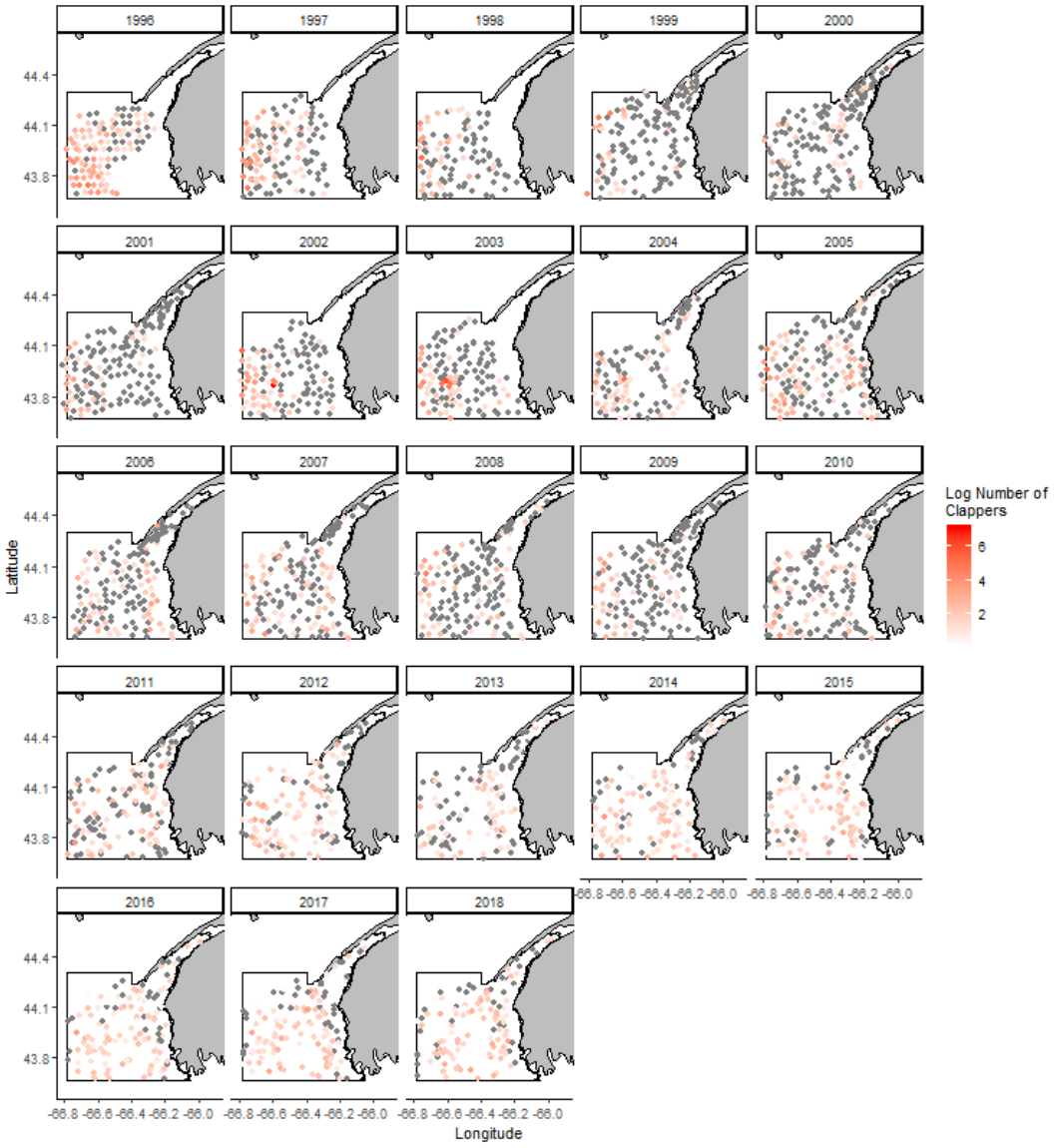

Figure B.3: Observed clapper abundance at every survey tow between 1996 and 2018. Grey dots are tows where no clappers were caught.

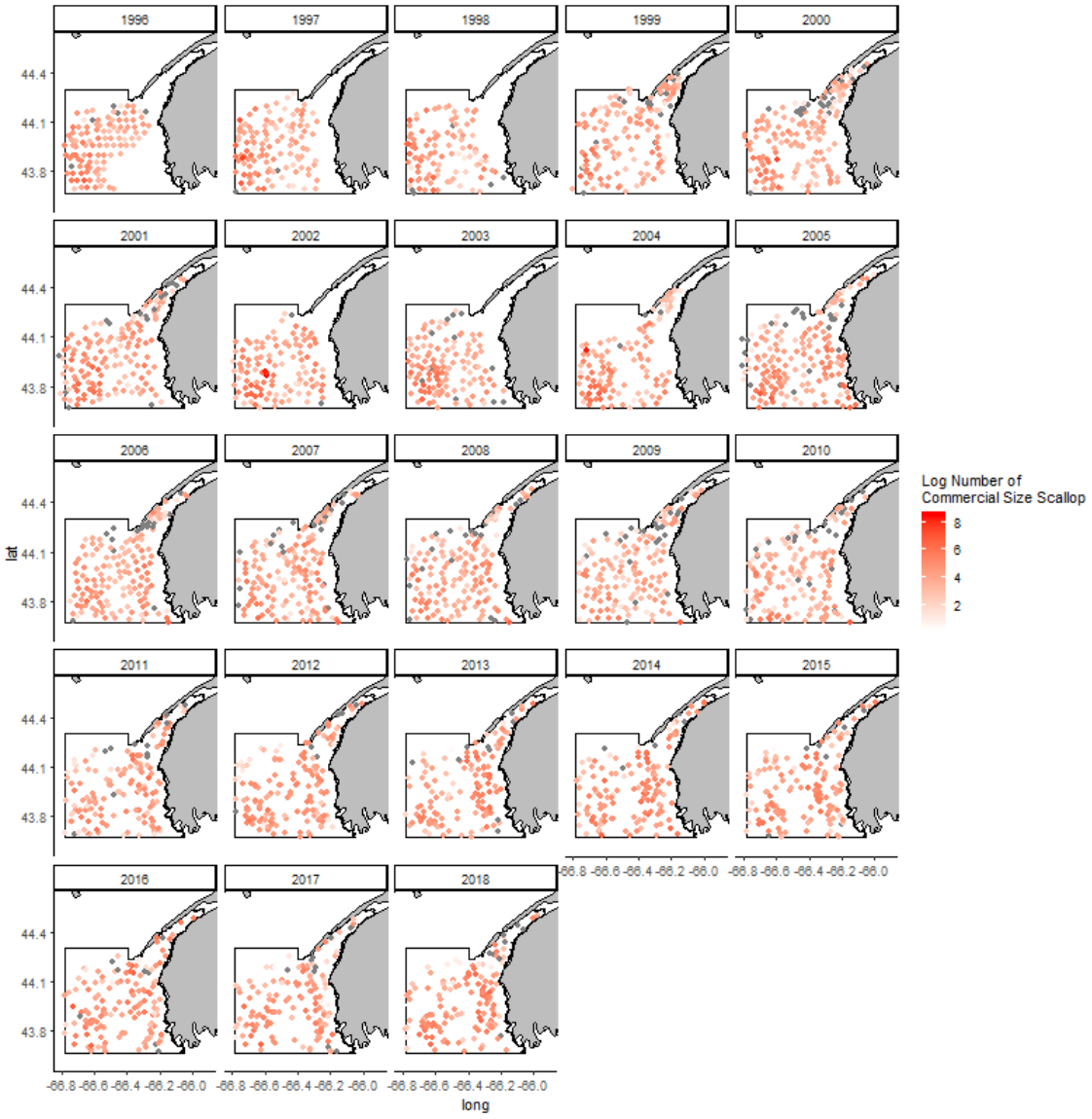

Figure B.4: Observed live scallop abundance at every survey tow between 1996 and 2018. Grey dots are tows where no live scallops were caught.

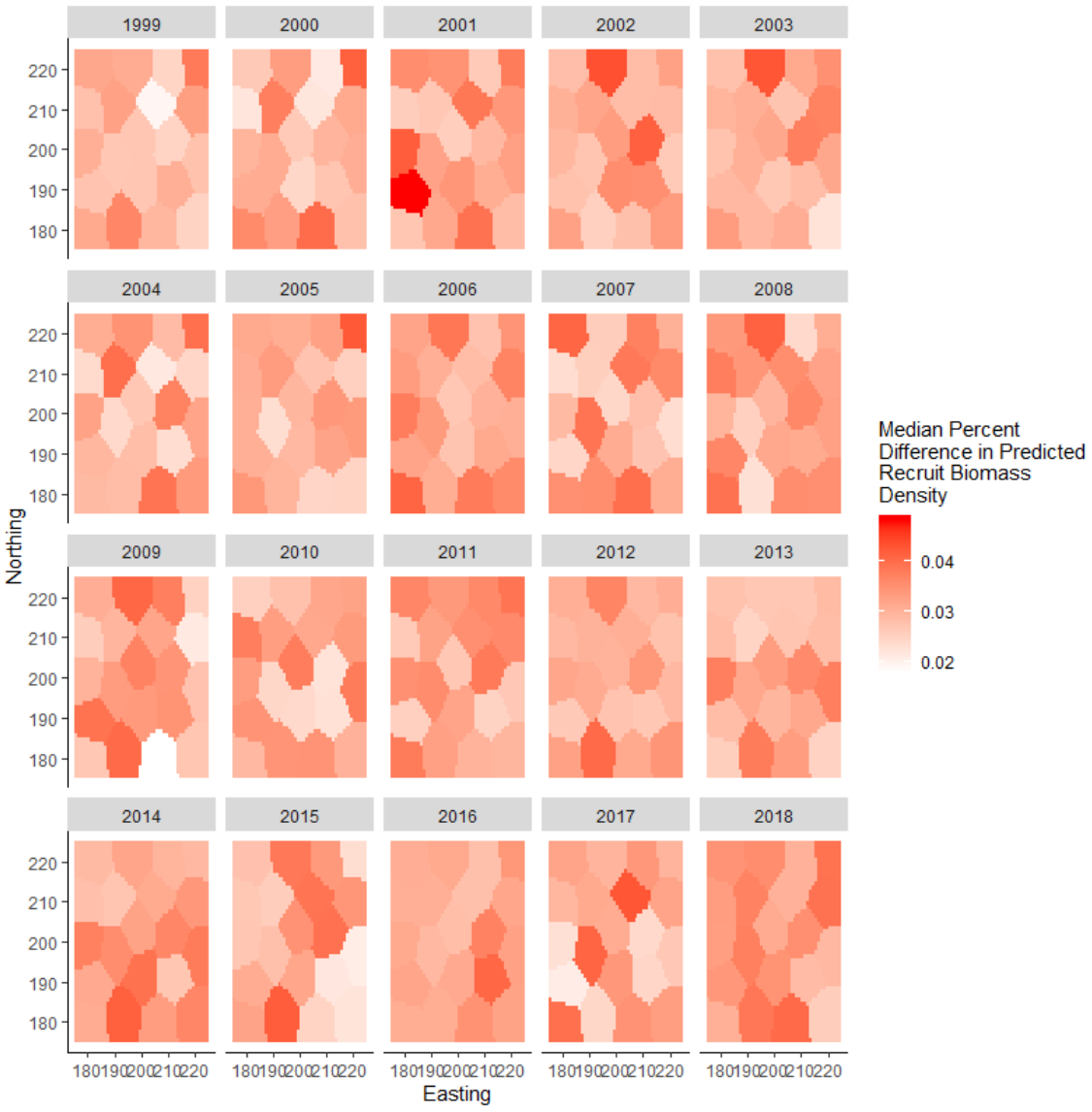

Figure B.5: Median percent difference recruit density ((predicted-true)/true) for setting A at every knot for 164 successful simulations of 20 years.

Figure B.6: Median percent difference natural mortality ((predicted-true)/true) for setting A at every knot for 164 successful simulations of 20 years.

Figure B.7: Median percent difference biomass density ((predicted-true)/true) for setting B at every knot for 176 successful simulations of 20 years.

Figure B.8: Median percent difference recruit density ((predicted-true)/true) for setting B at every knot for 176 successful simulations of 20 years.

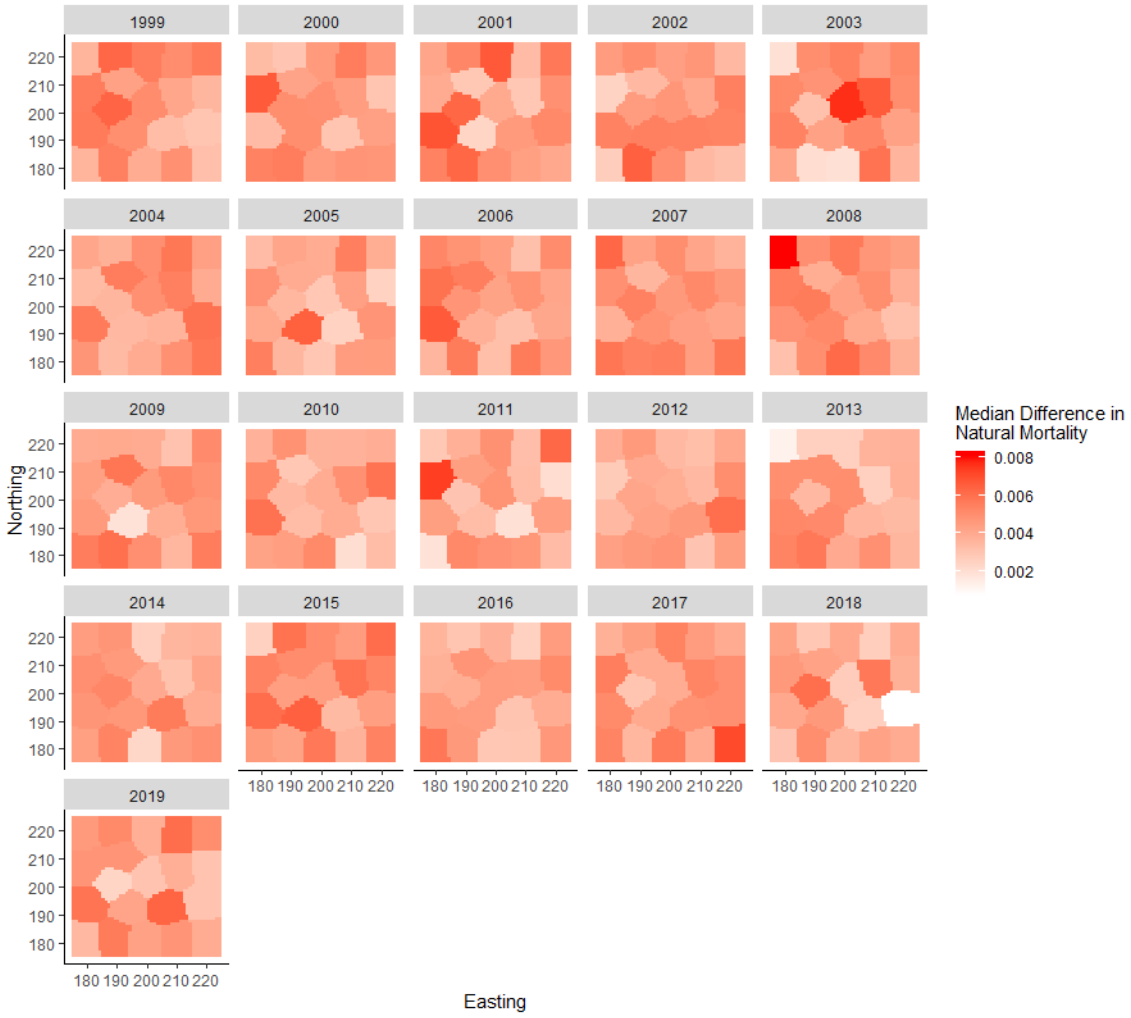

Figure B.9: Median percent difference natural mortality ((predicted-true)/true) for setting B at every knot for 176 successful simulations of 20 years.

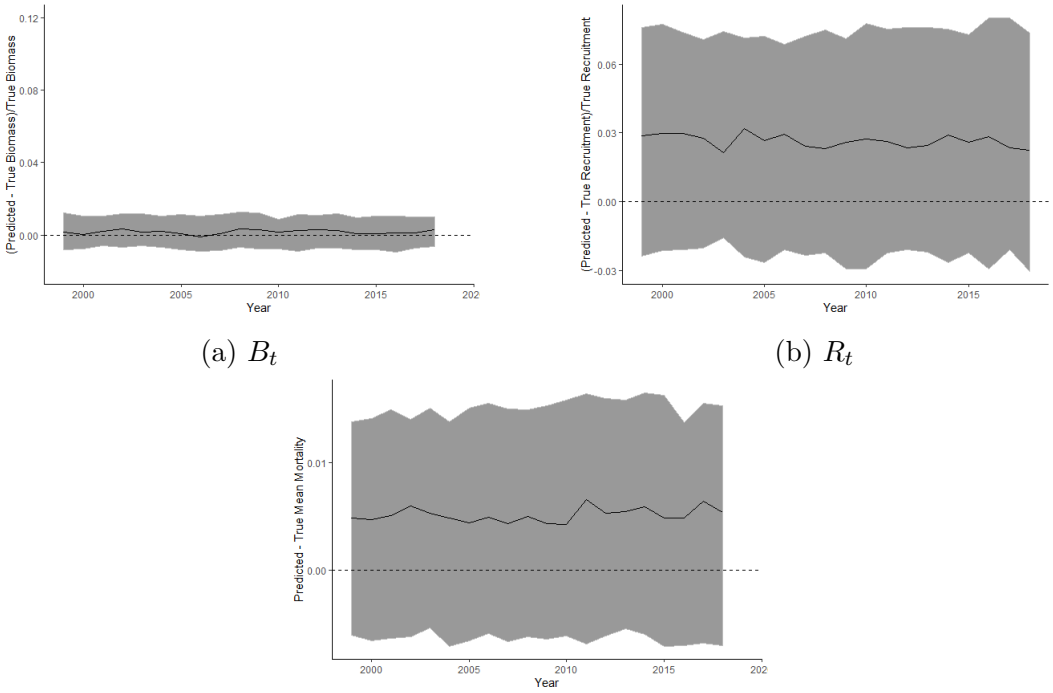

(a) B_t

(b) R_t

(c) m_t

Figure B.10: Functional boxplots (without whiskers) of the difference of the predicted random effects and their true value with horizontal dotted line at 0 and median difference shown by solid black line for setting B. B.10a and B.10b show the difference as a percentage of the true value (predicted - true / true) while B.10c simply shows the net difference (predicted - true).

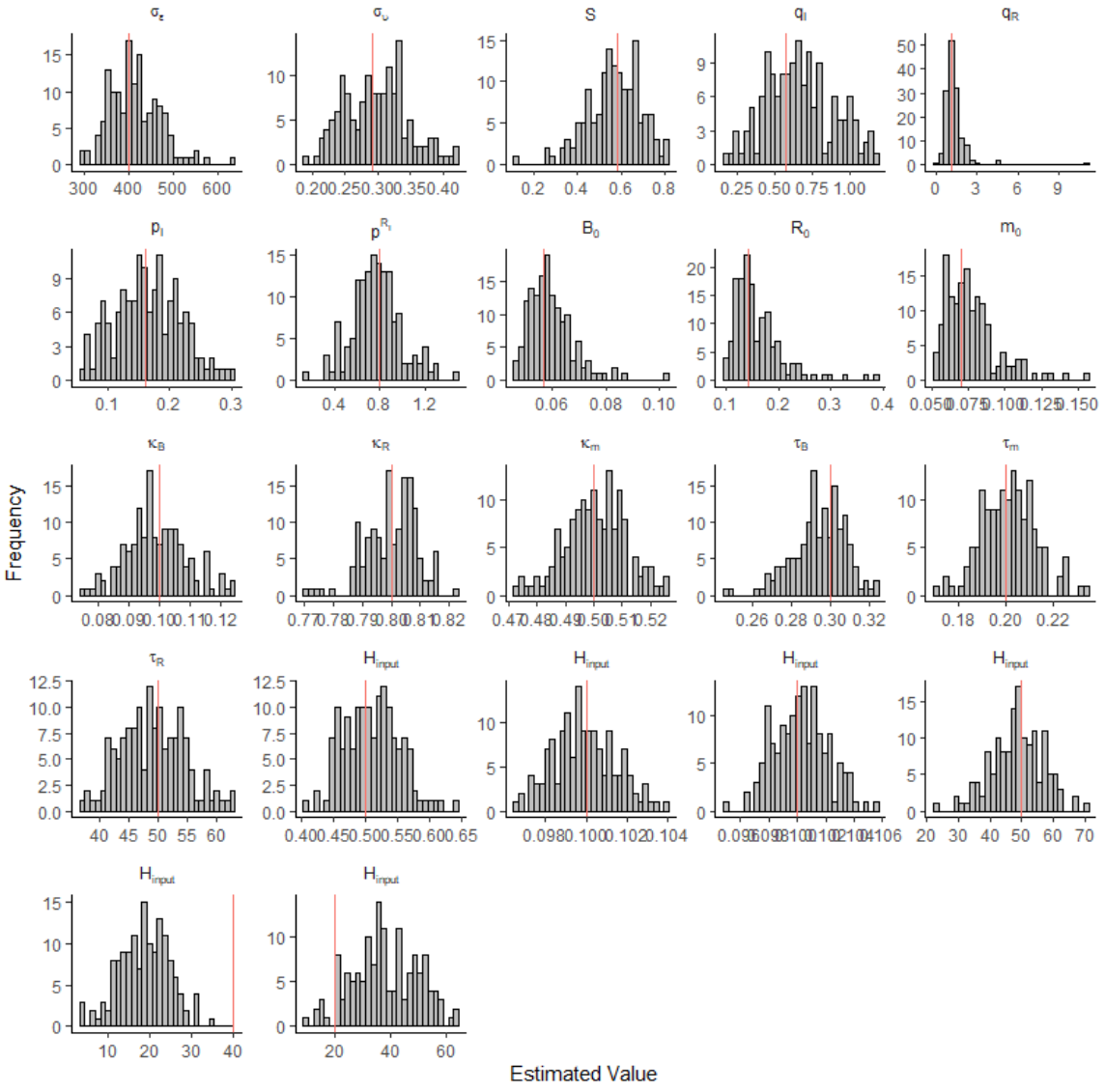

Figure B.11: Distribution of parameter estimates from setting C (163 simulations of 20 years). Red line denotes true value.

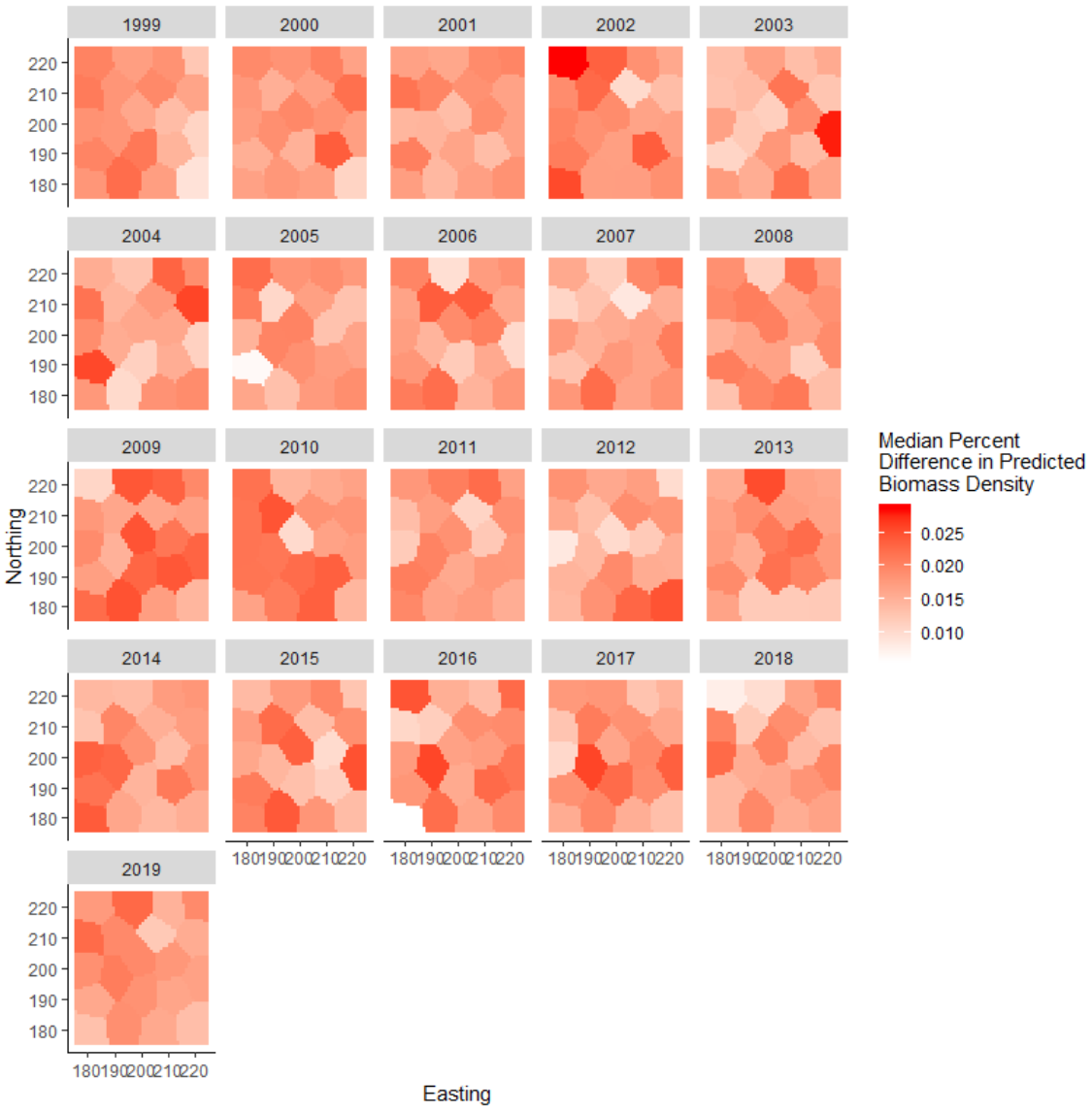

Figure B.12: Median percent difference biomass density ((predicted-true)/true) for setting C at every knot for 163 successful simulations of 20 years.

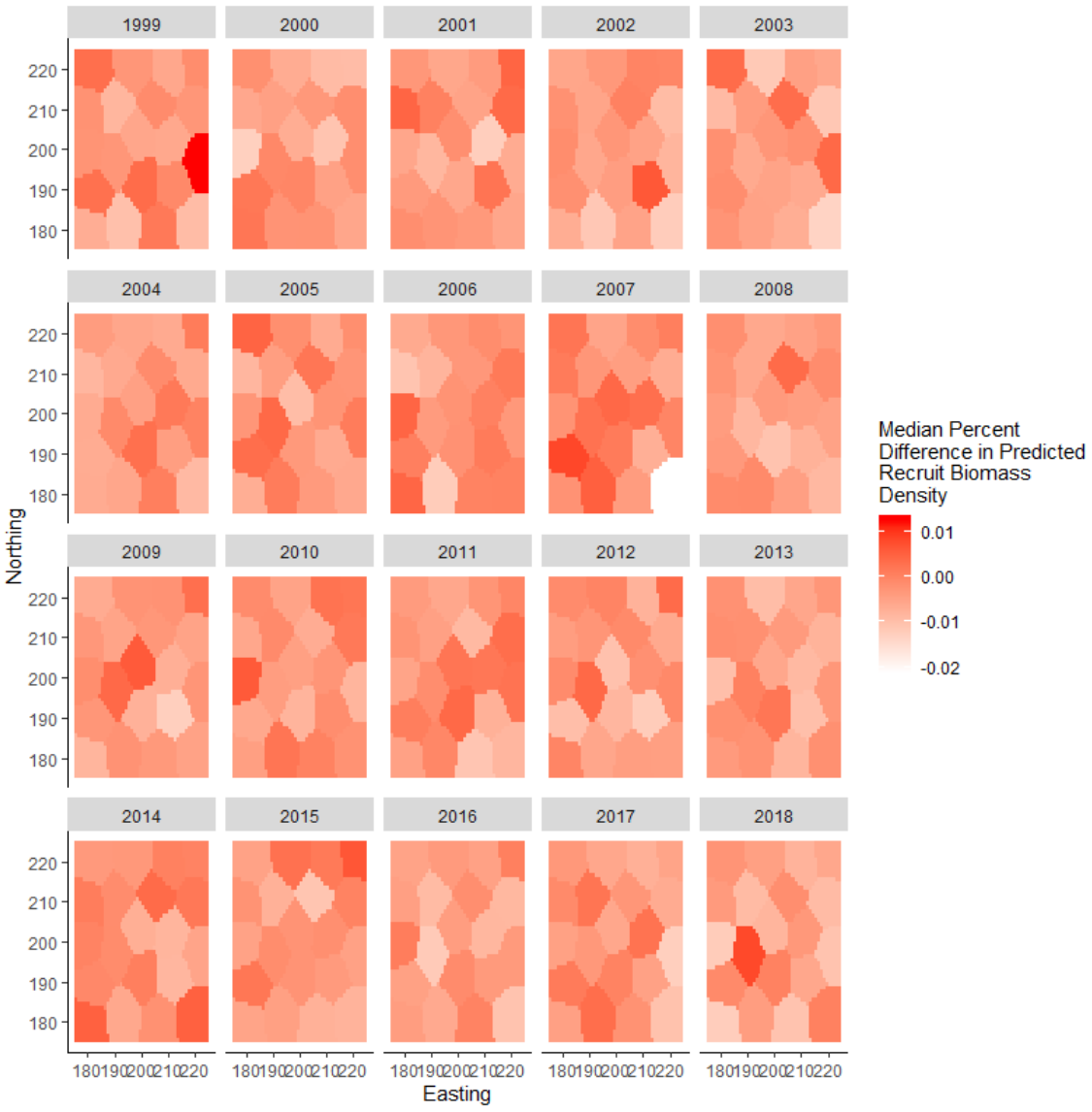

Figure B.13: Median percent difference recruit density ((predicted-true)/true) for setting C at every knot for 163 successful simulations of 20 years.

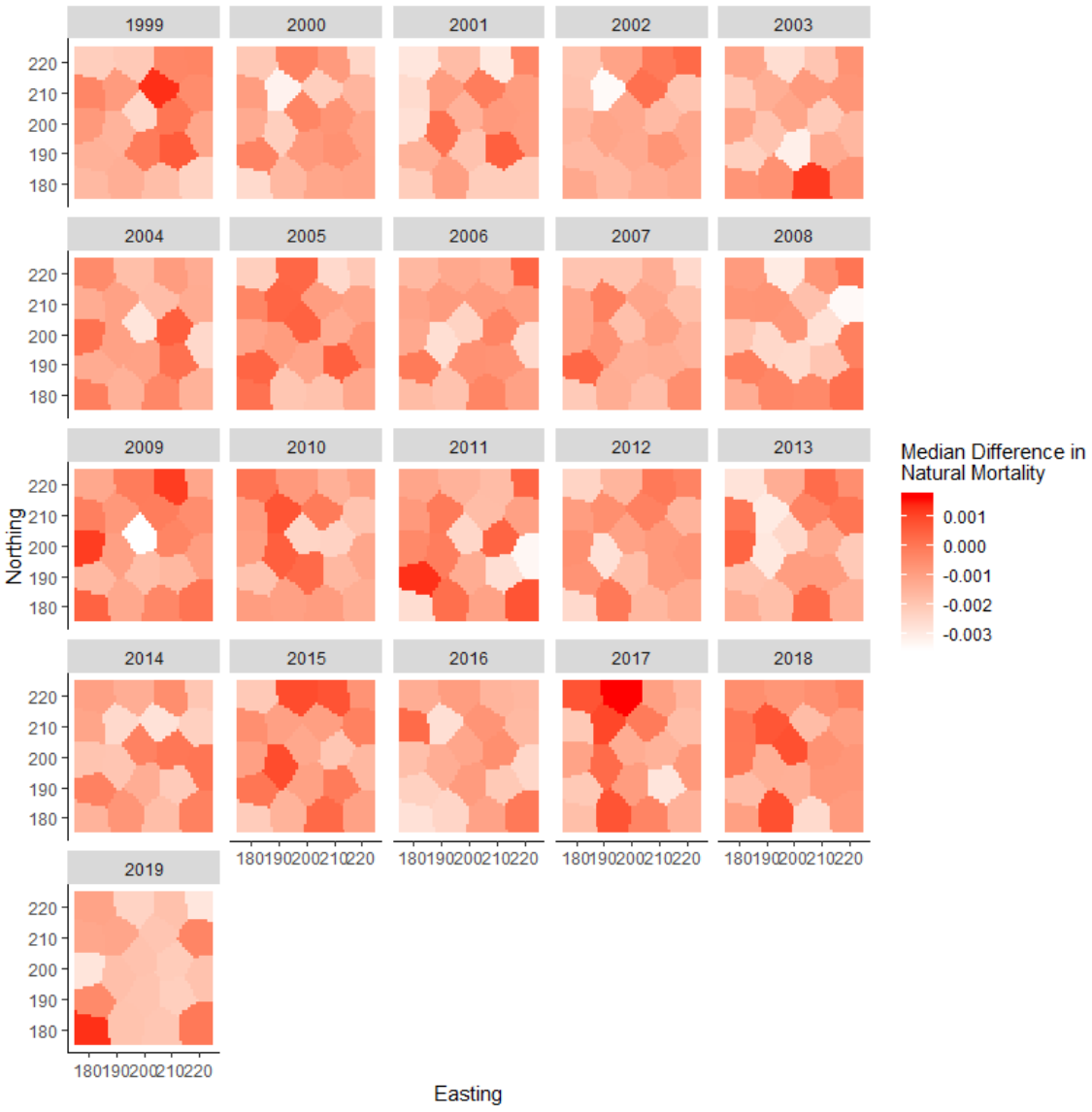

Figure B.14: Median percent difference natural mortality ((predicted-true)/true) for setting C at every knot for 163 successful simulations of 20 years.

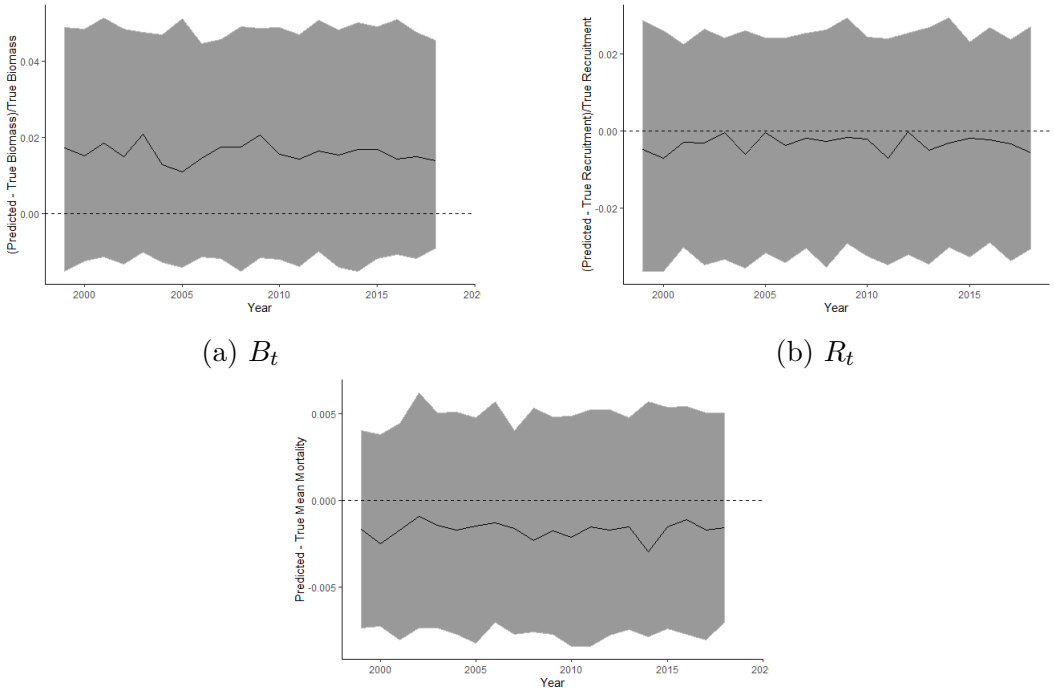

(a) B_t

(b) R_t

(c) m_t

Figure B.15: Functional boxplots (without whiskers) of the difference of the predicted random effects and their true value with horizontal dotted line at 0 and median difference shown by solid black line for setting C. B.15a and B.15b show the difference as a percentage of the true value (predicted - true / true) while B.15c simply shows the net difference (predicted - true).

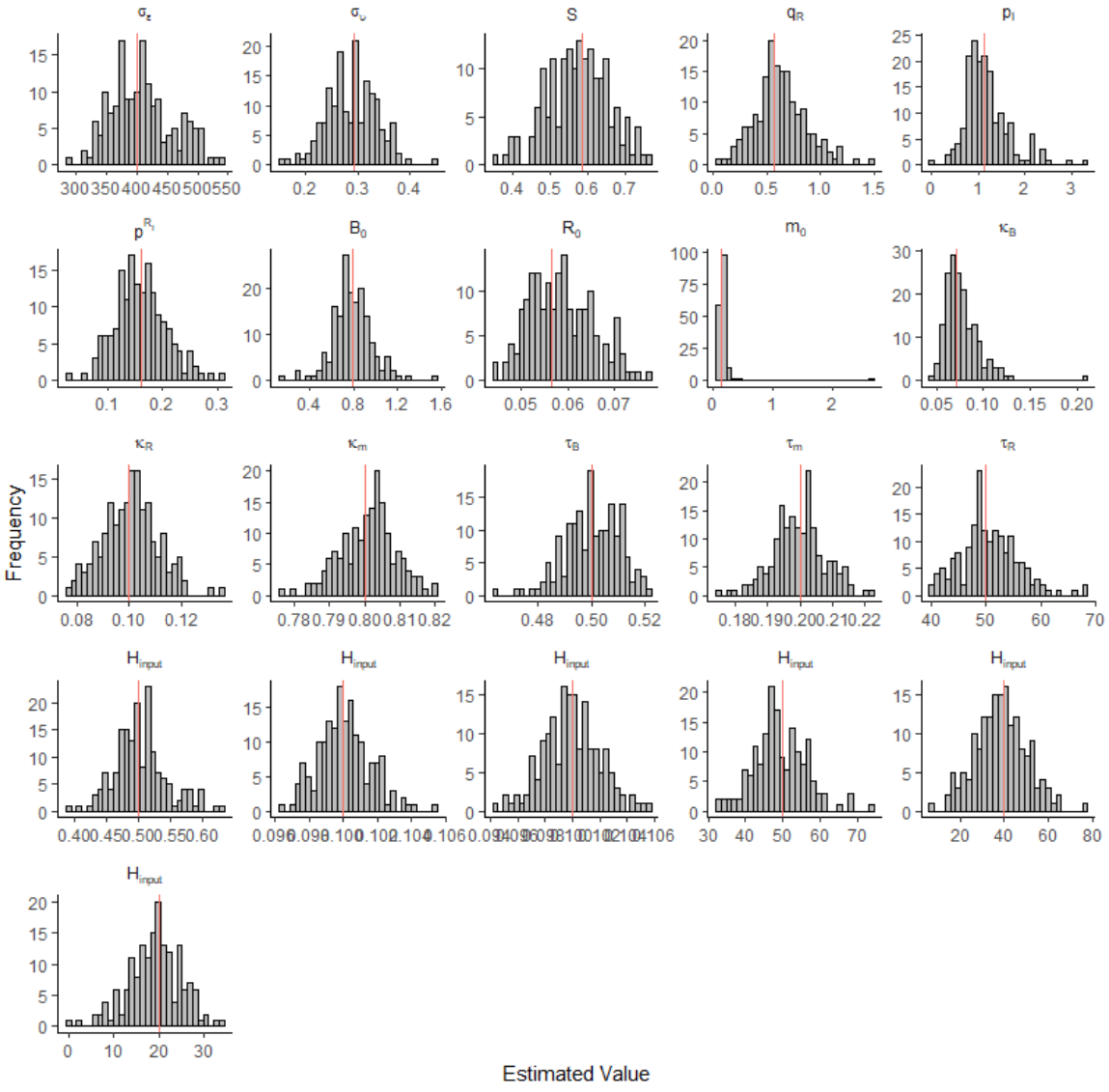

Figure B.16: Distribution of parameter estimates for setting D (146 simulations of 20 years). Red line denotes true value.

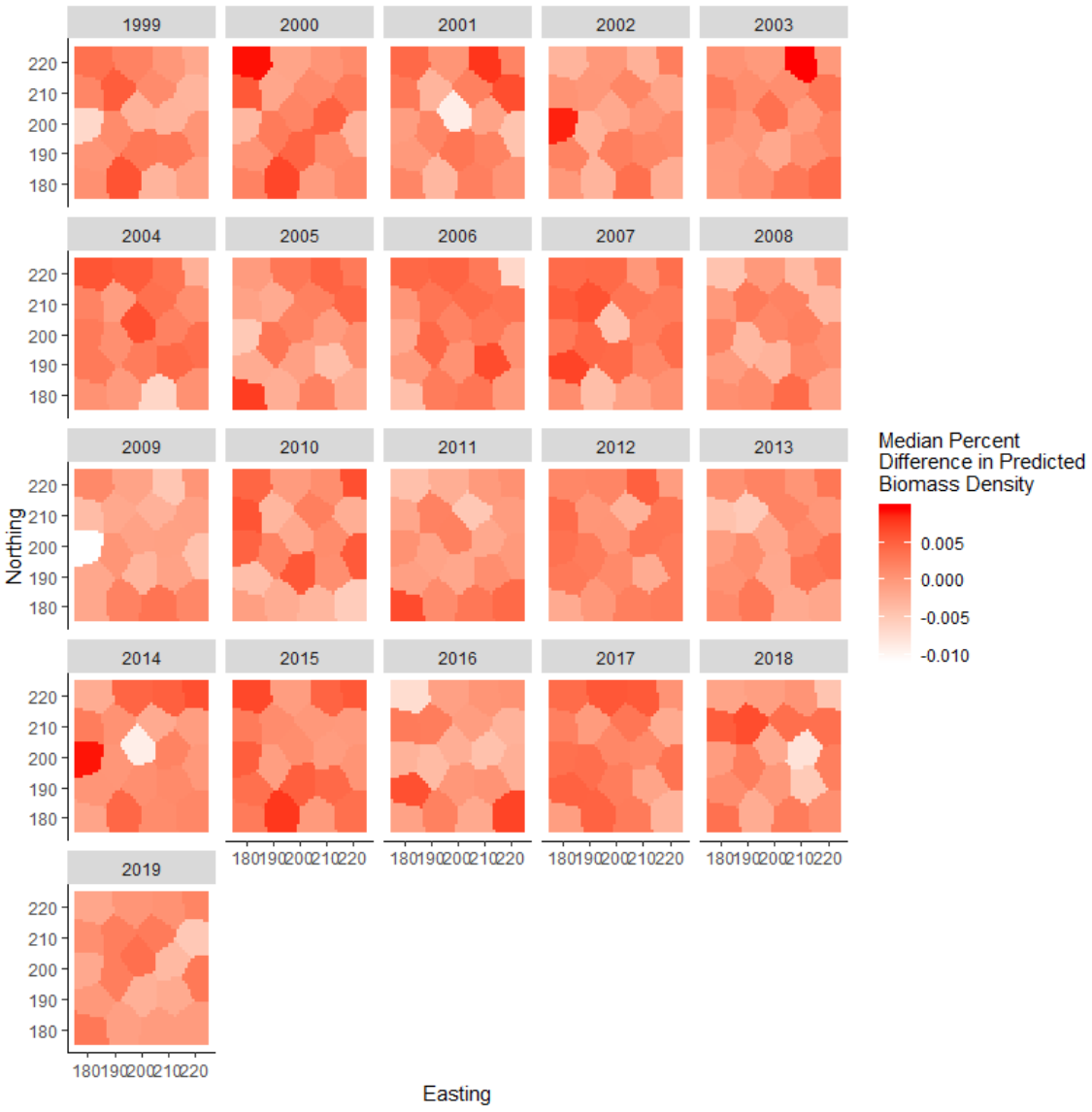

Figure B.17: Median percent difference biomass density ((predicted-true)/true) for setting D at every knot for 146 successful simulations of 20 years.

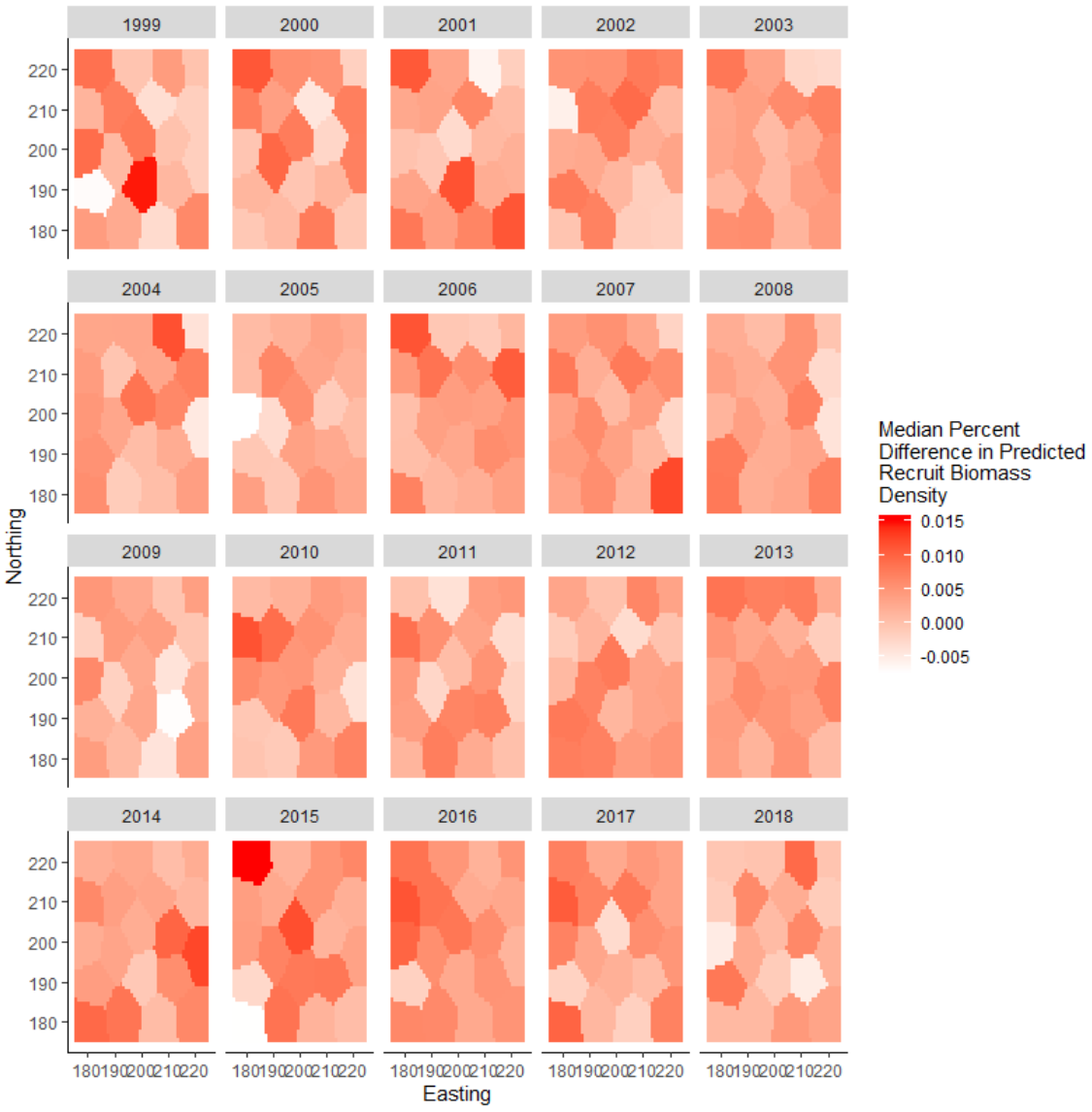

Figure B.18: Median percent difference recruit density ((predicted-true)/true) for setting D at every knot for 146 successful simulations of 20 years.

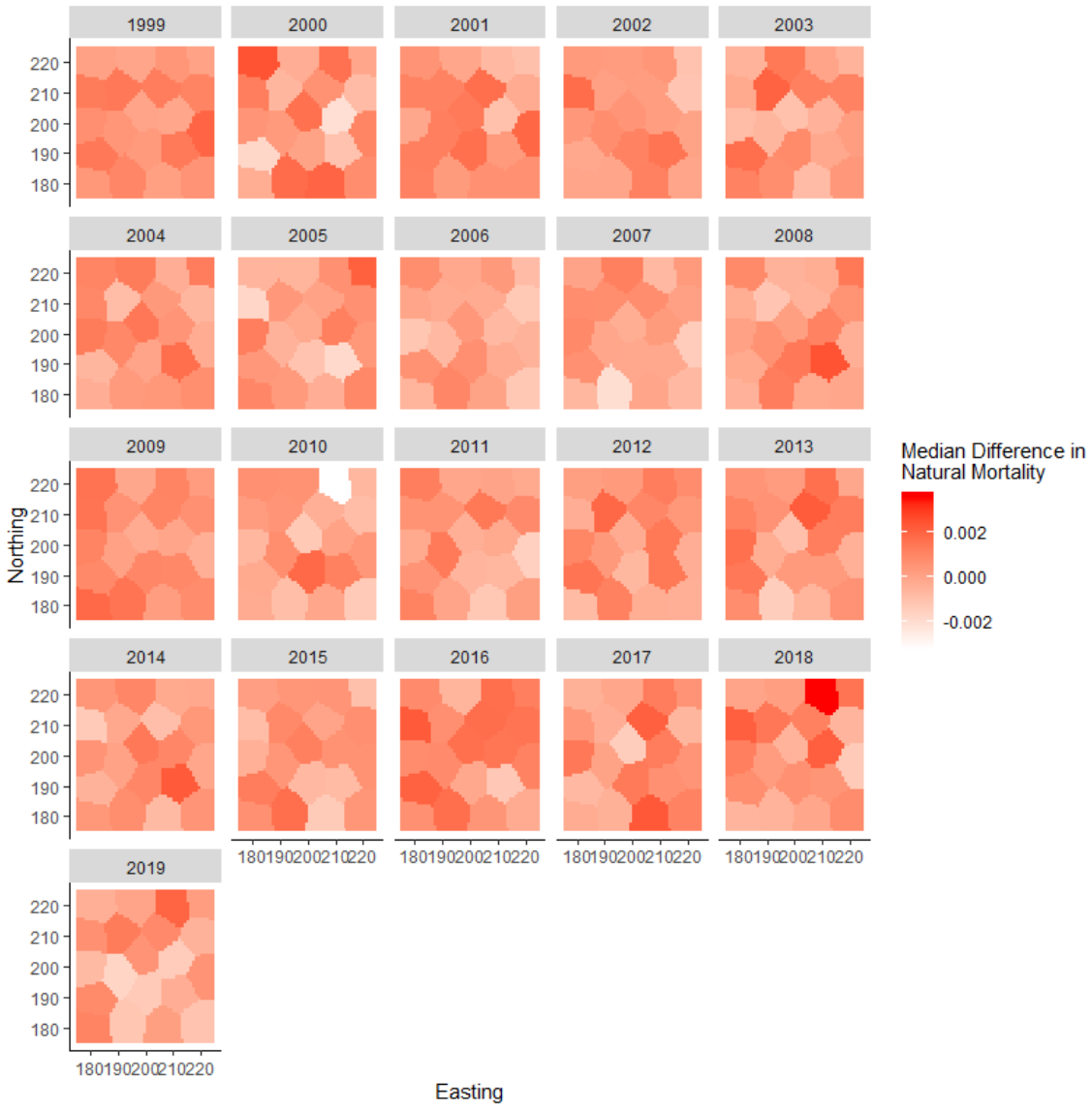

Figure B.19: Median percent difference natural mortality ((predicted-true)/true) for setting D at every knot for 146 successful simulations of 20 years.

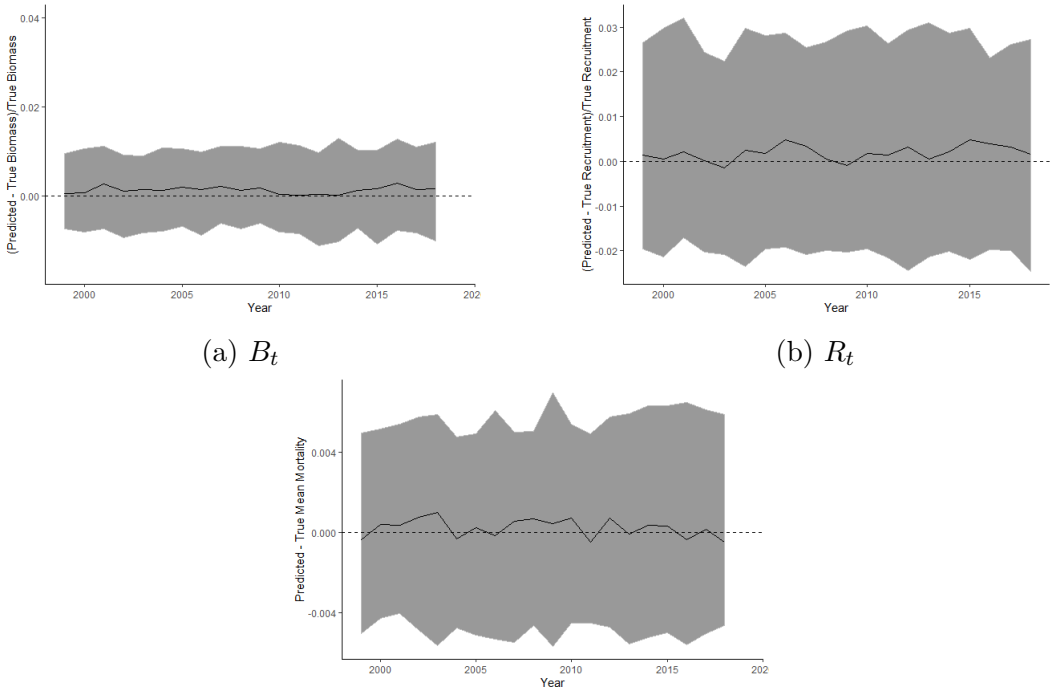

(a) B_t (b) R_t

(c) m_t

Figure B.20: Functional boxplots (without whiskers) of the difference of the predicted random effects and their true value with horizontal dotted line at 0 and median difference shown by solid black line for setting D. B.20a and B.20b show the difference as a percentage of the true value (predicted - true / true) while B.20c simply shows the net difference (predicted - true).

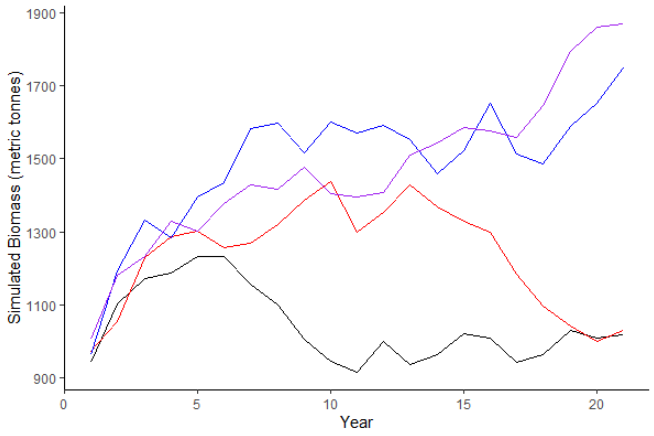

Figure B.21: Examples of simulated total biomass over 22 years by STM1.

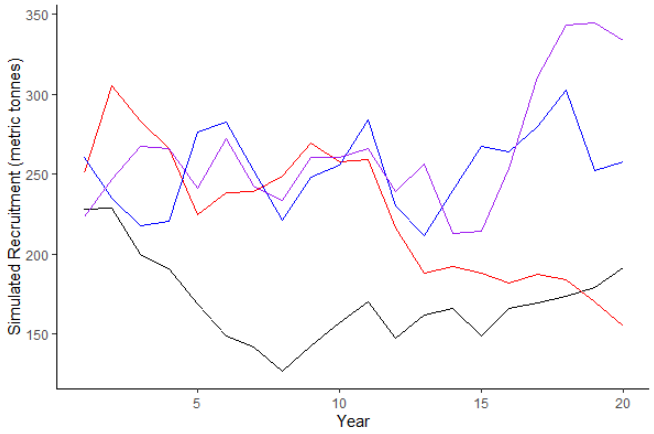

Figure B.22: Examples of simulated total recruit biomass over 22 years by STM1.

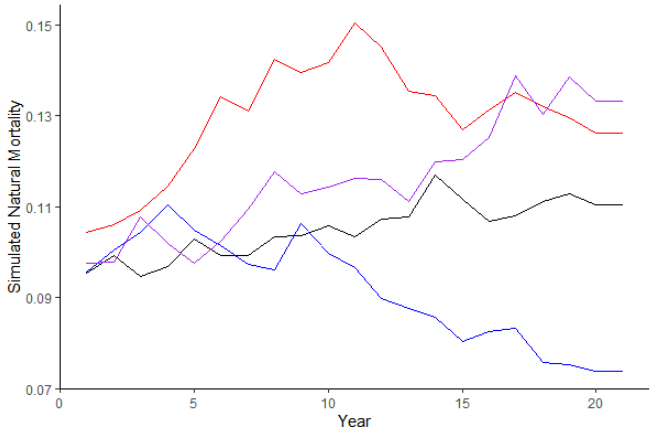

Figure B.23: Examples of simulated mean natural mortality over 22 years by STM1.

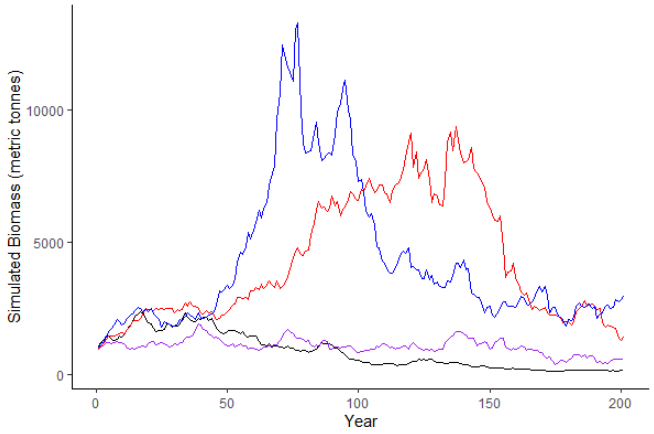

Figure B.24: Examples of simulated total biomass over 200 years by STM1.

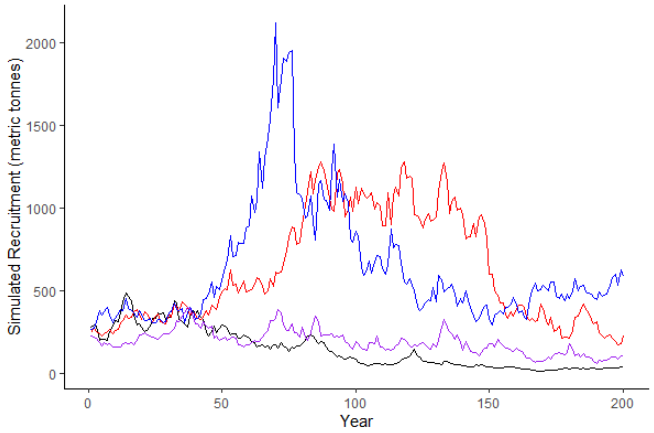

Figure B.25: Examples of simulated total recruit biomass over 200 years by STM1.

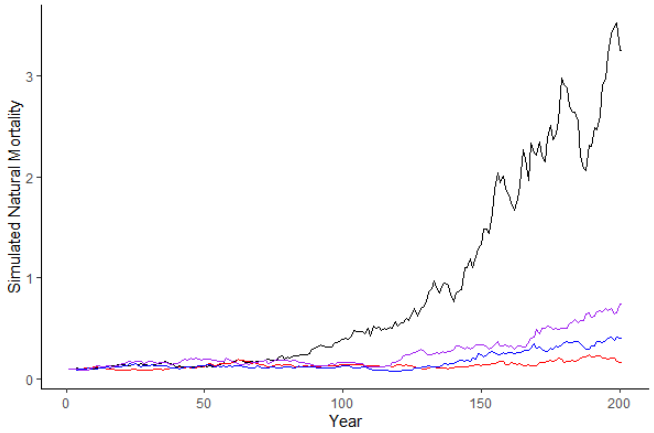

Figure B.26: Examples of simulated mean natural mortality over 200 years by STM1.

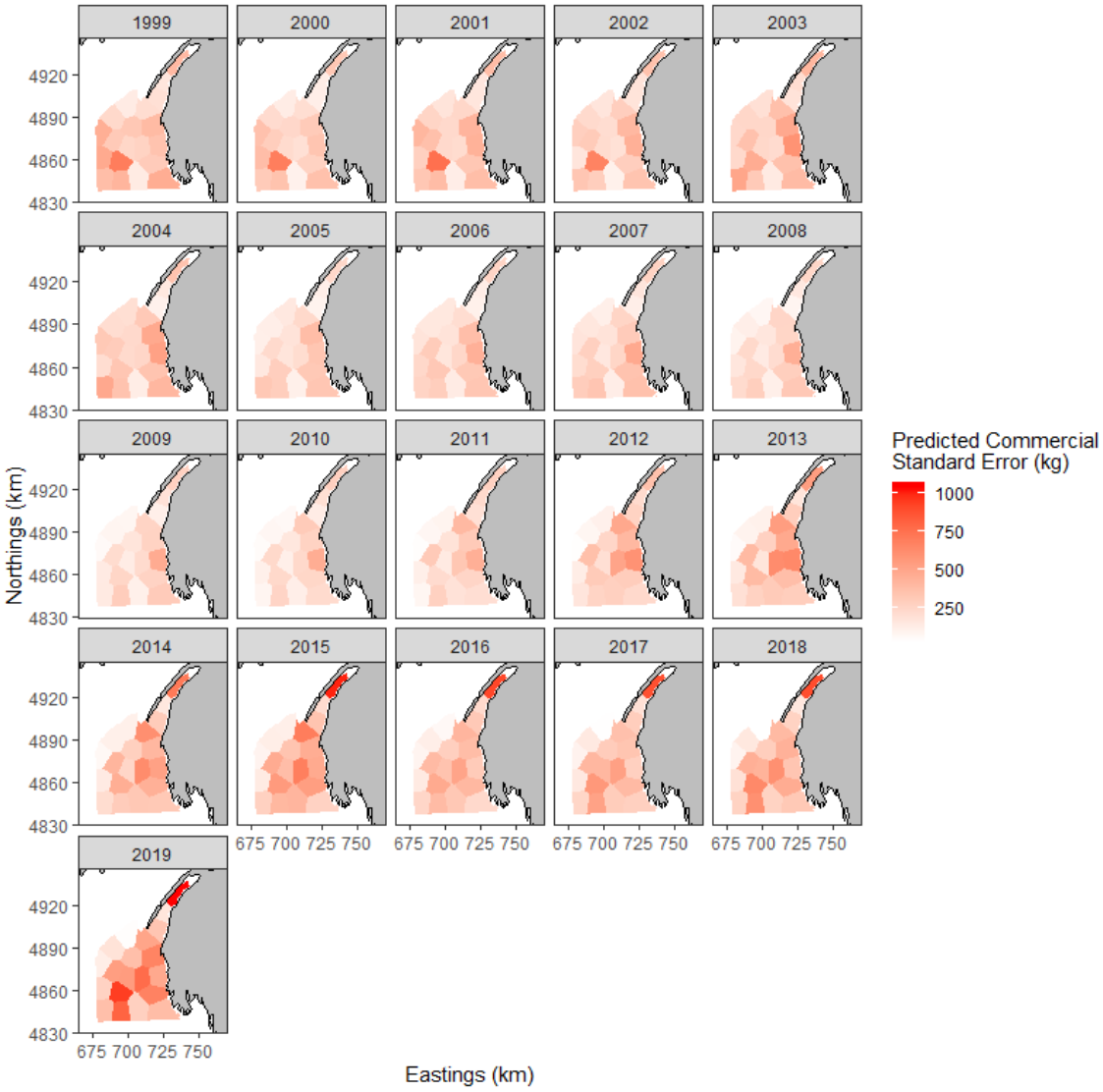

Figure B.27: Commercial size biomass density standard error (kg/km^2) at each knot between 1999 and 2019 for STM1 when q_I is fixed..

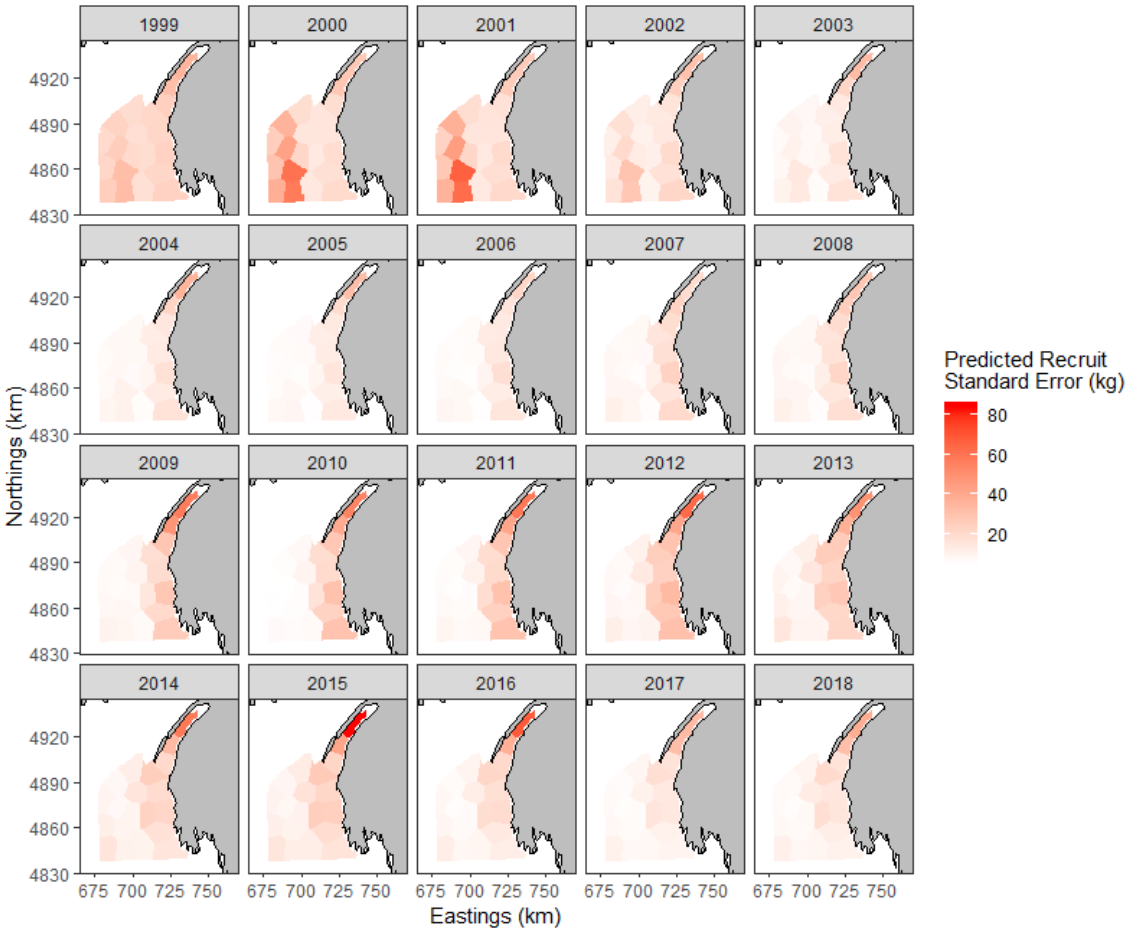

Figure B.28: Recruit biomass density standard error (kg/km^2) at each knot between 1999 and 2018 for STM1 when q_I is fixed..

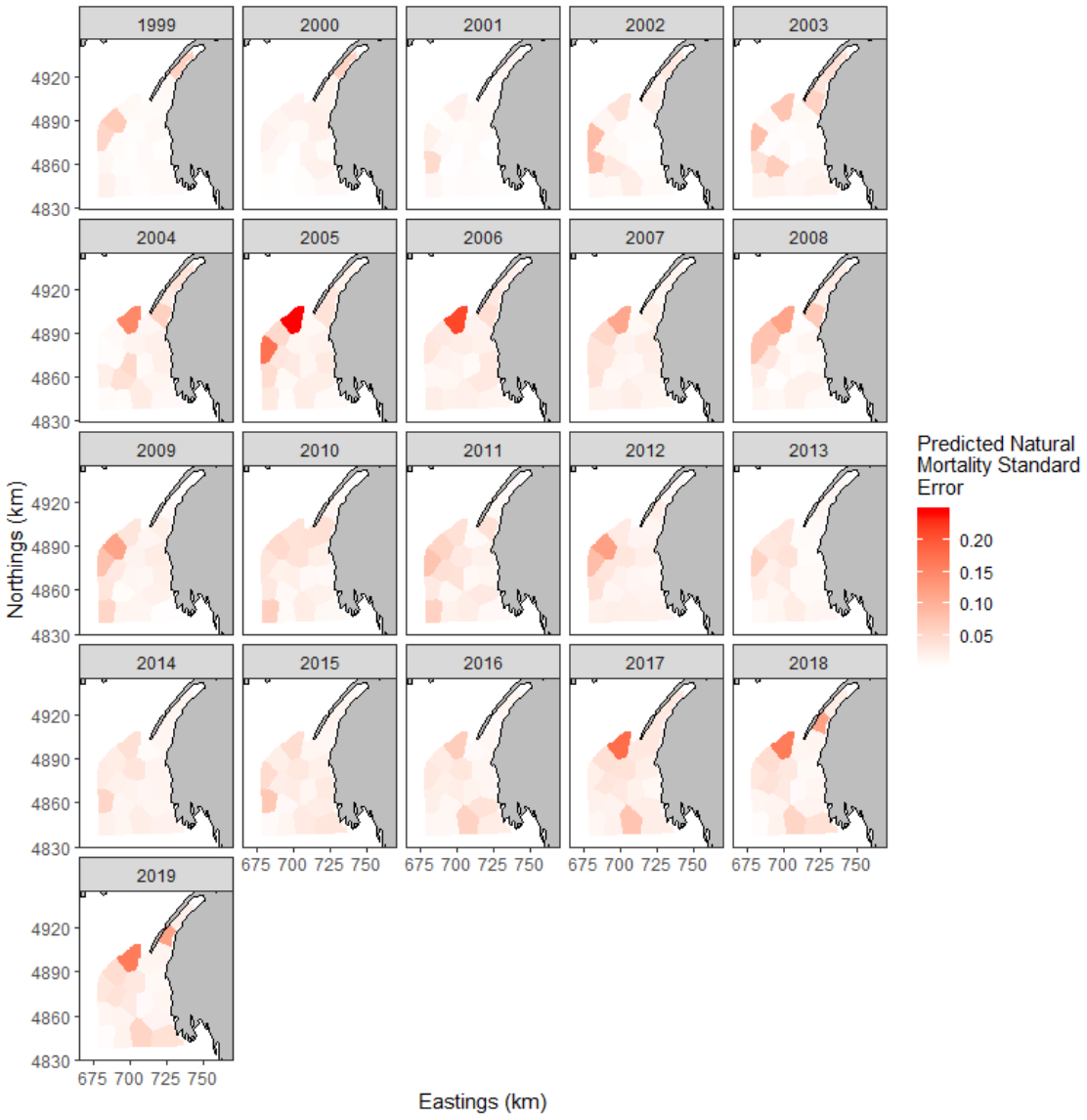

Figure B.29: Natural mortality standard error at each knot between 1999 and 2019 for STM1 when q_I is fixed.

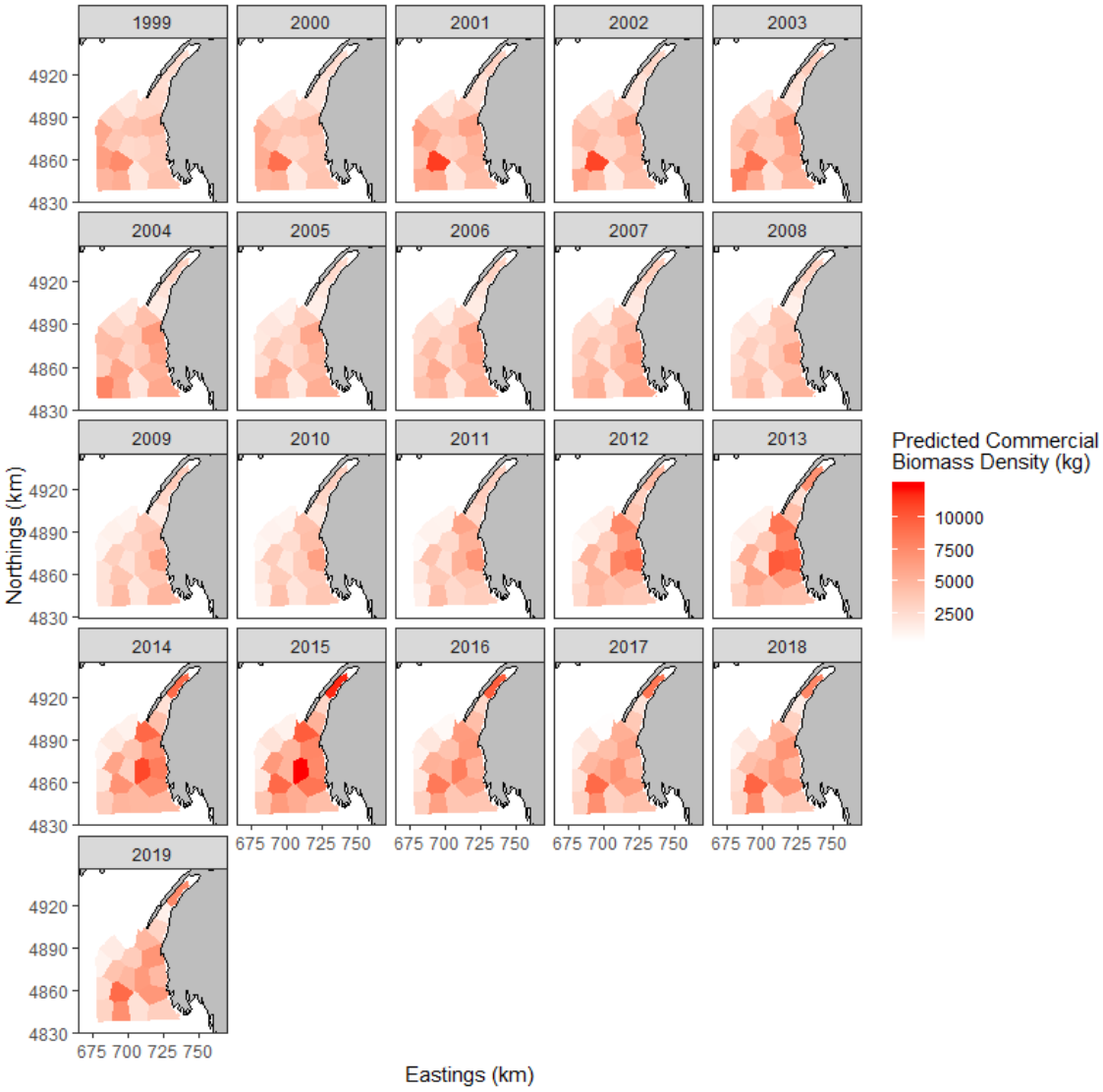

Figure B.30: Predicted commercial size biomass density (kg/km^2) at each knot between 1999 and 2019 for STM1 when q_I is estimated.

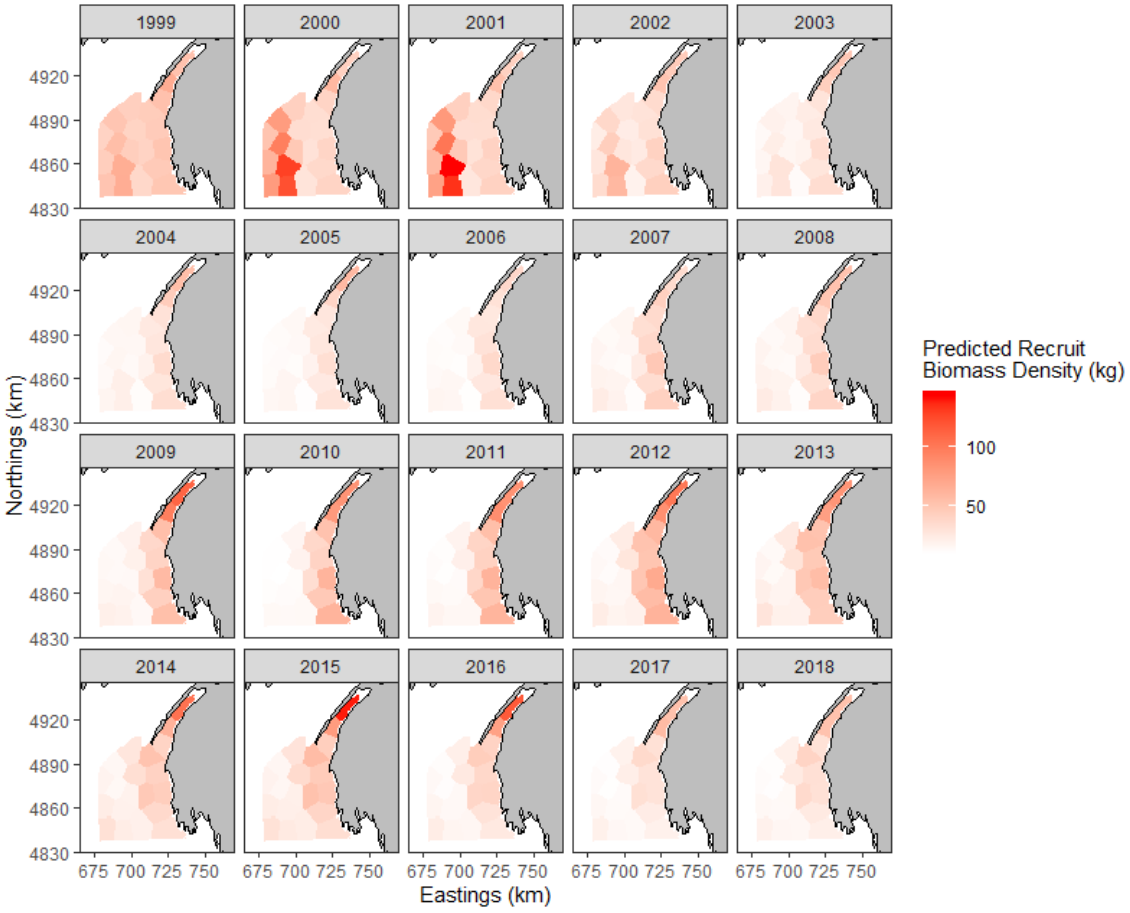

Figure B.31: Predicted recruit biomass density (kg/km^2) at each knot between 1999 and 2018 for STM1 when q_I is estimated.

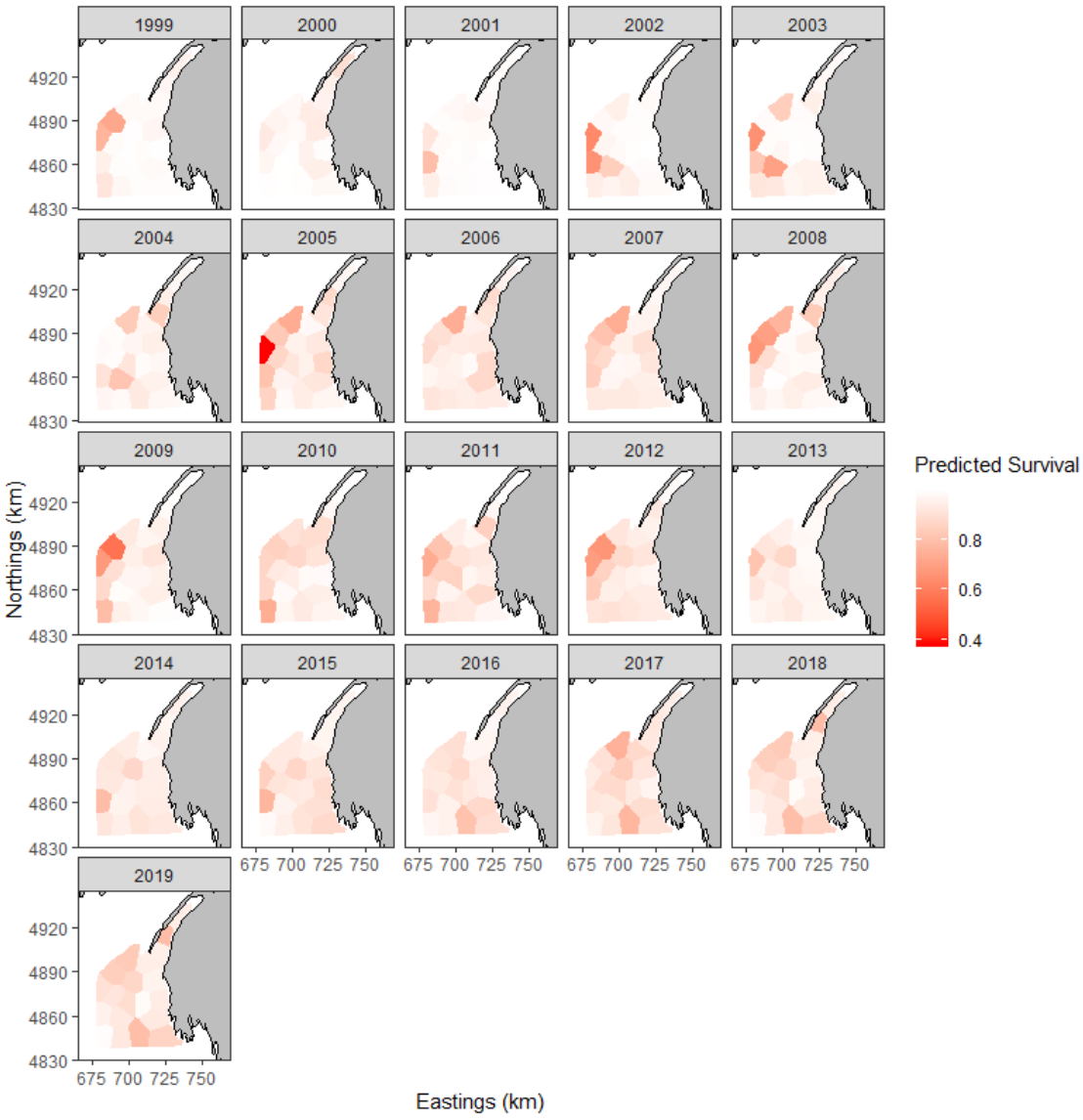

Figure B.32: Predicted survival at each knot between 1999 and 2019 for STM1 when q_I is estimated.

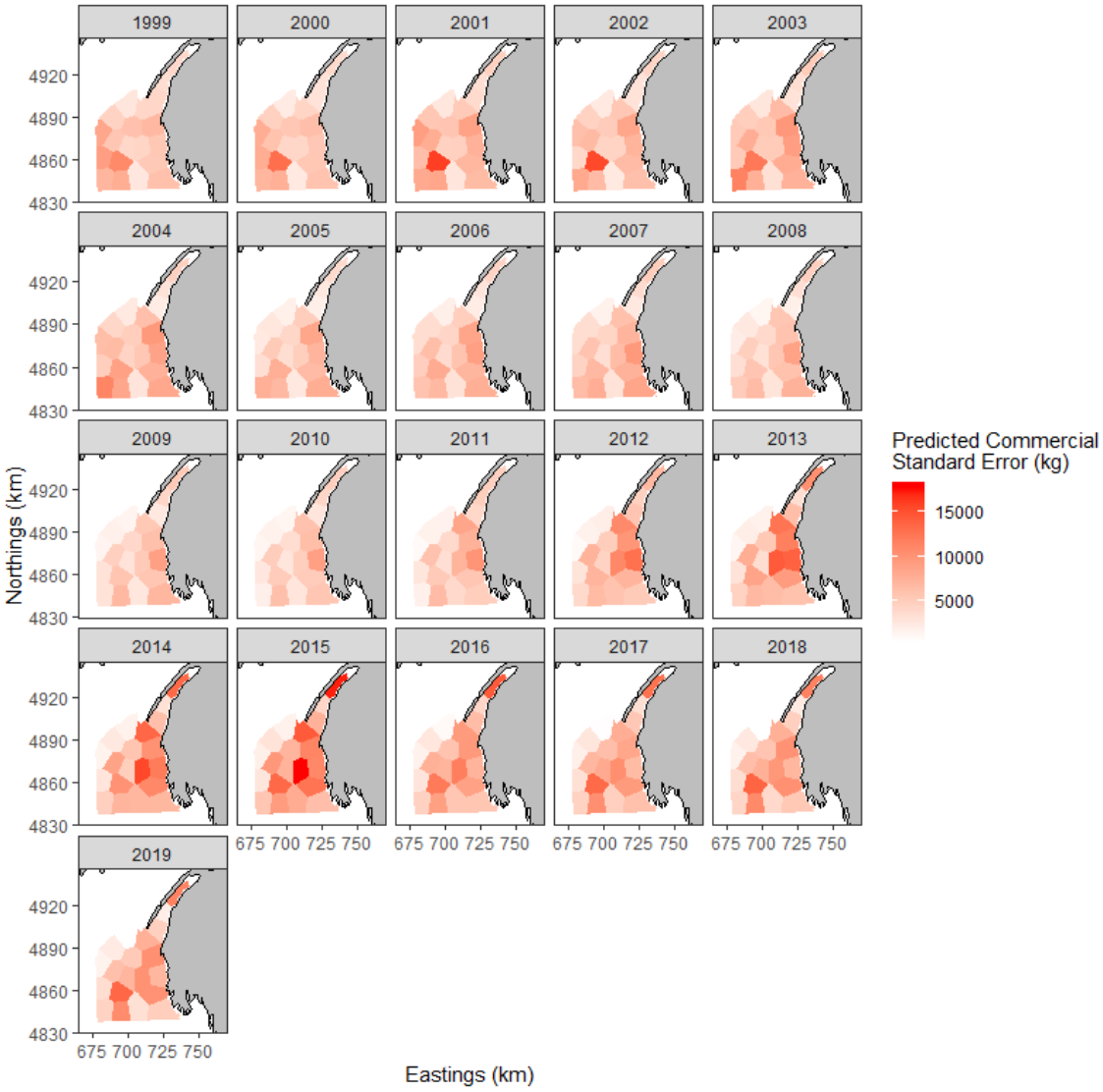

Figure B.33: Commercial size biomass density standard error (kg/km^2) at each knot between 1999 and 2019 for STM1 when q_I is estimated.

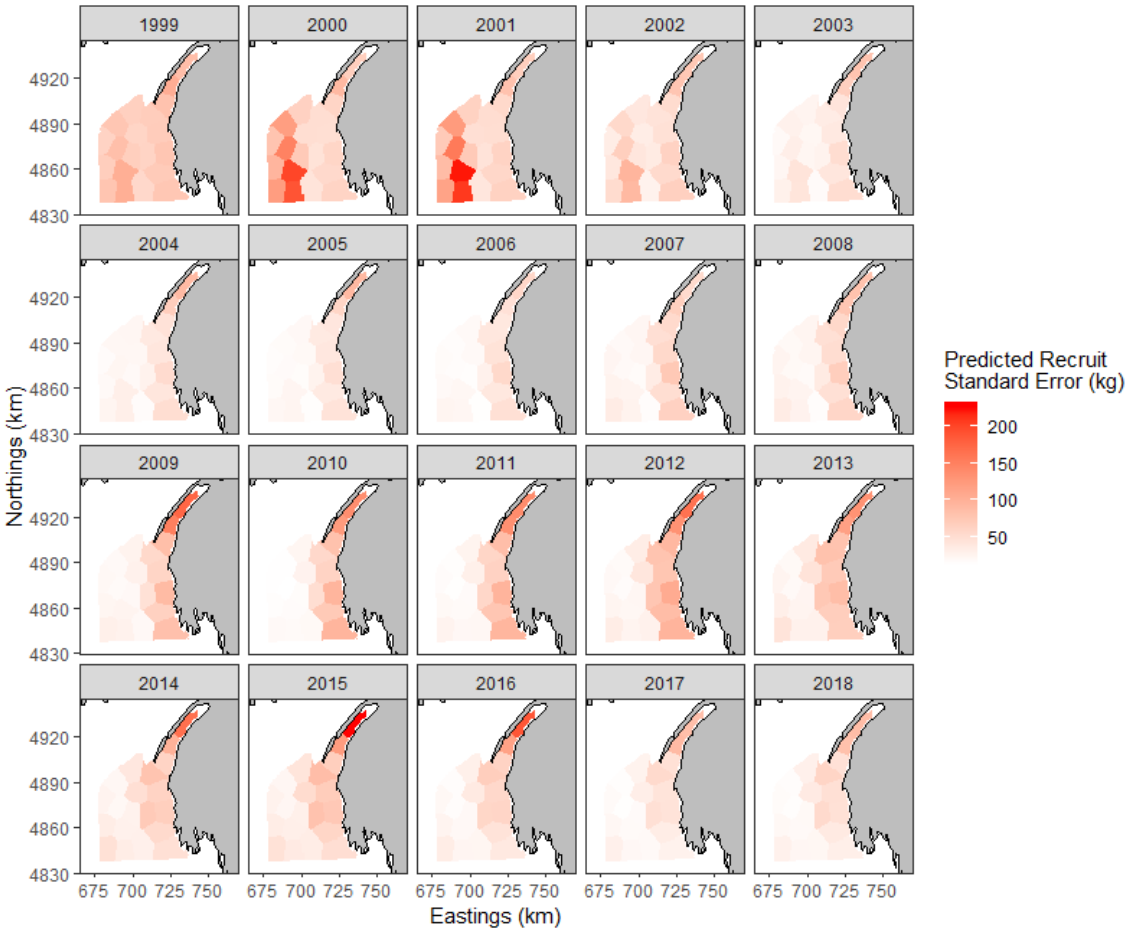

Figure B.34: Recruit biomass density standard error (kg/km^2) at each knot between 1999 and 2018 for STM1 when q_I is estimated.

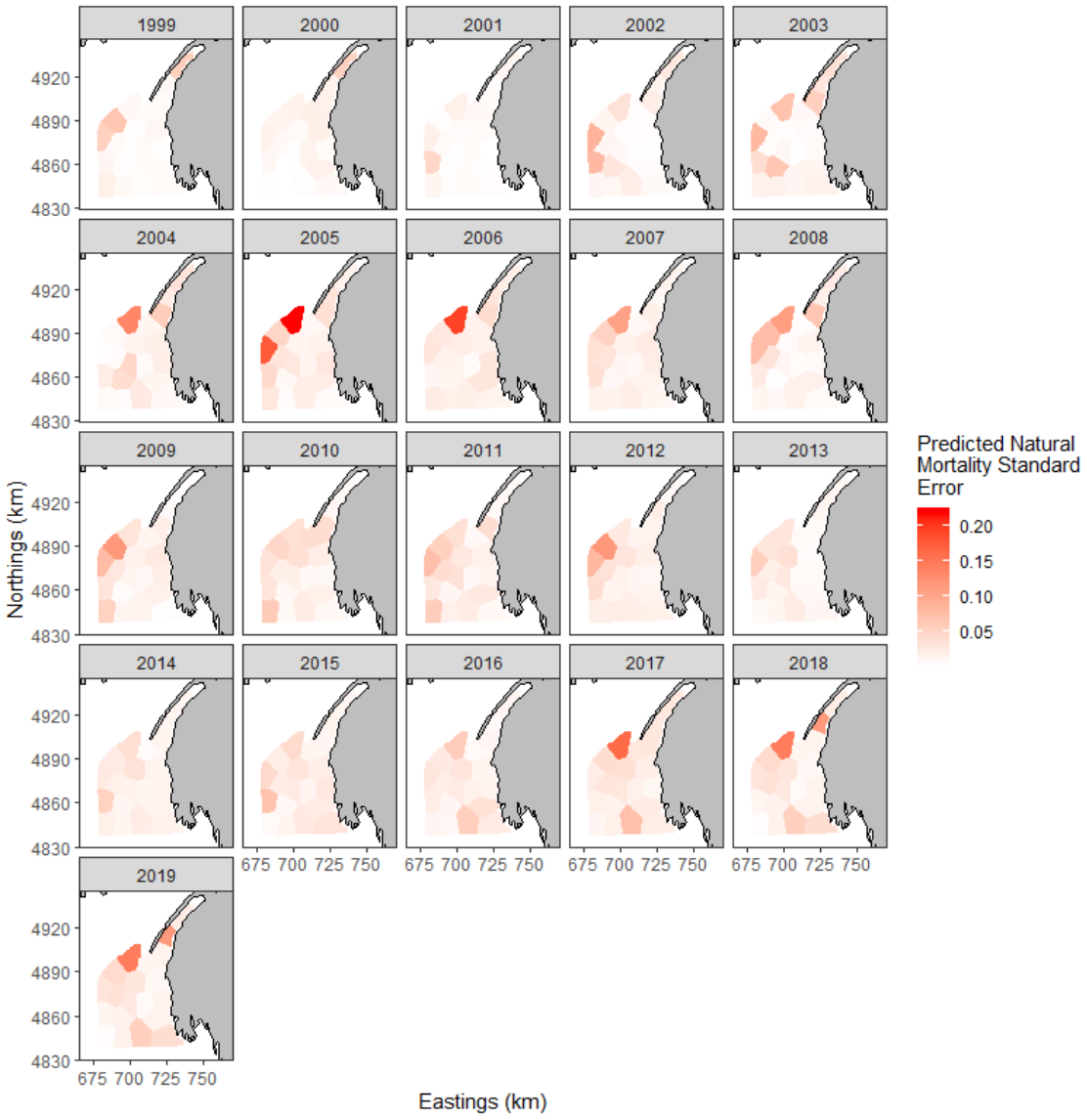

Figure B.35: Natural mortality standard error at each knot between 1999 and 2019 for STM1 when q_I is estimated.

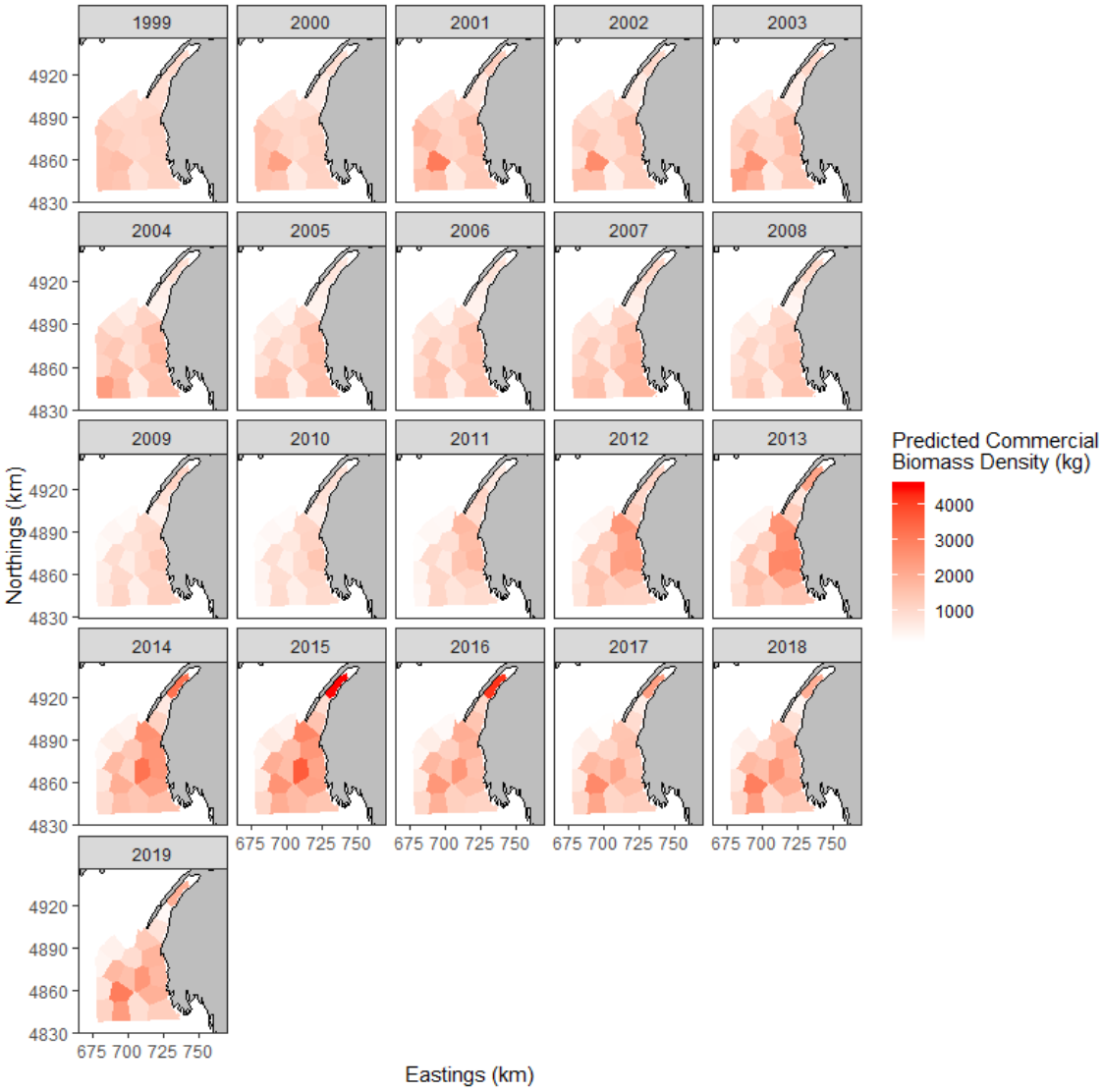

Figure B.36: Predicted commercial size biomass density (kg/km^2) at each knot between 1999 and 2019 for STM2 when q_I is fixed.

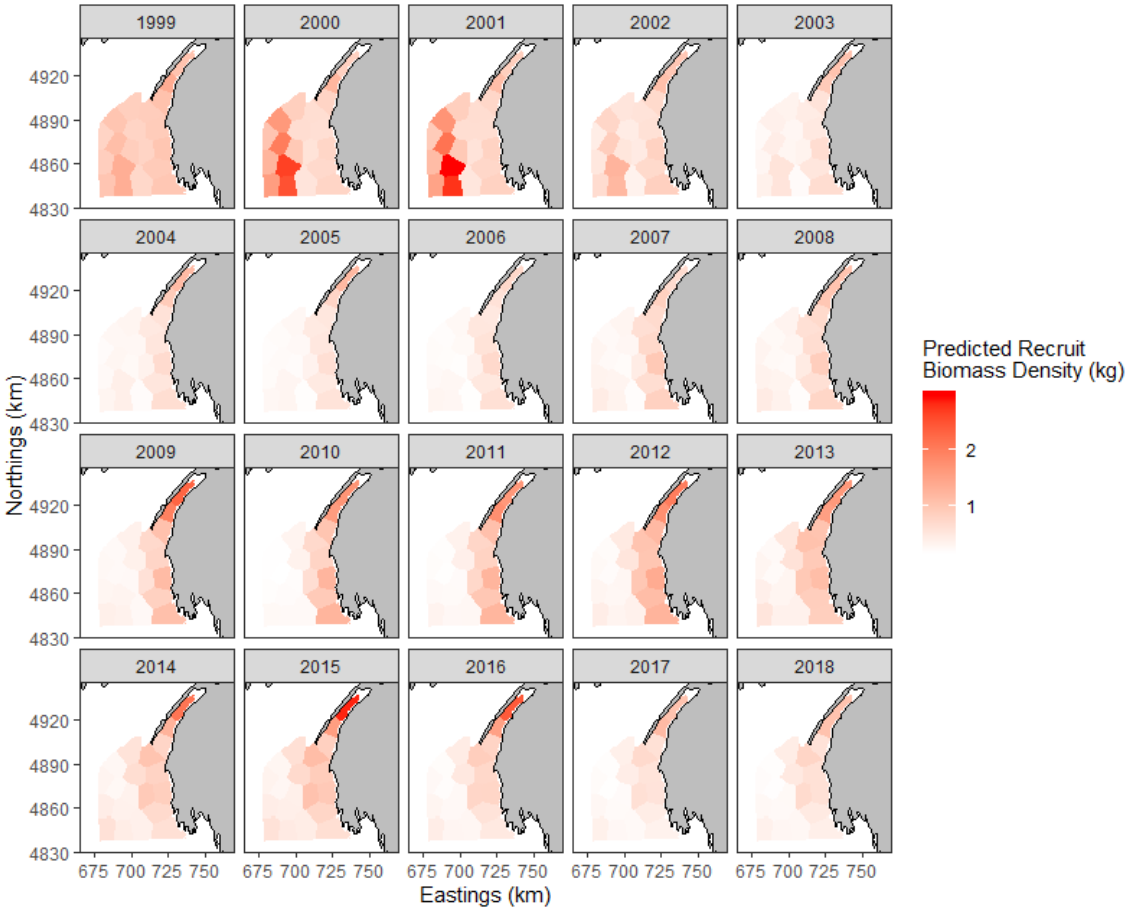

Figure B.37: Predicted recruit biomass density (kg/km^2) at each knot between 1999 and 2018 for STM2 when q_I is fixed.

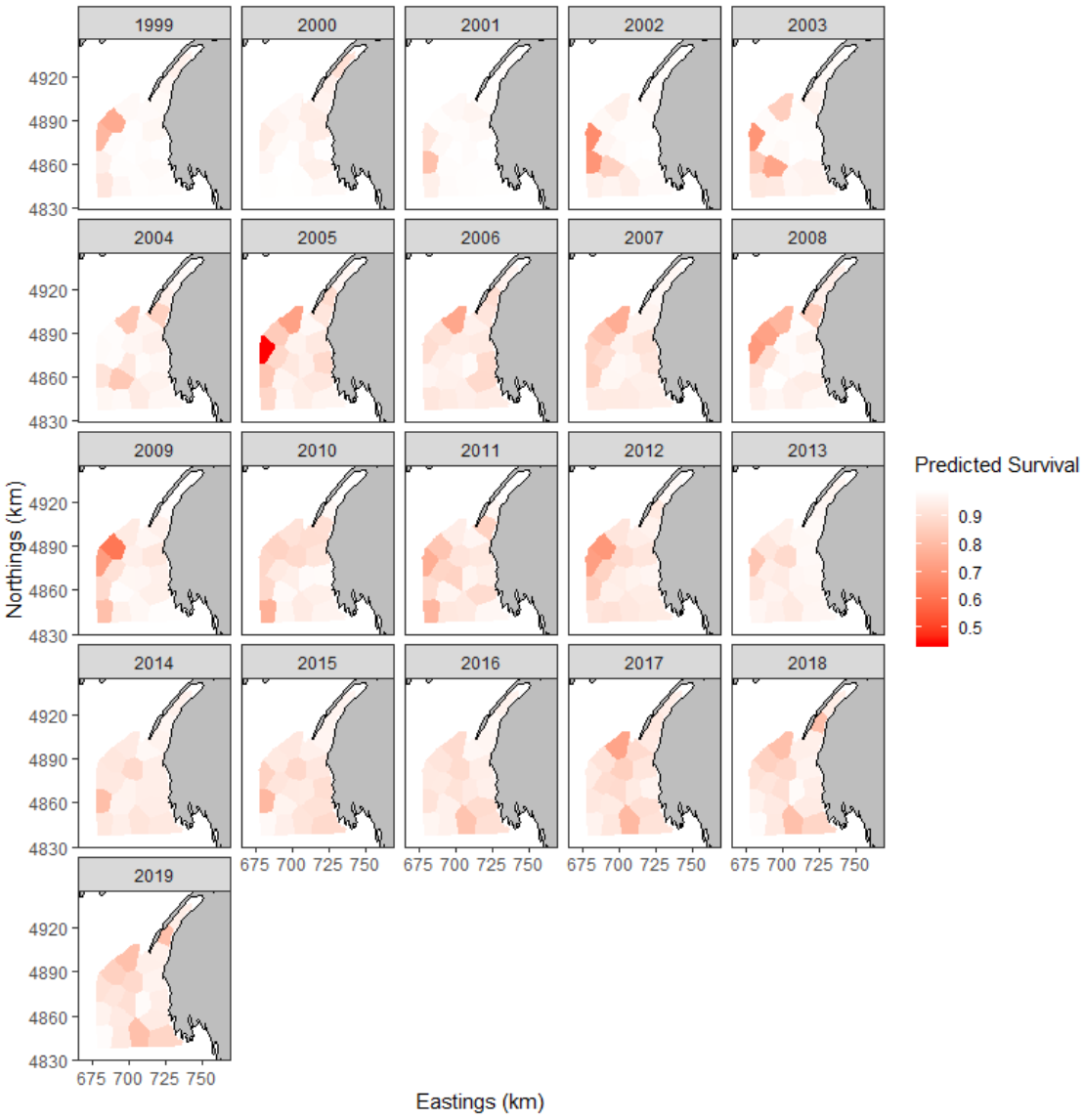

Figure B.38: Predicted survival at each knot between 1999 and 2019 for STM2 when q_I is fixed.

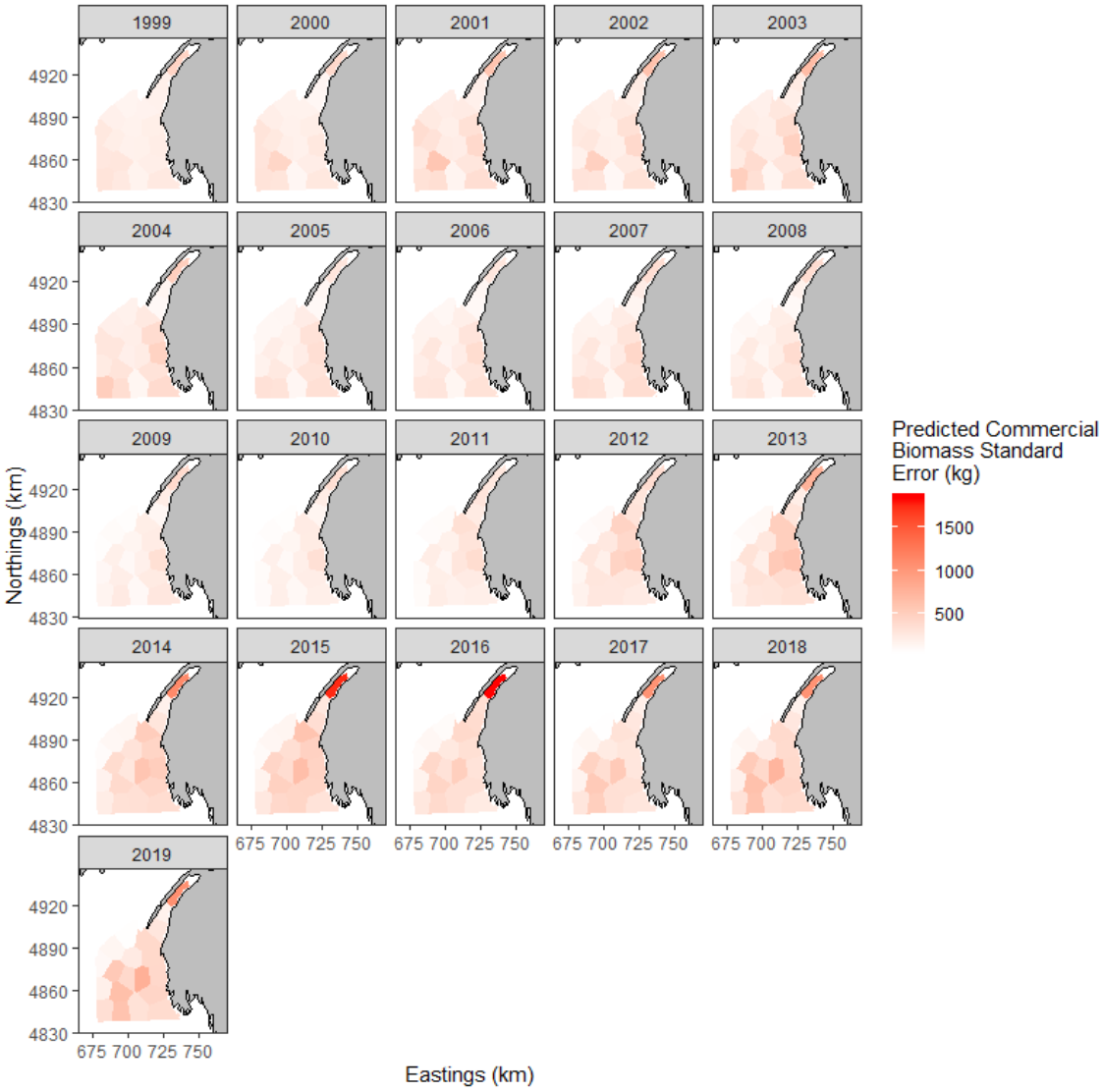

Figure B.39: Commercial size biomass density standard error (kg/km^2) at each knot between 1999 and 2019 for STM2 when q_I is fixed.

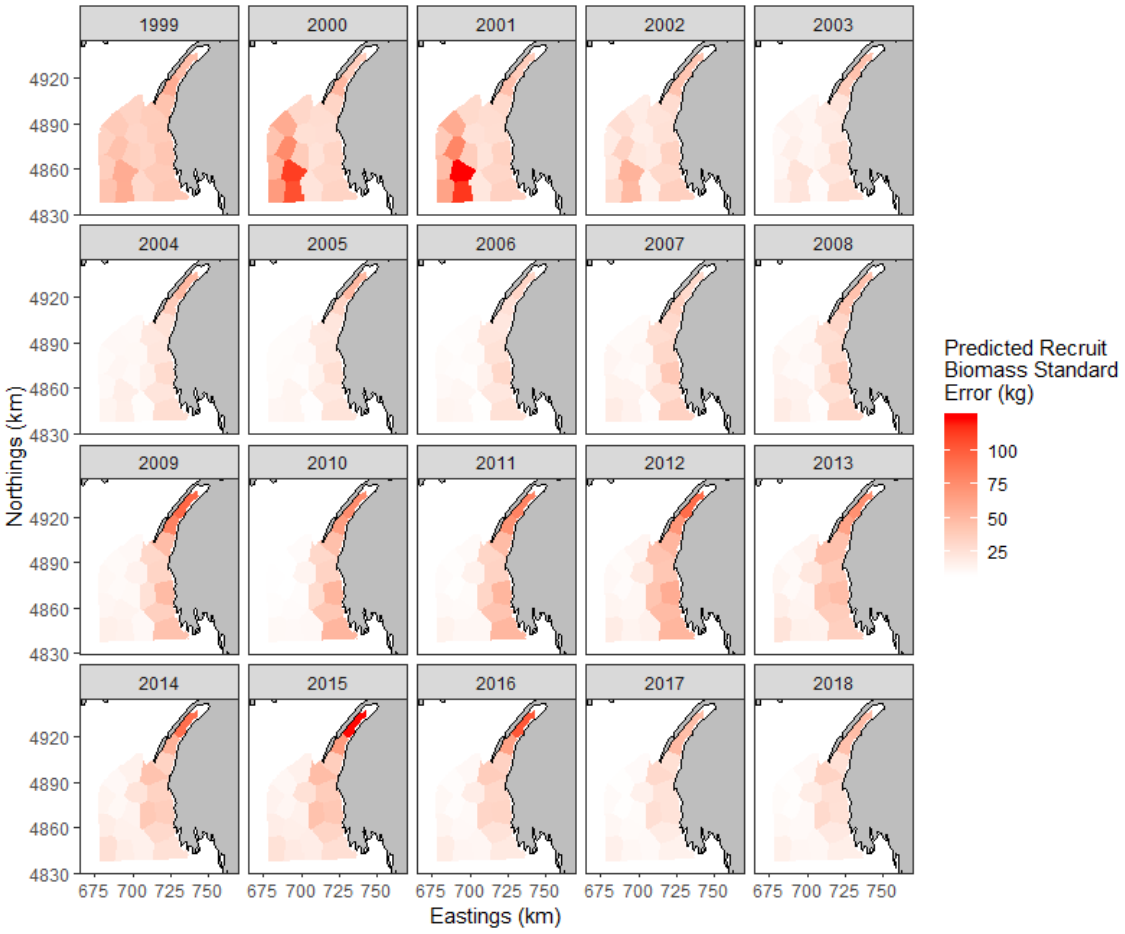

Figure B.40: Recruit biomass density standard error (kg/km^2) at each knot between 1999 and 2018 for STM2 when q_I is fixed.

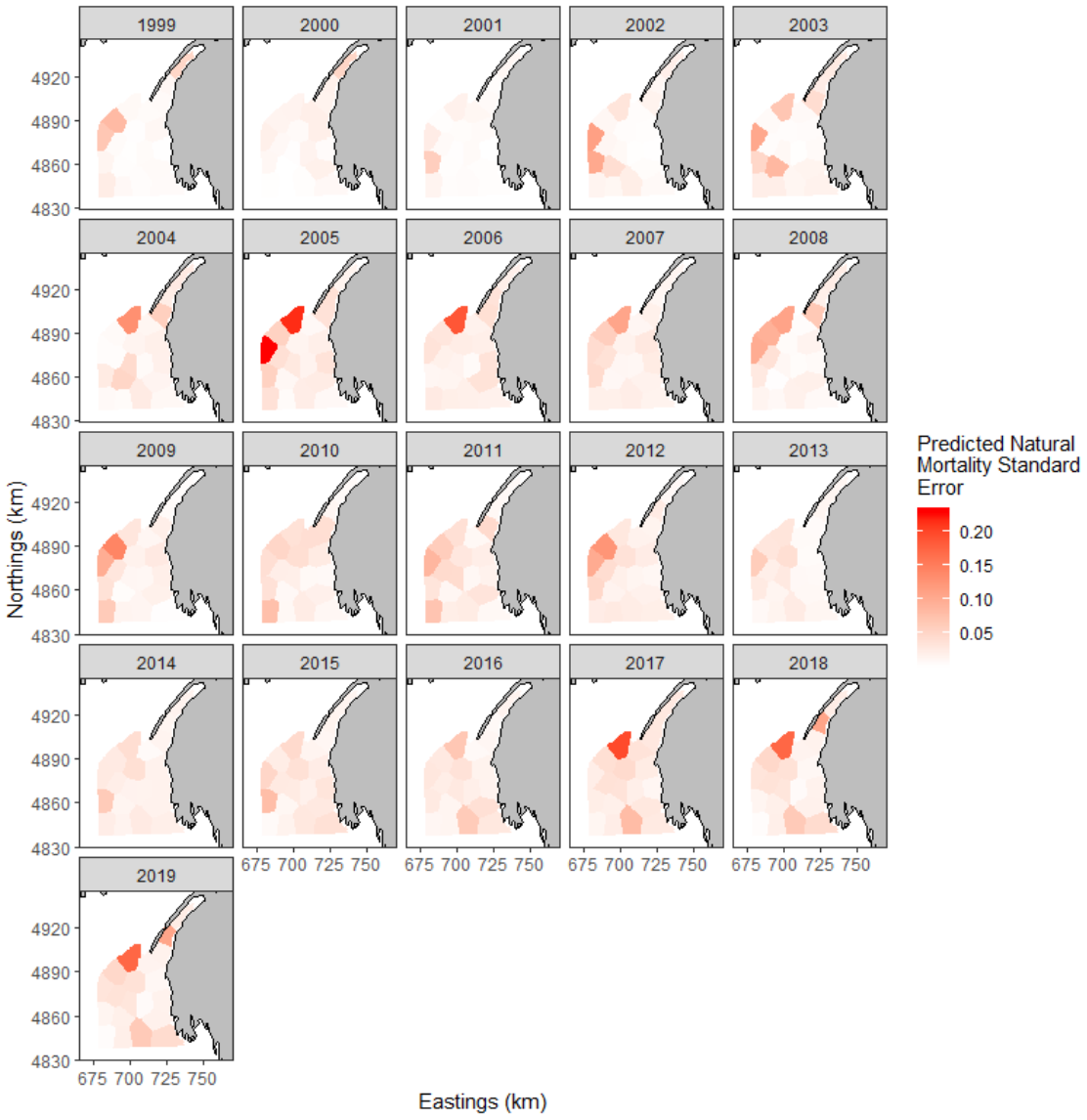

Figure B.41: Natural mortality standard error at each knot between 1999 and 2019 for STM2 when q_I is fixed.

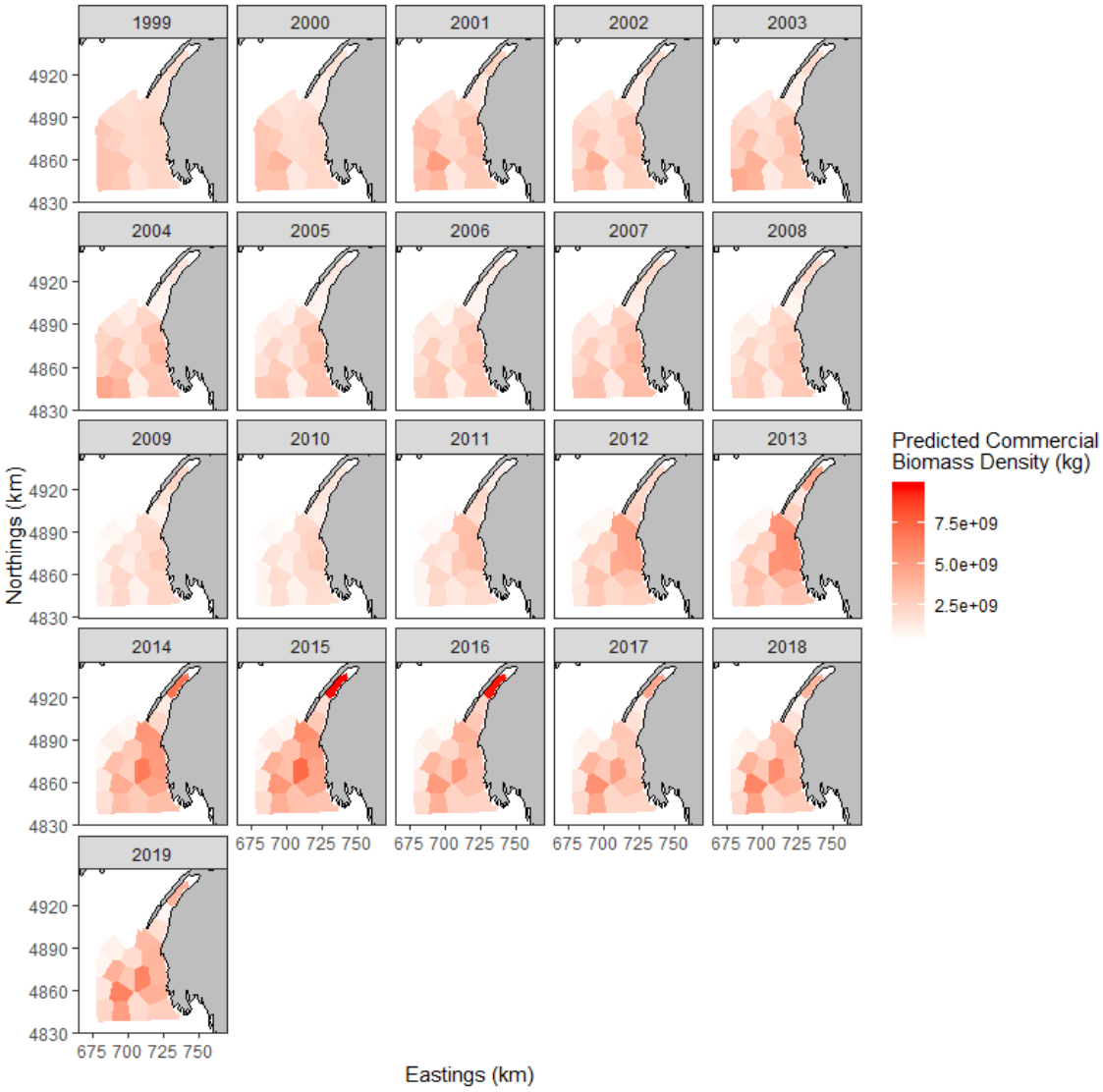

Figure B.42: Predicted commercial size biomass density (kg/km^2) at each knot between 1999 and 2019 for STM2 when q_I is estimated.

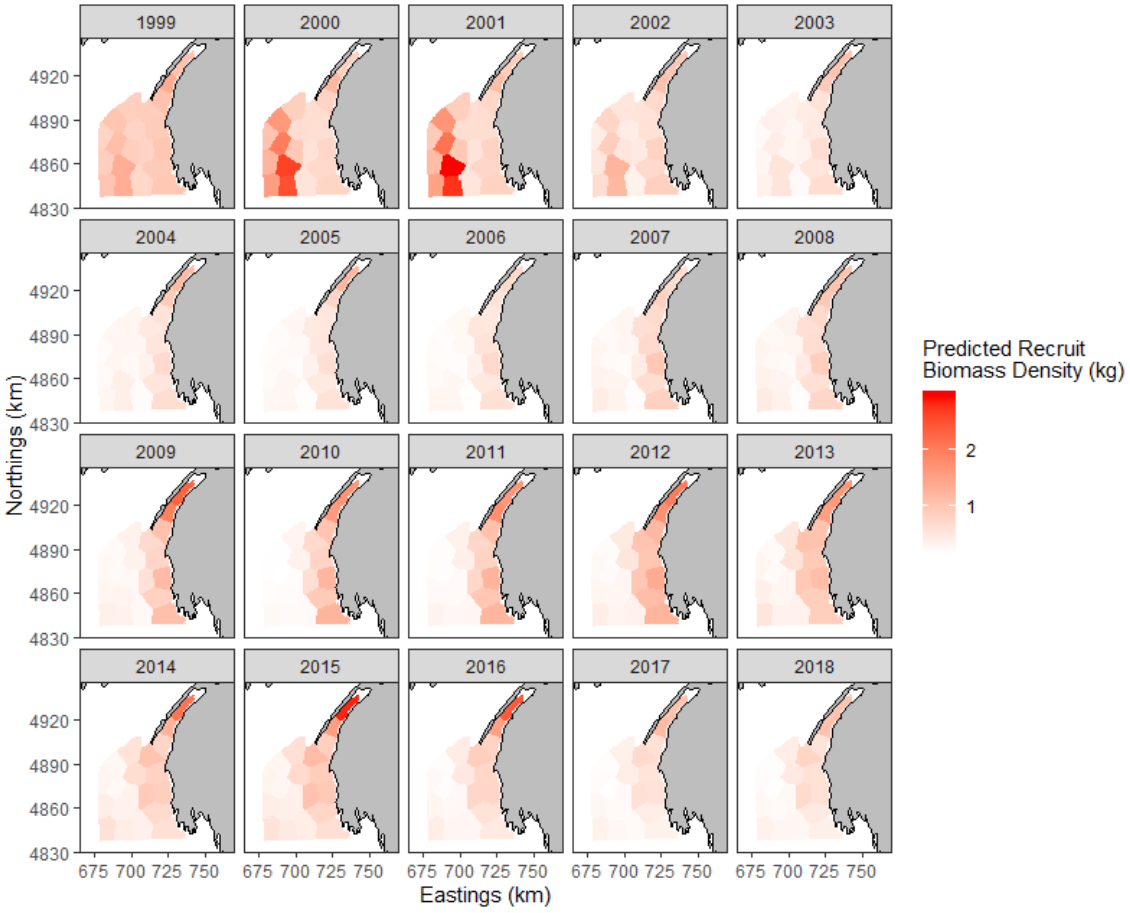

Figure B.43: Predicted recruit biomass density (kg/km^2) at each knot between 1999 and 2018 for STM2 when q_I is estimated.

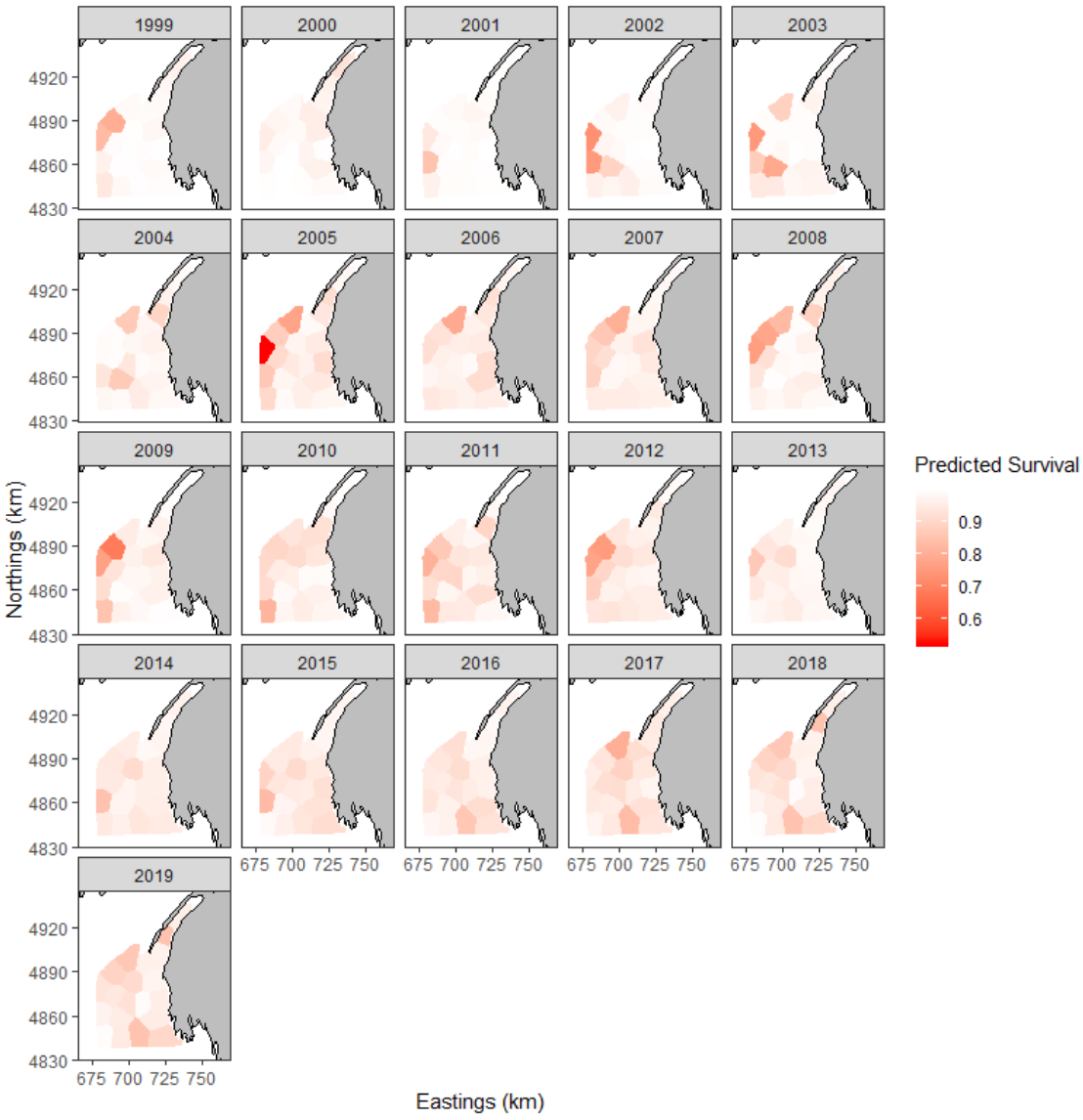

Figure B.44: Predicted survival at each knot between 1999 and 2019 for STM2 when q_I is estimated.

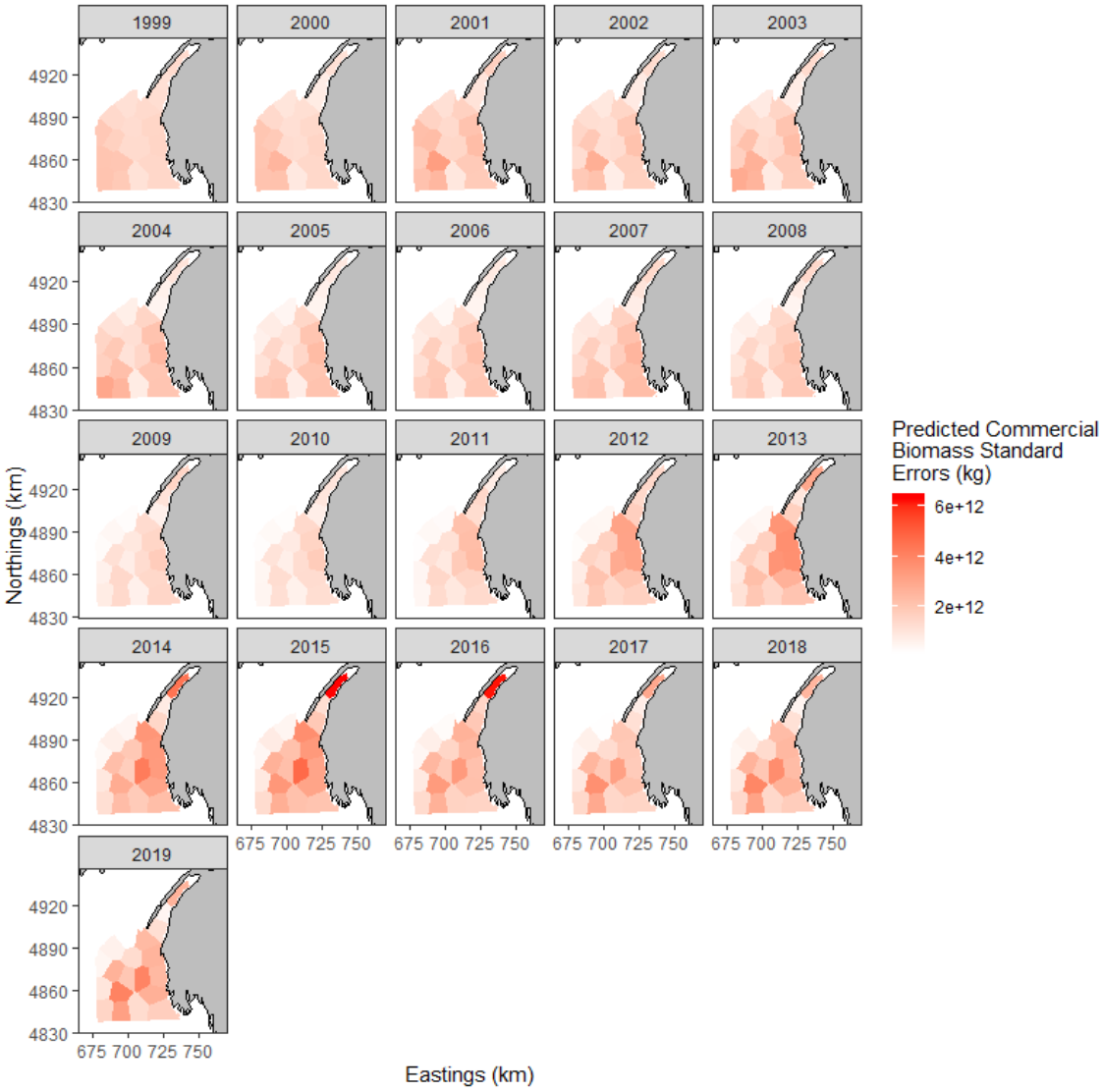

Figure B.45: Commercial size biomass density standard error (kg/km^2) at each knot between 1999 and 2019 for STM2 when q_I is estimated.

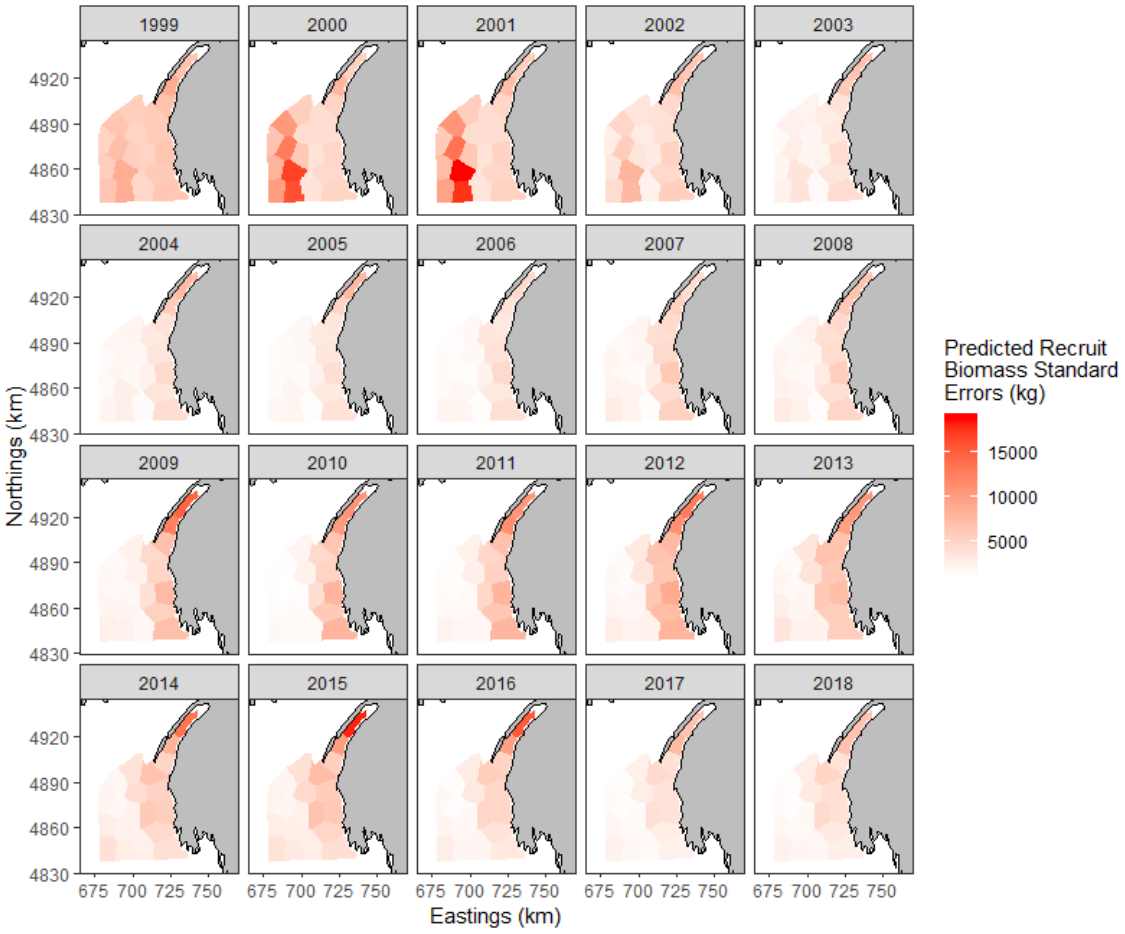

Figure B.46: Recruit biomass density standard error (kg/km^2) at each knot between 1999 and 2018 for STM2 when q_I is estimated.

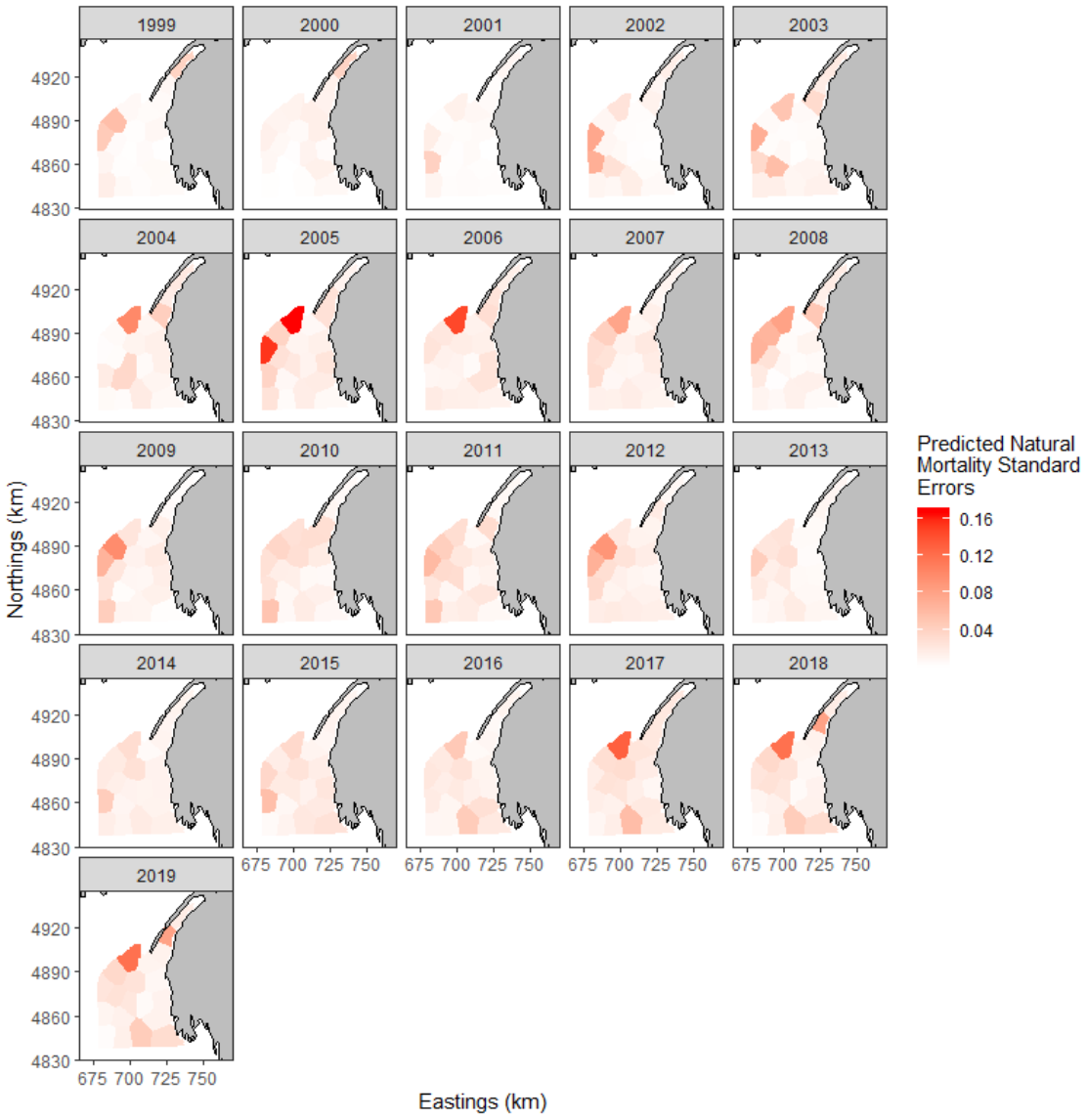

Figure B.47: Natural mortality standard error at each knot between 1999 and 2019 for STM2 when q_I is estimated.